Weakening Satellite Era and Future Tropical Atlantic Interannual Sea Surface Temperature Variability

Dissertation

in fulfillment of the requirements for the

degree of Dr. rer. nat of the Faculty of

Mathematics and Natural Sciences at Kiel

University

submitted by **Arthur Prigent**

Kiel, December 2021

GEOMAR

C|A|U

Christian-Albrechts-Universität zu Kiel

First referee: PD Dr. Joke F. Lübbecke

Second referee: Prof. Dr. Arne Biastoch

Day of Disputation: 23/02/2022

Approved for Publication: 23/02/2022

Abstract

Multidecadal changes in tropical Atlantic interannual sea surface temperature (SST) variability are investigated in this thesis during the satellite era, i.e. from the late 1970s to present-day, and in future projections. In particular, two El Niño-like phenomena driving high interannual SST variability in the eastern tropical Atlantic have been examined, namely: (1) the Atlantic Niños centered in the eastern equatorial Atlantic (ATL3, 20°W-0°; 3°S-3°N) and (2) the Benguela Niños developing in the Angola-Benguela area (ABA, 8°E-16°E; 20°S-10°S). The interannual SST variability in these two regions is important as both climate modes impact the climate of the surrounding countries. Furthermore, Benguela Niños have been shown to affect the marine ecosystems in the ABA.

Over the satellite era, multidecadal changes in interannual SST variability in the ATL3 region and in the ABA have been analyzed using observational data and reanalysis products. In the ATL3 region, the May-June-July interannual SST variability has weakened by 31% from 0.68 ± 0.09°C during 1982-1999 to 0.47 ± 0.05°C in 2000-2017. Relative to 1982-1999, during 2000-2017 all three components of the Bjerknes feedback decreased and the net heat flux damping, mainly through the latent heat flux damping, increased. Hence, both dynamical and thermodynamical processes are proposed to have contributed to weakened the ATL3 interannual SST variability. In the ABA it is shown that relative to 1982-1999, during 2000-2017 the March-April-May interannual SST variability has reduced by 30.5% from 1.08 ± 0.13°C to 0.75 ± 0.11°C. Compared to the pre-2000 period, during the post-2000 period the remote forcing had less influence on ABA SSTs. This is caused by smaller equatorial zonal wind variability reducing the equatorial Kelvin wave activity and thus weakening the ABA interannual SST variability. Due to the reduced equatorial forcing, the relative importance of the local forcing for the ABA interannual SST variability increased during 2000-2017.

Lastly, future projections of the ATL3 and ABA interannual SST variability under high CO_2 emission scenarios were assessed using the 5th and 6th phases of the Coupled Model Intercomparison Project (CMIP) models as well as the global coupled model Flexible Ocean and Climate Infrastructure (FOCI) with enhanced oceanic resolution over the tropical Atlantic. In the ATL3 region relative to 1950-1999, 80% of 40 CMIP5 and CMIP6 models agree on a reduction of the interannual SST in 2050-2099. The ATL3-averaged interannual SST variability change in CMIP5 and CMIP6 models can to a large part (61%) be related to the reduced thermocline feedback. In addition, it is shown that models with less SST bias tend to predict a stronger reduction of the ATL3 interannual SST variability. At last, the FOCI model, which is able to simulate a more realistic interannual SST variability in the ABA than the CMIP5 and CMIP6 models, is used to investigate future projections of the interannual SST variability in the ABA. As for the ATL3 region, in the ABA relative to 1970-1999, during 2070-2099 the interannual SST variability during the FOCI model peak season, May-June-July, decreases by about 24%. The reduction of the interannual SST and temperature variability in the ABA appears as a consequence of a smaller temperature response to thermocline depth variations. The weaker thermocline feedback is found to co-locate with the regions where the thermocline deepens the most.

Zusammenfassung

In dieser Arbeit werden multi-dekadische Änderungen der zwischenjährlichen Variabilität der Meeresoberflächentemperatur (SST) im tropischen Atlantik sowohl während des Satelliten-Zeitalters (seit Ende der 1970er Jahren bis heute) als auch in Zukunfts-Projektionen, untersucht. Insbesondere, zwei El-Niño ähnliche Phänomene, welche starke zwischenjährliche SST-Variabilität im östlichen tropischen Atlantik verursachen, werden analysiert: (1) der Atlantische Niño im östlichen, äquatorialen Atlantik (ATL3, 20°W-0°; 3°S-3°N) und (2) der Benguela Niño, welcher in der Angola-Benguela-Region entsteht (ABA, 8°E-16°E; 20°S-10°S). Zwischenjährliche SST-Variabilität in diesen beiden Regionen ist von großer Bedeutung, da beide Klima-Moden das Klima der umliegenden Länder beeinflussen. Es wurde außerdem nachgewiesen, dass Benguela Niños einen Einfluss auf marine Ökosysteme in der ABA-Region haben.

Während des Satelliten-Zeitalters wurden multi-dekadische Änderungen der zwischenjährlichen SST-Variabilität sowohl in der ATL3-Region als auch in der ABA-Region anhand von Beobachtungs- und Reanalyse-Daten analysiert. Es zeigt sich, dass sich die zwischenjährliche SST-Variabilität der Monate Mai bis Juli um 31% von 0.68 $\pm$ 0.09°C zwischen 1982-1999 auf 0.47 $\pm$ 0.05°C zwischen 2000-2017 verringert hat. Im Vergleich zu der Zeitspanne von 1982 bis 1999 haben sich zwischen 2000 und 2017 alle drei Komponenten des Bjerknes-Feedbacks abgeschwächt, während sich die Netto-Wärmefluss-Dämpfung hauptsächlich durch latente Wärmefluss-Dämpfung verstärkt hat. Daher wird angenommen, dass sowohl dynamische als auch thermodynamische Prozesse zu der Abschwächung der zwischenjährlichen SST-Variabilität in der ATL3-Region beigetragen haben. Es wird weiter für die ABA-Region gezeigt, dass sich relativ zu der Zeitspanne zwischen 1982 und 1999 die zwischenjährliche SST-Variabilität der Monate März bis Mai zwischen 2000 und 2017 um 30.5% von 1.08 $\pm$ 0.13°C auf 0.75 $\pm$ 0.11°C abgeschwächt hat. Verglichen zu der Zeitspanne vor 2000, hatten

nicht-lokale Prozesse während der Zeitspanne nach 2000 einen geringeren Einfluss auf die Meeresoberflächentemperaturen in der ABA-Region. Dies wird auf eine geringere Variabilität der zonalen Wind-Variabilität entlang des Äquators zurückgeführt, wodurch die Aktivität äquatorialer Kelvin-Wellen reduziert und folglich eine Abschwächung der zwischenjährlichen SST-Variabilität in der ABA-Region entsteht. Durch die Abschwächung des äquatorialen Antriebmechanismus hat sich die relative Bedeutung der lokalen Prozesse in Bezug auf die zwischenjährliche SST-Variabilität in der ABA-Region zwischen 2000 und 2017 verstärkt.

Zuletzt wurden Zukunftsprojektionen der zwischenjährlichen SST-Variabilität in der ATL3- und in der ABA-Region in hohen CO_2-Emissions-Szenarien sowohl anhand der fünften und sechsten Phase des "Coupled Model Intercomparison Projects" (CMIP) als auch des gekoppelten, globalen Modells "Flexible Ocean and Climate Infrastructure" (FOCI), mit besonders hoch-aufgelöstem tropischen Atlantik, analysiert. Für die ATL3-Region zeigt sich, dass im Vergleich zu 1950-1999 80% der 40 CMIP5- und CMIP6-Modelle eine Reduktion der zwischenjährlichen SST-Variabilität zwischen 2050-2099 vorhersagen. Die gemittelte Änderung der zwischenjährlichen SST-Variabilität in der ATL3-Region in den CMIP5- und CMIP6-Modellen kann zu einem Großteil (61%) der Abschwächung des Thermoklinen-Feedbacks zugeschrieben werden. Zusätzlich wird gezeigt, dass Modelle mit einem geringeren SST-Bias dazu tendieren eine stärkere Reduktion der zwischenjährlichen SST-Variabilität in der ATL3-Region vorherzusagen. Schließlich werden mithilfe des FOCI-Modells, welches im Gegensatz zu den CMIP5- und CMIP6-Modellen eine realistischere, zwischenjährliche SST-Variabilität in der ABA-Region aufweist, die Zukunftsprojektionen der zwischenjährlichen SST-Variabilität in der ABA-Region analysiert. Ähnlich zu der ATL3-Region zeigt sich für die ABA-Region, dass sich relativ zu der Zeitspanne zwischen 1970 und 1999 die zwischenjährliche SST-Variabilität zwischen 2070 und 2099 während der stärksten Jahreszeit im FOCI-Modell von Mai bis Juli um 24% abschwächt. Diese Abschwächung der zwischenjährlichen SST-Variabilität in der ABA-Region scheint die Folge einer schwächeren Temperatur-Reaktion auf Variationen der Thermoklinen-Tiefe zu sein. Es zeigt sich, dass in Regionen mit schwächerem Thermoklinen-Feedback auch die stärksten Änderungen in der Thermoklinen-Tiefe vorzufinden sind.

Table of Contents

List of Tables

List of Figures

List of Abbreviations

ABF	Angola-Benguela Front		**ITCZ**	Intertropical Convergence Zone
ABFZ	Angola-Benguela Frontal Zone		**OGCM**	Ocean General Circulation Model
AC	Angola Current		**SAA**	South Atlantic Anticyclone
AMO	Atlantic Multidecadal Oscillation		**SEUC**	South Equatorial Undercurrent
AMOC	Atlantic Meridional Overturning Circulation		**SECC**	South Equatorial Counter Current
AMM	Atlantic Meridional Mode		**SLP**	Sea Level Pressure
AMV	Atlantic Multidecadal Variability		**SLA**	Sea Level Anomaly
AZM	Atlantic Zonal Mode		**SSH**	Sea Surface Height
BC	Benguela Current		**SSP**	Shared Socioeconomic Pathway
BF	Bjerknes Feedback		**SST**	Sea Surface Temperature
BUS	Benguela Upwelling System		**STC**	Subtropical Cell
CMIP	Coupled Model Intercomparison Project		**TIWs**	Tropical Instability Waves
CTW	Coastal Trapped Waves		**WAM**	West African Monsoon
EBUS	Eastern Boundary Upwelling System		**WES**	Wind-Evaporation-SST
EKW	Equatorial Kelvin Waves		**WWV**	Warm Water Volume
ENSO	El Niño/Southern Oscillation		**Z20**	20°C isotherm depth
EUC	Equatorial Undercurrent		**Z23**	23°C isotherm depth
FOCI	Flexible Ocean Climate Infrastructure			
GCM	Global Climate Model			
IOD	Indian Ocean Dipole			

Chapter 1

Introduction

Tropical oceans are a key component of the climate system. Tropical regions, receive much of the solar radiation throughout the year. Thus, these regions are considerably warmer than the mid- and high latitudes. The excess of heat stored in the tropics drives the atmospheric and oceanic circulations that in turn help to distribute this heat to higher latitudes (Behera, 2021). In addition, the high sea surface temperature (SST) in the tropical oceans allows for strong interaction between the ocean and the atmosphere by deep atmospheric convection.

The tropical Pacific Ocean has received a lot of attention throughout the years because of the predominance of the El Niño/Southern Oscillation (ENSO), the strongest interannual climate variation (Philander, 1990). ENSO can impact the climate worldwide and further lead to dramatic socio-economic impacts. While ENSO contribution to interannual climate variability is the largest globally, it is not the only contributor. The contribution of the tropical Indian and Atlantic oceans has also been noted (Zebiak, 1993), and the latter is the focus of this study. Indeed, relatively strong interannual variations of SST, phase-locked to the seasonal cycle, occur in the tropical Atlantic. These large deviations of the SST from the climatological mean seasonal cycle have socio-economic repercussions (Hirst and Hastenrath, 1983). In fact, these SST anomalies can influence the regional climate as well as the marine ecosystems and fisheries. The tropical Atlantic mean-state and its seasonal cycle are introduced in sections 1.1 and 1.2, respectively. The tropical Atlantic SST variability is presented in section 1.3, with a particular focus on the interannual SST variability. Finally, the motivations, objectives and the outline of this thesis are drawn in section 1.4.

1.1 Tropical Atlantic mean-state

The equatorial Atlantic depicts a zonal temperature gradient, with warm waters located in the west and cool waters in the east (Figure 1.1a, shadings). Deep atmospheric convection and heavy rainfall occur in the western Atlantic over the warm waters, whereas there is net atmospheric subsidence over the colder waters in the eastern equatorial Atlantic. Rising motions in the western part and descending motions of the air masses in the eastern part establish an east-west atmospheric circulation called the Walker circulation (Figure 1.1b). In the annual mean, the maximum SSTs are located north of the equator (Figure 1.1a, shadings), setting the mean position of the Intertropical Convergence Zone (ITCZ, Figure 1.1a, indicated by mean precipitation contours). The ITCZ position to the north of the equator leads to cross-equatorial southeasterly winds over the equatorial Atlantic (Figure 1.1a). Surface wind induces a force on the ocean called the wind stress, which generates together with the Coriolis force a poleward Ekman transport on both sides of the equator. The divergence of the water masses results in an equatorial upwelling of cold subsurface waters. The upwelling of cold subsurface water helps to maintain the cross-equatorial SST gradient. In addition, the Walker circulation drives a westward transport of warm waters to the western equatorial Atlantic. As a result, the equatorial Atlantic isotherms are tilted up from west to east, with the thermocline located approximately at 130 m depth in the western part compared to approximately 60 m depth in the eastern part (Figure 1.1c). North and south of the equator, the complex equatorial Atlantic current system features an alternation of westward and eastward currents (Brandt et al., 2008). Below the surface currents, at the thermocline level, there are several eastward flowing subsurface currents that feed into the Angola Current (AC in Figure 1.1a), namely: the Equatorial Undercurrent (EUC), the South Equatorial Undercurrent (SEUC) and the South Equatorial Counter Current (SECC) (Peterson and Stramma, 1991; Rouault et al., 2007; Siegfried et al., 2019). The AC transports warm tropical waters with a mean southward transport at 11°S of 0.32 ± 0.046 Sv (1 Sv = 10^6 m^3s^{-1}) as estimated by Kopte et al. (2017) using moored velocity time series. Off South Africa and Namibia, the Benguela Current is flowing northwestward (BC in Figure 1.1a). The BC is the eastern boundary current of the South Atlantic subtropical gyre (Peterson and Stramma, 1991). The mean northward transport of the BC estimated by Majumder and Schmid (2018) in the upper 800 m between the conti-

nental shelf of Africa and 3°E amounts to 23 ± 3 Sv at 31°S and 11 ± 3 Sv at 28°S. The AC and the BC meet at the Angola-Benguela front (ABF) at around 16°S (Veitch et al., 2006) where a strong meridional SST gradient can be observed (ABF in Figure 1.1a).

In the southeastern tropical Atlantic Ocean and at the eastern flank of the South Atlantic Anticyclone (SAA, Figure 1.1a), which has its centre approximately at 8°W and 30°S (Reboita et al., 2019), the Benguela upwelling system (BUS) is located. The BUS is among the four major eastern boundary upwelling systems (EBUS), which are the most productive marine ecosystems in the world ocean (Bakun et al., 2015). The BUS shares with the other EBUS many characteristics, as for instance, a strong connection to the subtropical highs driving equatorward, upwelling favourable winds. Indeed, strong coastal southerly winds driven by the SAA prevail in the southeastern tropical Atlantic Ocean. These winds lead to the upwelling of cold nutrient rich subsurface water (Figure 1.1a) due to the offshore Ekman transport of surface waters at the eastern boundary. In addition, the cyclonic wind stress curl present near the coast drives an upward nutrient supply by Ekman suction. As a result, the BUS yields a high primary production favouring the growth of small pelagic fishes leading to an important pelagic fish stock (Chavez and Messié, 2009). The BUS also displays some unique features as it is surrounded by warm tropical water and by warm water coming from the Agulhas at its northern and southern boundaries, respectively. An additional remarkable feature of the BUS, is the presence of the AC (Kopte et al., 2017), flowing against the prevailing southerly winds.
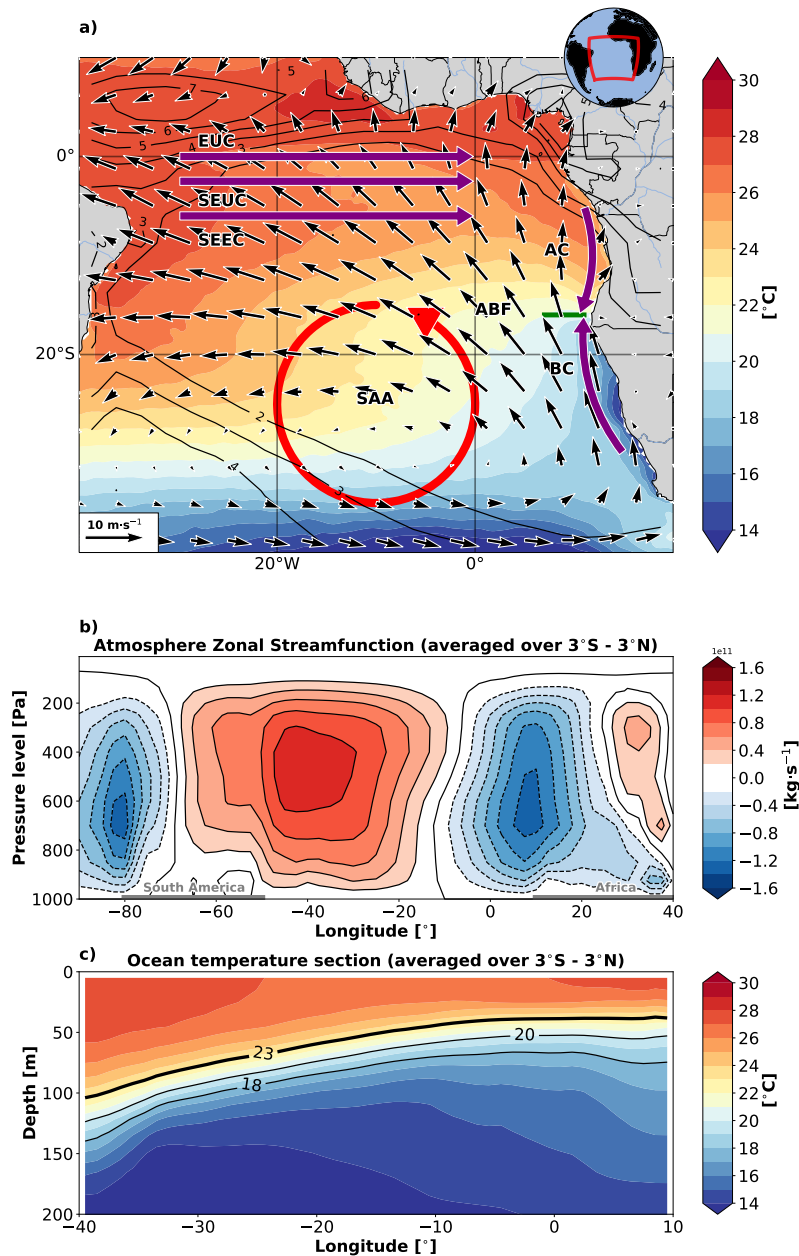
Figure 1.1: (a) Mean ERA5 winds (arrows, m·s^{-1}), SST (shadings, °C) and precipitation (contours, mm·day^{-1}) for the period 1982-2019. In purple five currents are schematized from north to south: The Equatorial Undercurrent (EUC), the South Equatorial Undercurrent (SEUC), the South Equatorial Counter Current (SECC), the Angola Current (AC) and the Benguela Current (BC). The green line indicates the mean position of the Angola Benguela front (ABF) around 16°S. The circled red arrows depict the mean position of the South Atlantic Anticyclone (SAA). (b) Zonal ERA-interim streamfunction representing the Walker circulation computed for the time periods 1982-2017 between 3°S and 3°N. Grey bold lines at the bottom indicate South America and Africa. (c) Top 200 m temperature section between 3°S and 3°N from ORA-S4. The 23°C isotherm is denoted by the thick black line.

1.2 Tropical Atlantic seasonal cycle

Both the equatorial Atlantic and the southeastern tropical Atlantic Ocean are characterized by pronounced seasonal cycles. In March-April-May (MAM) warm SSTs are located close to the equator (shadings in Figures 1.2a and 1.3a) setting the ITCZ at its southernmost position, over the equator (Figure 1.2a, contours). Due to the equatorial position of the ITCZ, the equatorial trade winds are at their weakest (Figures 1.2a and 1.3a) and the thermocline is at its deepest in the east (Figure 1.2c). The intensification of the equatorial trade winds from MAM to JJA (Figure 1.3a), due to the seasonal migration of the ITCZ and westward extension and intensification of the SAA (Reboita et al., 2019), drives a steepening of the thermocline (Figures 1.2c and 1.2d), an enhancement of the upwelling and vertical mixing. Hence, starting in April, the eastern equatorial Atlantic (ATL3, 20°W-0°; 3°S-3°N) SSTs decrease until August (Figures 1.2a and 1.2b). For instance, between 20°W and 0°W from MAM to JJA the temperature drops by $\sim 4°C$ (Figures 1.2a, 1.2b, 1.3a and 1.3b). The cooling observed in June-July-August (JJA) extending from the west African coast to the ATL3 region is referred to as the equatorial cold tongue (Figures 1.2b and 1.3a, shadings). In the western equatorial Atlantic, the seasonal adjustment of the ocean to the surface wind stress forcing results in a cycle of consecutive westward propagating Rossby and eastward propagating Kelvin waves (Figure 1.3a; Polo et al. (2008)). Yet, in the eastern equatorial Atlantic and along the southwest African coast a semiannual cycle is observed in the sea level anomalies (SLA, contours, Figures 1.3a and 1.3b). Ding et al. (2009) while investigating the dynamics of the seasonal cycle of the sea surface height (SSH) using ocean models, revealed that the semiannual cycle in SSH occurs because the semiannual cycle in surface winds resonantly excites the second baroclinic mode's basin mode.

The southwest African coast depicts two distinct regions, north and south of the ABF (Figure 1.3b). North of the ABF, between the equator and 15°S, a pronounced seasonal cycle is observed (Figure 1.3b) with warmest SSTs in February-March-April (FMA) and coolest SSTs in July-August-September (JAS). Throughout the year the southerly, upwelling favourable winds depict only little changes and remain relatively weak. Therefore, these winds cannot explain the strong cooling ($\sim 4°C$) observed from FMA ($\sim 27°C$) to JAS ($\sim 23°C$). The seasonal cycle of the SLA in the eastern equatorial Atlantic and along the southwest African coast (contours in Figures 1.3a
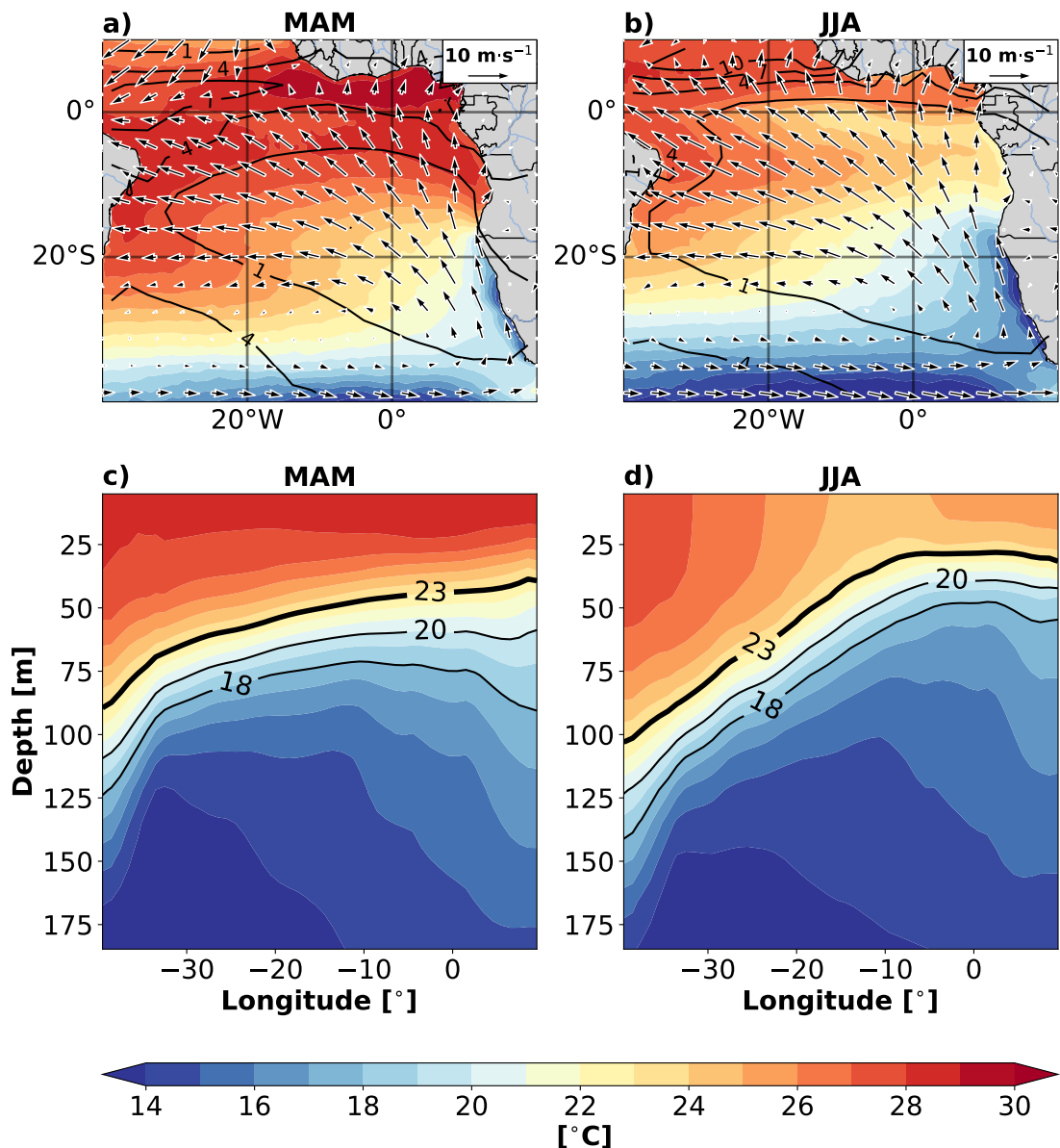
Figure 1.2: Mean ERA5 SST (shadings, °C), wind (arrows, m·s^{-1}) and precipitation (contours, mm·day^{-1}) in (a) MAM and in (b) JJA. Top 200 m temperature section between 3°S and 3°N from ORA-S4 in (c) MAM and in (d) JJA. The thick black line denotes the 23°C isotherm depth.

and 1.3b) follows a semiannual harmonic corresponding to the semiannual propagation of equatorial Kelvin waves (EKWs) along the equator that, when reaching the West African coast, transfer a part of their energy into poleward propagating coastally trapped waves (CTWs, Clarke (1983)). The seasonal variations of SSTs north of the ABF are dynamically driven via the propagation of EKWs and subsequent CTWs, which are associated with the upward and downward movements of the thermocline (Ostrowski
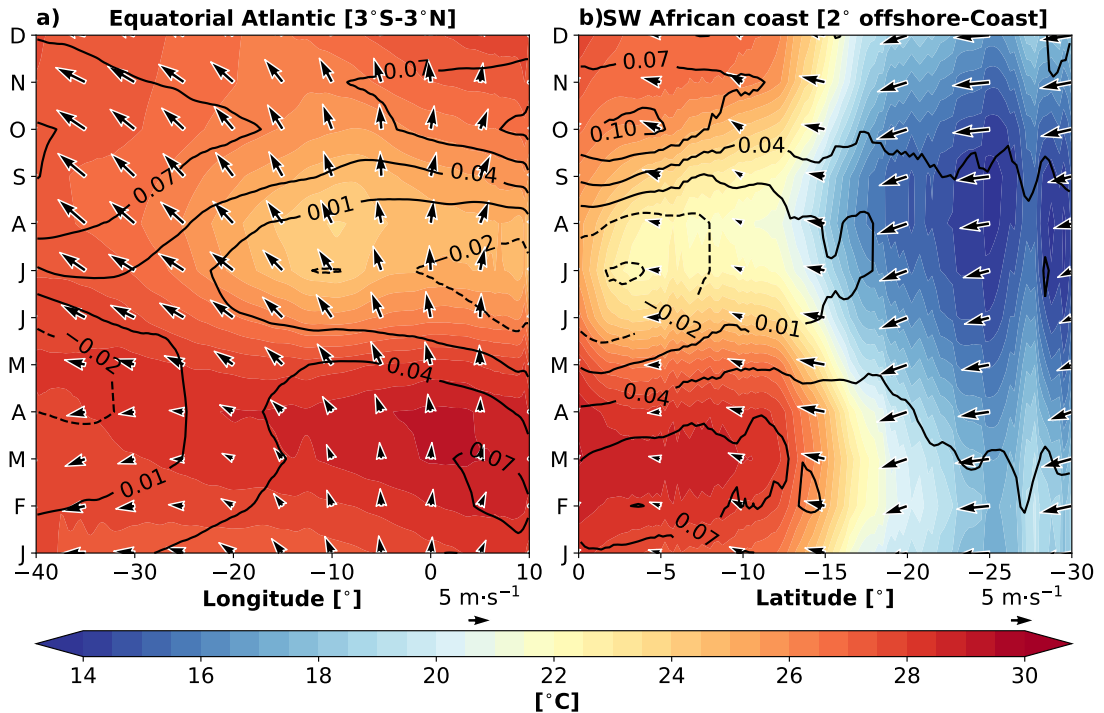
Figure 1.3: (a) Equatorial Atlantic SST (shadings, °C), winds (arrows, m·s^{-1}) and SLA (contours, m) averaged between 3°S and 3°N and plotted in function of the calendar month and longitude. (b) Southwest African SST (shading), winds (arrows) and SLA (contours) averaged on a 2° band and plotted as a function of the calendar month and latitude.

et al., 2009; Rouault, 2012). A downwelling (upwelling) CTW will drive a downward (upward) movement of the thermocline which can be observed in sea level anomaly data by elevated (lowered) sea level. South of the ABF from 17°S to 30°S relatively cool SSTs are observed throughout the year with coolest SSTs (around 14°C) found in JAS. In this region, the SST seasonal cycle is dominated by the alongshore, upwelling favourable winds.

1.3 Tropical Atlantic variability

The tropical Atlantic depicts SST variability on various spatial and temporal scales. At decadal to multidecadal time scales, the North Atlantic SSTs depicts a 65-80-year cycle with a range of 0.4°C (Enfield et al., 2001), referred to as the Atlantic multidecadal oscillation (AMO, Kerr (2000)), and nowadays referred to as the Atlantic multidecadal
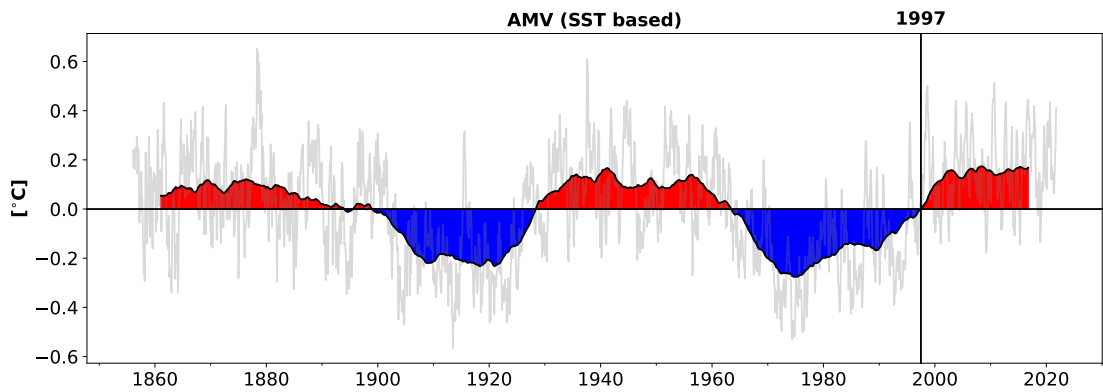
Figure 1.4: AMV index. The AMV index calculated from the Kaplan SST dataset (Kaplan et al., 1998) using the Enfield et al. (2001) methodology. This time series can be found at https://psl.noaa.gov/data/timeseries/AMO/.

variability (AMV, Figure 1.4). The AMV is the leading mode of internal multidecadal SST variability in the Atlantic Ocean (Knight et al., 2006; Martín-Rey et al., 2018).

A positive phase of the AMV is characterized by anomalously warm (cool) SSTs in the North Atlantic (south of the equator). The AMV has far reaching impacts as it can modulate the northeastern Brazilian and Sahelian rainfall (Knight et al., 2006) as well as the European summer climate (Sutton and Hodson, 2003). Martín-Rey et al. (2018) showed that the interannual tropical Atlantic variability differs depending on the AMV phases. They indicated that during a negative phase of AMV, the amplitude of the Atlantic Niño (this mode will be described in details in the following) increases up to 150% with respect to the positive phase of AMV. According to Martín-Rey et al. (2018), the increased equatorial Atlantic interannual SST variability during a negative phase of AMV is related to a shallower mean equatorial thermocline which results from an enhanced Azores high pressure system. The shallower mean thermocline would increase the effect of the Bjerknes feedback.

On interannual to decadal time scales, the tropical Atlantic is characterized by mainly two distinct patterns of SST variability (Sutton et al., 2000) displayed by the Empirical orthogonal Function (EOF) analysis (shadings in Figure 1.5): (i) the Atlantic meridional mode (AMM, Figure 1.5a) explaining 18.9% of the variance and (ii) the Atlantic zonal mode (AZM) or Atlantic Niño (Figure 1.5b), explaining 26.7% of the variance. Both climate modes are seasonally phase-locked and thus result in a year-to-year modulation of the seasonal cycle.

8
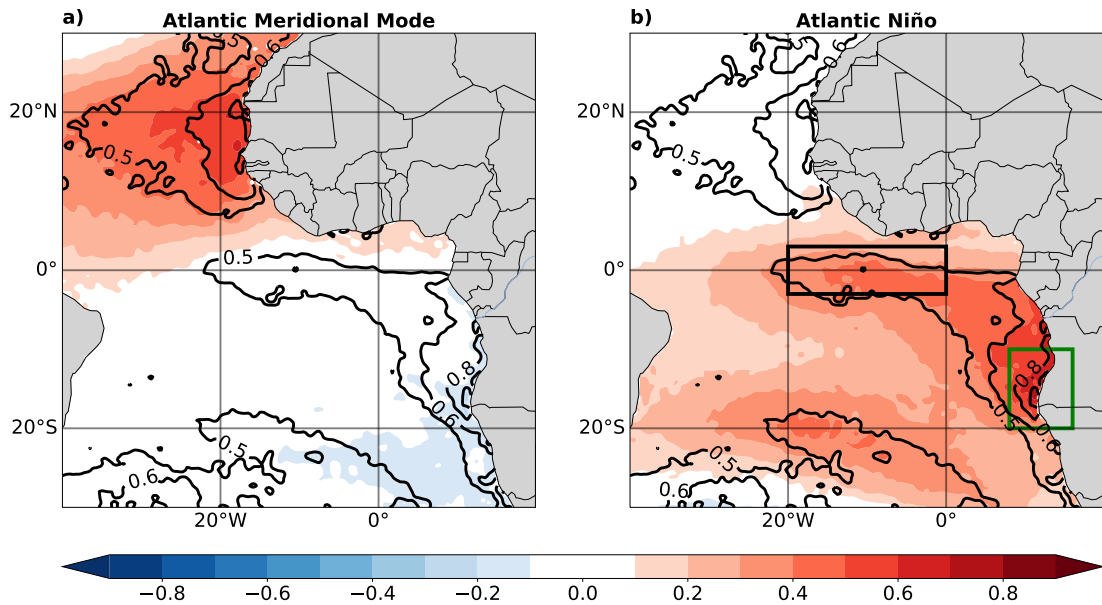
Figure 1.5: Second (a) and first (b) EOF of monthly ERA5 SST anomalies computed for the period 1980-2019 over the tropical Atlantic (40°W-20°E; 30°S-30°N). Each mode explains 18.9% and 26.7% of the variance, respectively. Black contours denote the standard deviation of the SST anomalies (°C) for the period 1980-2019.

The AMM has an interhemispheric pattern (Figure 1.5a) and is characterized by interannual and decadal anomalous meridional SST gradient between the tropical North and South Atlantic (Nobre and Shukla, 1996). The fluctuation of the meridional SST gradient modulates the seasonal migration of the ITCZ (Amaya et al., 2017), which in turn impacts regional rainfalls over northeast Brazil and the Sahel of Africa (Folland et al., 1986). For instance, anomalously warm (cold) SSTs in the tropical North Atlantic relative to the South Atlantic are associated with anomalous southerly (northerly) surface winds and northward (southward) displacement of the ITCZ (Foltz et al., 2012). The AMM generally occurs in boreal spring when the ITCZ is close to the equator. This mode is mainly driven by a positive thermodynamic air-sea feedback, the so-called Wind-Evaporation-SST (WES) feedback (Xie and Philander, 1994). During a positive phase of the AMM, positive (negative) SST anomalies are observed north (south) of the equator. The pressure anomalies induced by the anomalous meridional SST gradient drive cross-equatorial winds. Superimposed to the easterly trade winds, these wind anomalies increase (decrease) the wind speed south (north) of the equator, leading to intensified (reduced) evaporative cooling which acts to amplify the initial meridional

SST gradient (Xie, 2009).

The first mode of interannual SST variability in the tropical Atlantic is the zonal mode or Atlantic Niño (Figure 1.5b). The spatial pattern of the Atlantic Niño (shadings in Figure 1.5b and the standard deviation of the SSTa (contours in Figure 1.5b) reveal two centres of high interannual SST variability: (1) the eastern equatorial Atlantic (ATL3, 20°W-0°; 3°S-3°N, defined by Zebiak (1993)) and (2) the Angola-Benguela area (ABA, 8°E-14°E; 20°S-10°S, defined by Florenchie et al. (2003)). The climate modes driving interannual SST variability in these two regions are called the Atlantic Niños (Merle, 1980) and the Benguela Niños (Shannon et al., 1986), respectively. As these modes are strongly correlated, they could also be viewed as one single mode (Lübbecke et al., 2010, 2018; Illig et al., 2020). Yet, in the context of this study, Atlantic Niños and Benguela Niños are introduced in the following separate sections.

1.3.1 Atlantic Niños/Niñas

Atlantic Niños, and its cool phase Atlantic Niñas (Merle, 1980), are extreme warm and cold events occurring typically in boreal summer every few years in the eastern equatorial Atlantic. The centre of action of the Atlantic Niños is located at the position of the equatorial cold tongue in the ATL3 region (Figure 1.5b, black box; Zebiak (1993)). These events are characterized by SSTs deviating up to 1.5°C from the climatological mean as shown by the ATL3-averaged SST anomalies (Figure 1.6a). For instance, the ATL3 SST during the warm (cold) event of 1995 (2005) is shown in Figure 1.6b. It highlights that largest deviations of SST from the climatological mean seasonal cycle occur in boreal summer. This is confirmed by the seasonal cycle of the standard deviation of the SSTa (Figure 1.6c), which depicts a clear peak of variability in May-June-July (MJJ) with maximum of 0.67°C in June. A secondary peak (> 0.45°C) of interannual SST variability is observed in November-December (Figure 1.6c) and referred to as the Atlantic Niño II (Okumura and Xie, 2006).

Typical Atlantic Niño event

A typical Atlantic Niño event starts in March with weak positive SST anomalies on the equator and along the Angolan and Namibian coasts (Figure 1.7). SST anomalies along the southwest African coast are indicative of a Benguela Niño, and this climate

Figure 1.6: (a) Time series of ERA5 SST anomalies averaged over the ATL3 region. SST anomalies were computed by removing the climatological monthly mean seasonal cycle calculated over the period 1980-2019. Prior to computation of the SST anomalies the data was linearly detrended. $\pm\,\sigma$ denotes one standard (0.46°C) of the SST anomalies evaluated over the period 1980-2019. (b) Red (blue) line shows the ATL3-averaged SST warm (cold) event of 1995 (2005). The thick black line denotes the mean ATL3 seasonal cycle over the period 1980-2019. (c) ATL3-averaged mean seasonal cycle (black) and seasonal cycle of the standard deviation of the SST anomalies (red) over the period 1980-2019.

mode is described in the next section. Simultaneously, northwesterly wind and precipitation anomalies can be observed in the western equatorial Atlantic. In April, wind and precipitation anomalies continue to grow and peak in May. SST anomalies peak a month later in June (>1°C) and start decaying in July and August. Figure 1.7 shows a clear east-west distribution with reduced surface trade winds and maximum precipitation anomalies in the west and strongest SST anomalies (>0.4°C) in the east.

Generation mechanisms

Both dynamical and thermodynamical mechanisms play crucial roles in the generation and evolution of Atlantic Niño and Niña events. The underlying dynamical pro-
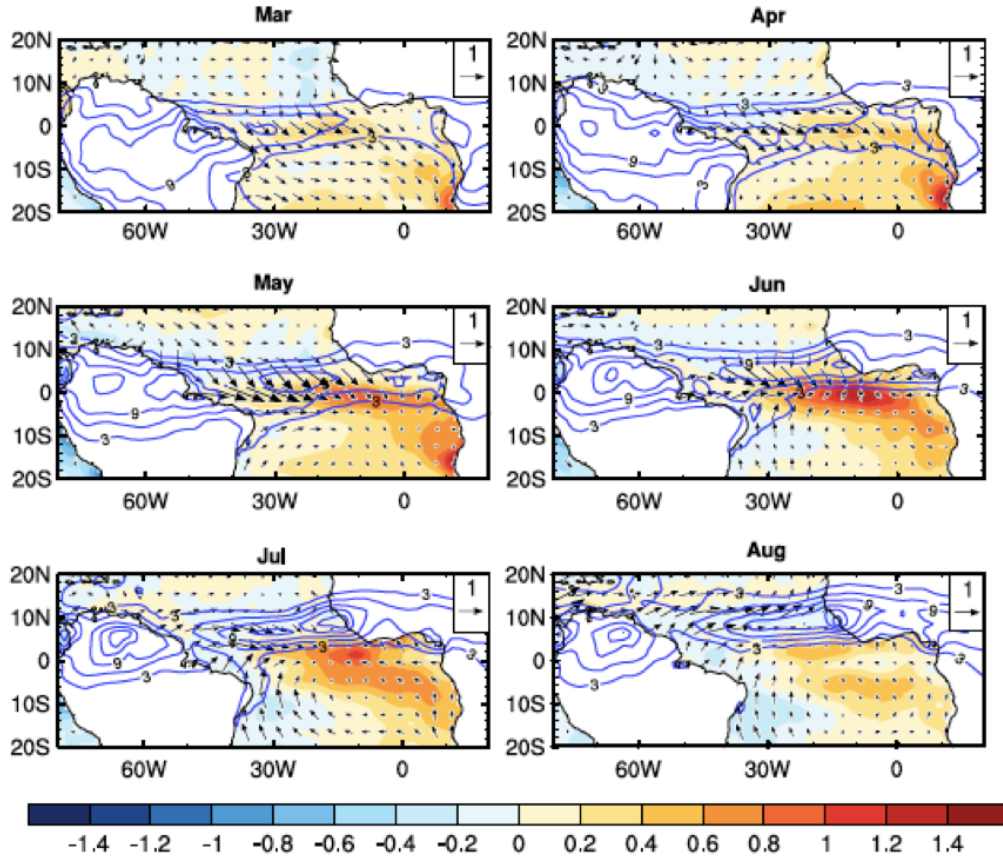
Figure 1.7: OI SST anomalies (shading, °C), ERA-interim surface wind anomalies (vectors; reference 1 m·s^{-1}) and total precipitation (contour lines, interval 3 mm·day^{-1}) composited on positive AZM events (1988, 1991, 1995, 1996, 1999, 2008). This figure is taken from Richter et al. (2017).

cesses of the Atlantic Niño are to some extent similar to those observed during ENSO in the Pacific Ocean (Servain et al., 1982; Zebiak, 1993; Keenlyside and Latif, 2007; Dippe et al., 2018; Lübbecke and McPhaden, 2013, 2017) as in both basins the Bjerknes feedback (Bjerknes, 1969) plays an important role. The Bjerknes feedback is a coupled air-sea feedback involving SSTs, winds and thermocline depth. Keenlyside and Latif (2007), using observational data, investigated the three components of the Bjerknes feedback which are: (1) the impact of SST anomalies in the east on western equatorial wind stress; (2) the thermocline slope response to western equatorial Atlantic wind anomalies; and (3) the local response of SST anomalies to thermocline depth variations. It is noteworthy that in the Pacific Ocean interactions of the Bjerknes feedback driving ENSO with the seasonal cycle occur, but do not dominate the SST variability. In con-

trast, in the tropical Atlantic, the Bjerknes feedback is seasonally active (Richter et al., 2017; Dippe et al., 2018). Furthermore, in comparison to ENSO, the SST variability is weaker and the extreme events are of shorter duration in the equatorial Atlantic (about 3 months for the Atlantic Niño and 9-12 months for El Niño). In addition, Lübbecke and McPhaden (2017) showed that while ENSO is asymmetric for warm and cold events in terms of amplitude, duration and localisation, the Atlantic Niño is symmetric, with cold events being the mirror images of the warm events.

Thermodynamical processes are also important for the Atlantic Niños. By comparing Global Climate Models (GCM) coupled to a slab ocean, i.e. without ocean dynamics, and fully coupled GCMs, Nnamchi et al. (2015) showed that thermodynamical processes could explain a large fraction of the amplitude of the Atlantic Niño events. While Nnamchi et al. (2015) argued that the thermodynamical feedbacks constitute the main source of Atlantic Niño variability, Jouanno et al. (2017) showed that ocean dynamics control a large fraction of the equatorial Atlantic SST variability, and that thermodynamical processes in the tropical Atlantic mainly act to dampen the SST anomalies. Hence, the relative importance of thermodynamical and dynamical processes for the generation of Atlantic Niños is still under debate. However, both processes are important for the evolution of these extreme events.

Richter et al. (2013) indicated that some equatorial Atlantic warm events developed despite easterly wind anomalies in the preceding months. These "non-canonical" events cannot be explained by the Bjerknes feedback which should generate cooling under such conditions. Instead, they suggested based on model simulations that non-canonical events are resulting from the meridional advection of temperature anomalies from north of the equator by the mean circulation. While investigating the non-canonical cold event of 2009, Foltz and McPhaden (2010) and later Burmeister et al. (2016) highlighted the important contribution of the reflection of Rossby waves into EKWs at the western boundary to the onset of non-canonical events. Lastly, Brandt et al. (2011b) revealed that the vertically alternating zonal currents, i.e. the equatorial Atlantic deep jets, which are independent from the atmospheric forcing, propagate their energy upwards and thus affect SST, wind and rainfall in the tropical Atlantic.

Atlantic Niño/Niña impacts

Atlantic Niños/Niñas have an influence on the climate of the surrounding countries, but can also have extratropical impacts, however, not discussed here in detail. Interannual SST variability in the eastern equatorial Atlantic has an influence on the rainfall over the Gulf of Guinea and neighbouring coastal regions (Brandt et al., 2011a; Caniaux et al., 2011). The West African Monsoon (WAM) starting in boreal summer and developing over the Guinea coast and Sahel, is influenced by the equatorial Atlantic SST variability. For instance, the Atlantic Niño would reduce (increase) the rainfall over the Sahel (Gulf of Guinea) (Cabos et al., 2019; Lübbecke et al., 2018). In addition, Nobre and Shukla (1996) showed that equatorial Atlantic interannual SST variability may delay the northward migration of the ITCZ and, hence, impact the rainfall over the Northeast South American region. In addition, Chenillat et al. (2021) showed that Atlantic Niños affect to a large extend the interannual concentration of chlorophyll-*a*, with an Atlantic Niña (Niño) event associated to high (low) concentrations of chlorophyll-*a* in the eastern equatorial Atlantic. Accordingly, the implications of such a chlorophyll-*a* concentration interannual variability driven by Atlantic Niños for the marine ecosystems requires more research.

1.3.2 Benguela Niños/Niñas

Every few years, SSTs off the coast of Angola and Namibia can deviate up to 2°C from the climatological mean (Figure 1.8a). These extreme warm (cold) events are called the Benguela Niños (Niñas) (Shannon et al., 1986). They occur generally in boreal spring and can last from a few months to half a year (Imbol Koungue et al., 2019).
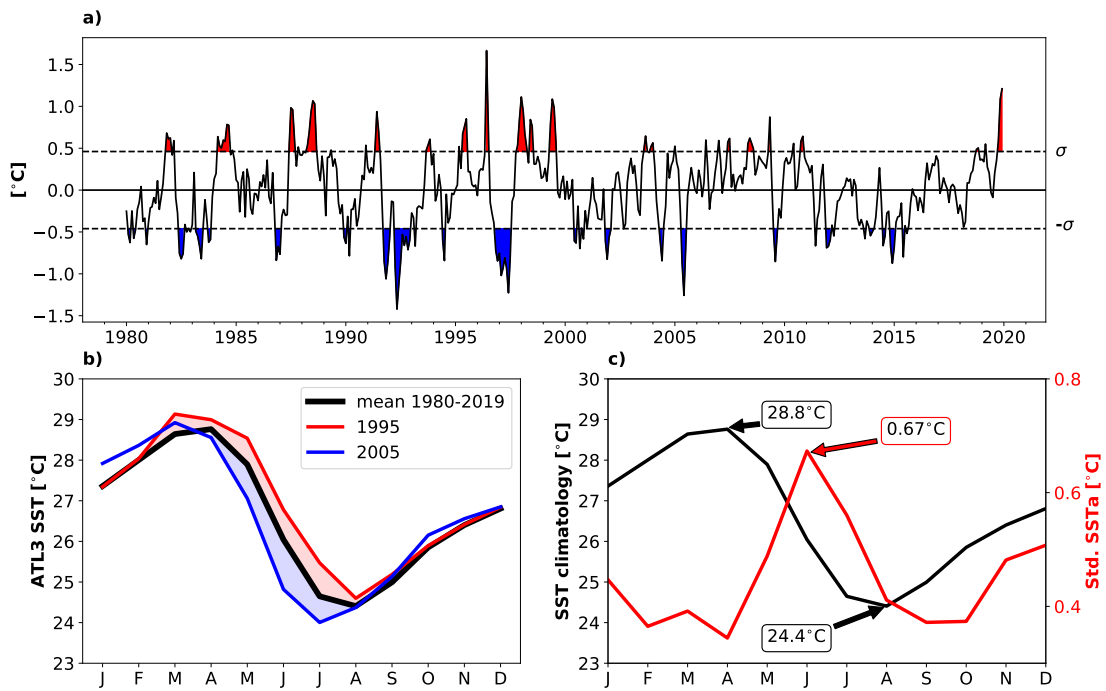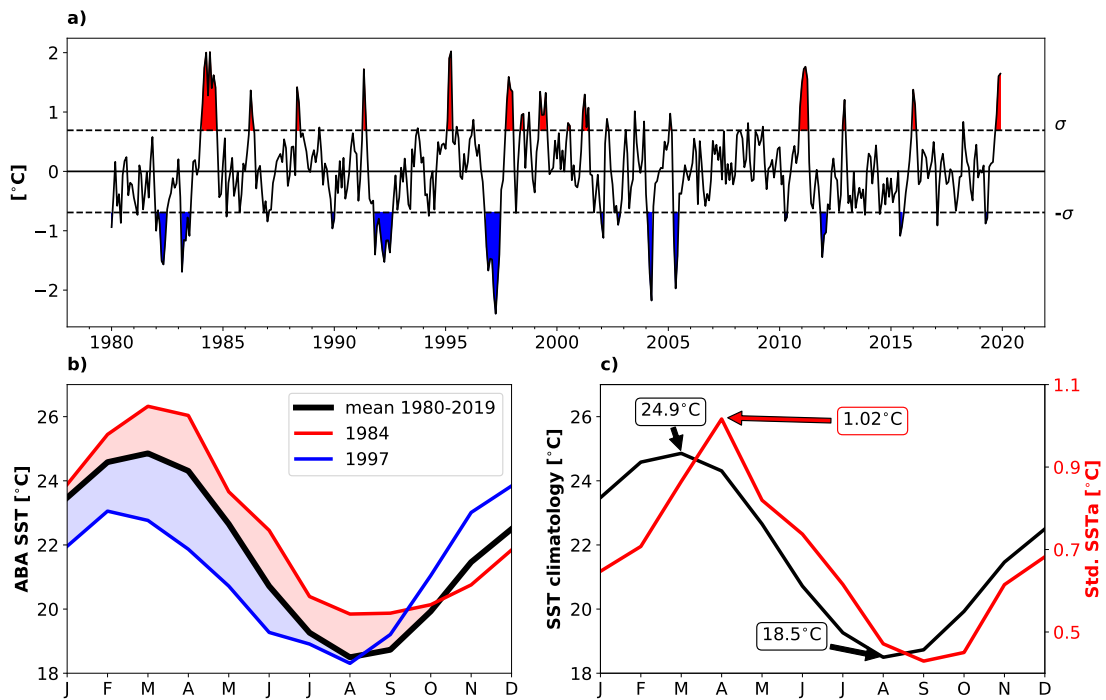
Figure 1.8: (a) Time series of SST anomalies averaged over the ABA. SST anomalies were computed by removing the climatological monthly mean seasonal cycle calculated over the period 1980-2019. Prior to computation of the SST anomalies the data was linearly detrended. $\pm\sigma$ denotes one standard (0.69°C) of the SST anomalies evaluated over the period 1980-2019. (b) Red (blue) line shows the ABA-averaged SST during the warm (cold) event in 1984 (1997). The thick black line denotes the mean ABA seasonal cycle over the period 1980-2019. (c) ABA-averaged mean seasonal cycle (black) and seasonal cycle of the standard deviation of the SST anomalies (red) over the period 1980-2019.

This is consistent with the ABA-averaged SST during the warm and cold events of 1984 and 1997 (Figure 1.8b), which reveals largest SST deviation from the climatological mean seasonal cycle in boreal spring (MAM). The SST variability in the ABA is phase-locked to the seasonal cycle (Figure 1.8c) with largest SST variability occurring in MAM, with a maximum of 1.02°C in April, one month after the warmest SSTs. Hence, the Benguela Niños/Niñas can be seen as a year-to-year modulation of the seasonal cycle.

15

Typical Benguela Niño event

Using the 10 m depth temperature and surface wind stress anomalies from an ocean general circulation model (OGCM) and a composite of four selected warm events, Imbol Koungue et al. (2019) described the typical evolution of a Benguela Niño. Three months prior to the event peak (Figure 1.9a), no significant temperature anomalies are found along the southwest African coast, and northeasterly wind anomalies are found north of the equator. Two months before the event (Figure 1.9b) the first signs of anomalously warm waters ($\sim 0.5^\circ$C) can be observed along the Angolan and Namibian coast and alongshore wind anomalies remain relatively weak. One month before the peak of the event (Figure 1.9c), a basin-wide weakening of the SAA can be observed, consistent with Lübbecke et al. (2010) and Richter et al. (2010), and with westerly wind anomalies in the western and central equatorial Atlantic as well as alongshore wind anomalies in the southeastern tropical Atlantic. In addition, temperature anomalies exceed 1°C from 5°S to 20°S along the west African coast. During the peak of the event, the Benguela Niño signature is fully developed, with ocean temperature anomalies larger than 2°C between 10°S and 20°S where the wind stress anomalies converge (Figure 1.9d). One month after the peak of the event (Figure 1.9e), a similar pattern to during the peak of the event is observed, but at lower amplitude. Two months after the peak of the event (Figure 1.9f), weak temperature anomalies are observed off Angola and Namibia and alongshore winds reinforce. We note that the warm temperature anomalies spread northwestward towards the equatorial cold tongue region, suggesting the onset of an Atlantic Niño. This is consistent with Lübbecke et al. (2010) who suggested that Benguela Niños tend to lead Atlantic Niños by a few months. They proposed that the lag between the Benguela and Atlantic Niños is caused by the difference in thermocline depths between the two regions and to a different phase-locking of the interannual SST variability and seasonal cycle. Illig et al. (2020) further investigated the lag between Atlantic Niños and Benguela Niños using different Tropical Atlantic Ocean model experiments. They revealed that only coastal wind stress anomalies along the coast of Angola and Namibia are responsible for the lag between Atlantic and Benguela Niños. Hu and Huang (2007) suggested that the SST anomalies along the West African coast and near the equator are physically connected. They proposed that the coastal warming (cooling) may induce wind convergence (divergence) over the basin, which can cause prevailing

16
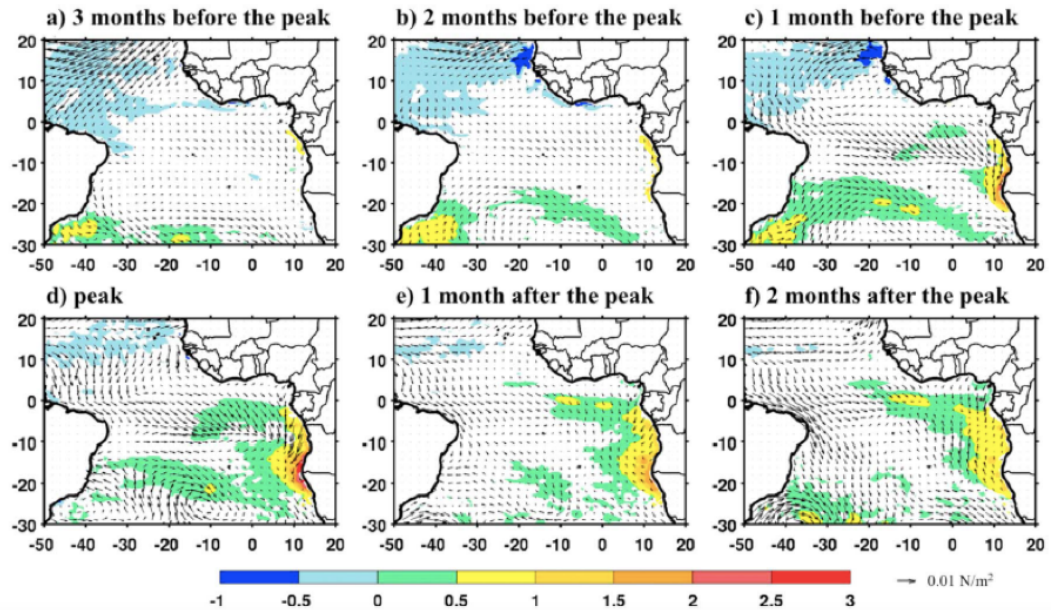
Figure 1.9: Composite maps of detrended 10m temperature anomalies (T10, shading in °C) and surface wind stress (arrows in N·m^{-2}) computed from four selected Benguela Niños (1976/1977, 1984, 1995 and 2001) and averaged during (a) December–January (three months before peak), (b) January–February (two months before the peak), (c) February–March (one month before the peak), (d) March–April (peak), (e) April–May (one month after the peak), and (f) May–June (two months after the peak). The shaded areas (detrended anomalies of T10) represent the 90% statistically significant areas. This figure is taken from Imbol Koungue et al. (2019).

westerly (easterly) anomalies in the southern tropical and equatorial Atlantic. These wind anomalies could then participate to the onset of an Atlantic Niño. These studies highlight the strong connection between the Atlantic Niños and Benguela Niños. Yet, unlike Atlantic Niños/Niñas, Benguela Niños/Niñas show some asymmetry. Imbol Koungue et al. (2019) showed that Benguela Niñas tend to last longer and cover a larger area than Benguela Niños.

Generation mechanisms

The two main generation mechanisms of the Benguela Niños/Niñas have been shown to be (1) the remote equatorial forcing and (2) the local forcing. First, the remote equatorial forcing portrays the strong relation between the EKW activity and the interannual variability along the coast of Angola and Namibia. This forcing is associated with

the eastward propagating upwelling (downwelling) EKW triggered by the intensification (relaxation) of the trade winds in the western or central equatorial Atlantic (Illig et al., 2004). When reaching the west African coast, a fraction of the EKW energy is transferred into poleward propagating CTW (Polo et al., 2008) reaching the BUS ($\sim$ 30°S, Bachèlery et al. (2020)). While propagating southward, the CTWs trigger vertical displacements of the thermocline which can affect the local stratification, alongshore currents and biogeochemical conditions (Bachèlery et al., 2016b,a; Rouault, 2012; Imbol Koungue et al., 2017). For instance, the propagation of a downwelling (upwelling) CTW along the west African coast deepens (shoals) the thermocline and can be observed in altimetry by an increase (decrease) of the sea level. In an ocean modelling study, Bachèlery et al. (2020) showed that over the period 1958-2008, that remote forcing from the equatorial Atlantic explains around 50% (70%) of the SST (SLA) interannual variability in the ABA. Second, a study by Richter et al. (2010), using observations and GCM simulations, showed the important role played by the local alongshore wind in the generation of the Benguela Niños. They revealed that SST anomalies in the ABA are preceded by westerly wind anomalies on the equator and northerly wind anomalies along the southwest African coast. These wind anomalies are related to a basin-wide weakening of the SAA (Lübbecke et al., 2010). In addition, alongshore wind anomalies may also trigger CTW at the eastern boundary and fluctuations of the coastal currents (Junker et al., 2017). While investigating the origins and developments of the Benguela Niños and Niñas, Florenchie et al. (2004) and Rouault et al. (2007) analysed the potential role of surface heat fluxes during extreme events. They found that during an extreme event, large latent heat flux anomalies could be observed acting to dampen the SST anomalies. An atypical warm event occurred in 2016 off Angola and Namibia and was investigated by Lübbecke et al. (2019). Unlike classical Benguela Niños, this event was short, peaked early in the year and was not predominantly forced by the remote equatorial forcing. Instead, this event was a combination of local processes involving reduction of alongshore winds and local upwelling, anomalous heat fluxes, freshwater input and advection. The relative importance of the remote and local forcing is still under debate and might change on decadal to multi-decadal timescales.

Benguela Niño/Niña impacts

The BUS is characterized by high primary production favouring rich and diverse marine ecosystems. Benguela Niños have dramatical impacts on the local marine ecosystems and fisheries (Gammelsrød et al., 1998; Binet et al., 2001). Bachèlery et al. (2016a) revealed that the equatorial remote forcing through CTW propagations explains more than 85% of coastal interannual nitrate and oxygen fluctuations off Angola and Namibia, using a coupled physical/biogeochemical model. Hirst and Hastenrath (1983) and Nicholson and Entekhabi (1987) established the impact of anomalously warm SSTs along the Benguela coast on coastal rainfall from near the equator to approximately 25°S. Building on the previous studies, Rouault et al. (2003) confirmed that during warmest SSTs (FMA), warm SST anomalies in the southeastern tropical Atlantic can amplify local atmospheric instability, evaporation and rainfall. They indicated the anomalous strong rainfall during a Benguela Niño might extend to southern Africa if the large-scale circulation is favourable. Koseki and Imbol Koungue (2021) investigated the response of the atmosphere to cold events using reanalysis data and a high-resolution atmospheric model. They found that rainfall in western Angola during Benguela Niñas is reduced significantly.

1.3.3 Interbasin interaction between the tropical Atlantic and Pacific

The tropical Atlantic interannual variability may also be influenced remotely by ENSO. The interaction between ENSO and Atlantic Niños is complex (Cai et al., 2019; Lübbecke et al., 2018) as both modes of variability may interact with each other. The connection between the two modes is directed both from the Pacific to the Atlantic and from the Atlantic to the Pacific. The first connection, from the Pacific to the Atlantic is of particular interest here as it may influence the tropical Atlantic interannual SST variability. Latif and Grötzner (2000) over the period 1903-1994, showed that the equatorial Atlantic exhibited a delayed response to ENSO with the equatorial Pacific SST anomalies leading by 6 months those of the equatorial Atlantic. They found that an ENSO event could induce zonal wind anomalies in the western equatorial Atlantic. These zonal wind anomalies generate subsurface anomalies propagating eastward which may

contribute to the development of an Atlantic Niño event. In line with Latif and Grötzner (2000), Delecluse et al. (1994) showed that the 1984 Atlantic Niño was partially initiated by zonal wind anomalies related to the major 1982-1983 El Niño event. Chang et al. (2006) found that ENSO has two competing impacts on the equatorial Atlantic, hence the net response of the equatorial Atlantic to ENSO can be occasionally weak. Lübbecke and McPhaden (2012), using observational and GCM data, found a robust response of the tropical Atlantic winds to ENSO, with weakened (strengthened) northeast (southeast) trade winds north (along and south) of the equator. However, they argue that the relationship between SST anomalies in the eastern equatorial Pacific and Atlantic is inconsistent, as in some years El Niño events were followed by warm and in other years by cold SST anomalies. Lübbecke and McPhaden (2012) could partially attribute the inconsistency of the relationship to a delayed negative feedback occurring in years with warm or neutral response in the eastern equatorial Atlantic. In boreal spring of these years, the northeast trades weaken and the north tropical Atlantic SSTs warm, setting up a meridional SST gradient. This leads to negative wind stress curl anomaly to the north of the equator that generates downwelling Rossby waves. The reflection of these waves at the western boundary can eventually lead to a warming in the equatorial Atlantic cold tongue region in boreal summer. The Pacific – Atlantic relationship is subject to modulation by the background mean-state. Martín-Rey et al. (2014), using observational data, showed that the AMV modulates the connection between ENSO and the Atlantic Niño modes. They found that the link between the two basins is strong during the negative phase of the AMV. The impact of ENSO on the ABA interannual SST variability has not been investigated. However, as ENSO can impact the eastern equatorial Atlantic variability, and given that Atlantic Niños and Benguela Niños are strongly correlated, it is likely that it may also influence the Benguela Niños.

1.3.4 Atlantic Niños and Benguela Niños in global coupled climate models

Coupled GCMs are key tools to explore and understand climate change impacts on tropical Atlantic variability. However, the representation of the tropical Atlantic mean-state by GCMs suffer from severe biases. As described in section 1.1, the equatorial Atlantic has a pronounced zonal gradient with warmer water in the west and cooler

water in the east. Yet in coupled GCMs, due to a strong warm bias in the eastern equatorial Atlantic, this zonal gradient is generally too weak, or even often reversed (Davey et al., 2002). In addition, coupled GCMs tend to have an ITCZ too south in the annual mean, a westerly bias in the equatorial surface winds, resulting in a struggle to represent the equatorial cold tongue in boreal summer (Richter and Xie, 2008). Richter and Tokinaga (2020) showed that relative to the Coupled model Intercomparison Project Phase 5 (CMIP5), the new generation of GCMs, CMIP6, shows on average only little improvements. Yet, a few models show now small biases. Using CMIP5 and CMIP6 models, Imbol Nkwinkwa et al. (2021) showed that high atmospheric resolution plays some role in substantially reducing the warm bias in the eastern equatorial Atlantic. Despite the strong biases in the equatorial Atlantic, many GCMs produce almost realistic Atlantic Niños, although the simulated SST variability is generally too weak and peaks one month later than observed (Richter et al., 2014). Deppenmeier et al. (2016) showed that the Bjerknes feedback is active in the CMIP5 models and that the first component, the impact of SST anomalies in eastern equatorial Atlantic on western equatorial Atlantic wind stress, is relatively well captured in the majority of the models. However, the third component, the thermocline depth variations impact on the SST which is the most important for the eastern tropical Atlantic according to Lübbecke and McPhaden (2013), is generally too weak in CMIP5 models. The southeastern tropical Atlantic also features strong biases, with warm SST biases, often exceeding 5°C, and strong surface wind biases (Richter, 2015). The interannual SST variability in the ABA is underestimated by the CMIP6 GCMs and occurs three months later than the observed peak of variability in April (Richter and Tokinaga, 2020). This poor representation of the Benguela Niños in GCMs leads to only few studies using them in this region. Harlaß et al. (2018) revealed that increasing the atmosphere model resolution, and particularly its vertical resolution, enables to simulate realistic interannual SST variability in the eastern equatorial Atlantic with the same ocean model resolution. However, in the southeastern tropical Atlantic, the relatively coarse atmospheric resolution in GCMs is likely responsible for unrealistic alongshore wind variability contributing to the bad representation of the SST variability (Small et al., 2015; Kurian et al., 2021).

1.4 Motivations, Objectives and outline

1.4.1 Motivations and objectives

Over the years, the tropical Atlantic variability has been intensively examined (Lübbecke et al., 2018; Cabos et al., 2019; Richter and Tokinaga, 2021). The underlying mechanisms and potential impacts of the Atlantic Niños/Niñas (Zebiak, 1993; Keenlyside and Latif, 2007; Deppenmeier et al., 2016; Jouanno et al., 2017; Lübbecke et al., 2018; Dippe et al., 2018) and Benguela Niños/Niñas (Shannon et al., 1986; Florenchie et al., 2003, 2004; Rouault et al., 2003, 2007, 2018; Bachèlery et al., 2016b,a, 2020; Imbol Koungue et al., 2017, 2019; Imbol Koungue and Brandt, 2021; Lübbecke et al., 2019) have been investigated in detail. Yet, the characteristics changes of the Atlantic Niños and Benguela Niños with the tropical Atlantic mean-state over the past decades as well as their projections under global warming has still not been investigated much. Tokinaga and Xie (2011), using a suite of bias-corrected observations, found a weakening of the equatorial Atlantic cold tongue intensity over the period 1950-2009. This reduction of SST variability in the eastern equatorial Atlantic was attributed to increased SSTs in the eastern equatorial Atlantic along with a weakening of easterly winds and to a deepening of the thermocline (Tokinaga and Xie, 2011). Servain et al. (2014) also found a substantial warming ($> 1°C$) over the time period from 1964-2012 in the eastern tropical ocean. Yet, in contrast with Tokinaga and Xie (2011), they observed strengthened trade winds. Hence, the main motivation of this study is to further investigate the relationship between the tropical Atlantic mean-state and the Atlantic Niños and Benguela Niños under past, present and future conditions. To do so, this thesis will address the following research questions:

- **How did the interannual SST variability in the eastern equatorial Atlantic change over the satellite era? What are the mechanisms driving this change? Is this change related to mean-state changes?**

- **How did the interannual SST variability in the southeastern tropical Atlantic change over the satellite era? What are the origins of this interannual SST variability change? Is this change in interannual SST variability related to mean-state changes?**

- **How is global warming influencing the Atlantic Niño? What are the future changes in interannual SST variability in the eastern equatorial Atlantic?**

- **How does the interannual SST variability change in the southeastern tropical Atlantic under a global warming scenario? What are the mean-state changes?**

1.4.2 Outline

To address those questions, interannual SST variability changes as well as tropical Atlantic mean-state changes in the tropical Atlantic Ocean are examined over the satellite era and in future projections. Time series of the ATL3-averaged (Figure 1.6a) and ABA-averaged (Figure 1.8a) SST anomalies reveal that fewer Atlantic and Benguela Niños/Niñas occurred during the period 2000-2017 relative to the period 1982-1999, respectively. Therefore, in Chapter 2, the change in interannual SST variability in the eastern equatorial Atlantic is examined. To do so, the different components of the Bjerknes feedback as well as the thermal damping are estimated for the two periods and discussed. In addition, their potential link to mean-state changes occurring during these periods are discussed. Chapter 3 focuses on the changes in interannual SST variability in the southeastern tropical Atlantic Ocean during the satellite era. Both the remote equatorial forcing and the local forcing, the main drivers of interannual SST variability in this region, are assessed. The potential relationship between the interannual SST variability changes in the ABA and the mean-state changes are also discussed. Chapter 4 focuses on the future interannual SST variability changes in the eastern equatorial Atlantic. CMIP5 and CMIP6 models are used in order to investigates these changes. In Chapter 5, using a global coupled model with regionally enhanced ocean model resolution in the tropical Atlantic, the future changes in interannual SST variability off the Angolan and Namibian coasts are investigated. Chapter 6 summarizes the answers to the research question raised in the previous section along with a discussion and the perspectives of this work.

Chapter 2

Weakened SST variability in the tropical Atlantic Ocean

While ENSO showed some multidecadal changes in interannual SST variability around the year 2000 (Hu et al., 2013; McPhaden, 2012; Lübbecke and McPhaden, 2014), such multidecadal changes in interannual SST variability in the eastern equatorial Atlantic has not been investigated much yet. Only Tokinaga and Xie (2011) indicated that, over the period 1950-2009, the equatorial Atlantic cold tongue weakened. Here in Chapter 2, we examined observational data and reanalysis products in order to assess the interannual SST variability change that occurred in the tropical Atlantic around the year 2000.

Citation: **Prigent, A.**, Lübbecke, J. F., Bayr, T., Latif, M., & Wengel, C. (2020a). Weakened SST variability in the tropical Atlantic Ocean since 2000. Climate Dynamics, 54, 2731–2744. https://doi.org/10.1007/s00382-020-05138-0

The candidate carried out all the analyses, produced all the figures and authored the manuscript from the first draft to the final published version.

Abstract

A prominent weakening in equatorial Atlantic sea surface temperature (SST) variability, occurring around the year 2000, is investigated by means of observations, reanalysis products and the linear recharge oscillator (ReOsc) model. Compared to the time period 1982-1999, during 2000-2017 the May-June-July SST variability in the eastern equatorial Atlantic has decreased by more than 30%. Coupled air-sea feedbacks, namely the positive Bjerknes feedback and the negative net heat flux damping are important drivers for the equatorial Atlantic interannual SST variability. We find that the Bjerknes feedback weakened after 2000 while the net heat flux damping increased. The weakening of the Bjerknes feedback does not appear to be fully explainable by changes in the mean state of the tropical Atlantic. The increased net heat flux damping is related to an enhanced response of the latent heat flux to the SST anomalies (SSTa). Strengthened trade winds as well as warmer SSTs are suggested to increase the air-sea specific humidity difference and hence, enhancing the latent heat flux response to SSTa. A combined effect of those two processes is proposed to be responsible for the weakened SST variability in the eastern equatorial Atlantic. The ReOsc model supports the link between reduced SST variability, weaker Bjerknes feedback and stronger net heat flux damping.

2.1 Introduction

The equatorial Atlantic Ocean is characterized by interannual variations of sea surface temperature (SST), which can have significant impacts on the climate over the adjacent landmasses (Hirst and Hastenrath, 1983; Folland et al., 1986; Nobre and Shukla, 1996). The dominant mode of tropical Atlantic interannual SST variability, which has its center of action in the equatorial cold tongue region, is referred to as the Atlantic Niño or Atlantic zonal mode because of its east-west orientation (see Lübbecke et al. (2018) for a review). The underlying dynamics of the Atlantic Niño are to some extent similar to those observed during El Niño/Southern Oscillation (ENSO) in the Pacific Ocean (Servain et al., 1982; Zebiak, 1993; Keenlyside and Latif, 2007). They involve a coupling of SST anomalies (SSTa), zonal wind stress and ocean heat content anomalies as described by the Bjerknes feedback (Bjerknes, 1969). The Atlantic Niño exhibits

a clear seasonal phase locking with largest SSTa occurring in boreal summer (Richter et al., 2017) and a secondary maximum peaking in November-December referred to as Atlantic Niño II by Okumura and Xie (2006). While the Atlantic Niño shares many characteristics with ENSO, it is more damped (Zebiak, 1993; Lübbecke and McPhaden, 2013), and the events are of shorter duration than for the Pacific counterpart. Compared to ENSO, each of the three Bjerknes feedback components, i.e (1) the zonal wind response to eastern equatorial SSTa, (2) the thermocline slope response to western equatorial wind anomalies and (3) the local response of SSTa to thermocline depth anomalies, explains less variance in the tropical Atlantic (Keenlyside and Latif, 2007), allowing other processes to play an important role as well. Nnamchi et al. (2015) showed that thermodynamic forcing by stochastic atmospheric perturbations can explain a significant amount of the observed SST variability in the equatorial Atlantic. Yet, recent studies assessing the relative importance of dynamic versus thermodynamic processes conclude that the dynamic and in particular the Bjerknes feedback is a main driver for the Atlantic zonal mode (Jouanno et al., 2017; Dippe et al., 2019).

Some studies have addressed multidecadal change of SST variability both in the equatorial Pacific (Hu et al., 2013; Lübbecke et al., 2014; Guan and McPhaden, 2016; Xu et al., 2019; Hu et al., 2017) and in the equatorial Atlantic (Tokinaga and Xie, 2011). While Tokinaga and Xie (2011) investigated trends in Atlantic cold tongue variability over the time period 1950-2009, several studies have discussed a shift in equatorial Pacific variability that occurred around the year 2000 and is clearly visible in many ENSO characteristics. This shift has been explained by changes in the equatorial thermocline tilt along with a strengthening of the trade winds, which has hampered the eastward migration of warm water along the equatorial Pacific and hence reduced ENSO amplitude (Hu et al., 2013). A more recent study from Xu et al. (2019), also investigating the weakening of ENSO amplitude since the late 1990s, put it in the context of the transition from the Aleutian Low mode to the North Pacific Oscillation in the atmosphere that is responsible for a westward extension of negative sea level pressure anomalies. This shift is proposed to have weakened the atmospheric responses to the zonal equatorial SSTa, and hence ENSO amplitude.
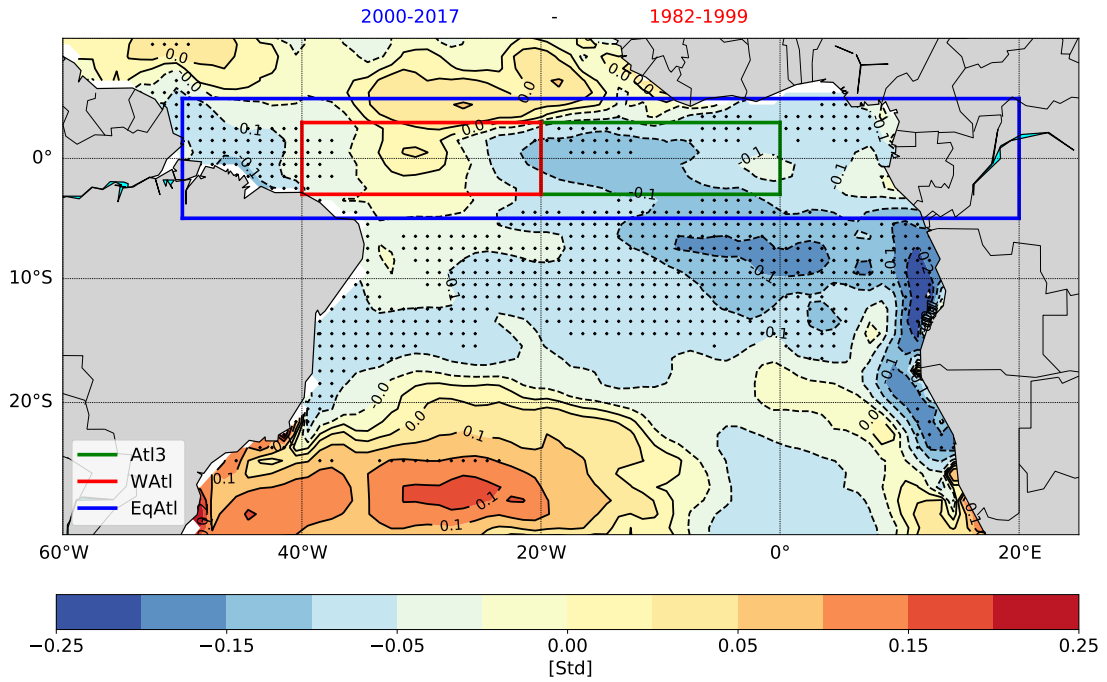
Figure 2.1: Difference of ORA-S4 standard deviation of SST (°C) anomalies between 2000-2017 and 1982-1999. Three regions used in the following are indicated by boxes: the Atlantic 3 region (Atl3; 3°S–3°N, 20°W–0°) in green, the western Atlantic region (WAtl, 3°S–3°N, 40°W–20°) in red and the Equatorial Atlantic region (EqAtl, 5°S–5°N, 50°W–20°E) in blue. Dots represent where standard deviation of the SSTa of the two periods are significantly different at the 95%-level according to the Welch's t-test.

In the present study, we want to investigate a shift in SST variability in the eastern equatorial Atlantic that has occurred around the year 2000. The paper is structured as follows: The data and methods used are described in section 2.2. In section 2.3, the shift in interannual SST variability and mean state changes are investigated. Summary and discussion are presented in section 2.4.

28

2.2 Data and methods

2.2.1 Data

Ocean variables wind and precipitation datasets

Nine reanalysis and observational datasets with monthly resolution are used for SST over the time period 1982-2017. The analyzed datasets are: the Hadley Centre Sea Ice and Sea Surface Temperature dataset version 1.1 (HadI-SST 1.1, Rayner (2003)), which is an EOF-based reconstruction, available at 1° by 1° horizontal resolution and spanning the period 1870/01-2018/12; The Ocean Reanalysis System version 4 (ORA-S4, Balmaseda et al. (2013)) from the European Centre for Medium-range Weather Forecast (ECMWF) available at 1° by 1° horizontal resolution for the time period 1958/01 to 2017/12; the Optimum Interpolation SST Analysis Version 2 (OI-SST, Reynolds et al. (2007)) available at 1° by 1° horizontal resolution for the time period 1981/12 to 2019/05; the Climate Forecast System Reanalysis Version 1 and 2 (CFSR, Saha et al. (2014) available at 2.5° by 2.5° horizontal resolution for the time period 1979/01 to 2019/08; The ECMWF Re-Analysis 5 (ERA5) product (Hersbach, Hans and Dee, 2016) available at 0.5° by 0.5° horizontal resolution for the time period 1979/01 to 2019/06; The ECMWF Re-Analysis (ERA)-interim product (Dee et al., 2011) available at 0.5° by 0.5° horizontal resolution for the time period 1979/01-2018/12; the Woods Hole Oceanographic Institution Objectively Analyzed air sea Fluxes (OAflux; Yu, Lisan and Jin, Xiangze and Weller (2008)) and National Centers for Environmental Prediction/National center for Atmospheric Research (NCEP/NCAR) Reanalysis 1 (NCEP-R1, Kalnay et al. (1996)) and NCEP/DOE Reanalysis 2 (NCEP-R2, Kanamitsu et al. (2002)) available at 2.5° by 2.5° horizontal resolution spanning the time periods from 1979/01 to 2018/12 for OAflux and NCEP-R2 and from 1948/01 to 2019/05 for NCEP-R1.

Ocean subsurface temperature data to calculate the depth of the 23°C isotherm as a proxy for thermocline depth (Lübbecke and McPhaden, 2013) is taken from the ORA-S4 reanalysis dataset. Wind speed and wind stress data spanning the time period 1982-2017 are taken from ERA-interim, ERA5, CFSR, NCEP-R1, and NCEP-R2. Monthly precipitation data is taken from the Global Precipitation Climatology Project version 2.3 (GPCP, Adler et al. (2018)), which is a blend of satellite and station data, available

at 2.5° by 2.5° horizontal resolution for the time period 1979/01-2019/04.

Reanalysis datasets are known to have large biases in the tropical regions (Kumar and Hu, 2012) and particularly in the tropical Atlantic Ocean (Huang et al., 2007). These biases may have an impact on the ocean-atmosphere feedbacks and overshadow the changes between the two periods. However, the use of several datasets allows us to assess the robustness of our results.

Heat flux products

Six monthly heat flux products are used for the time period 1982-2017: OAflux, ERA-interim, NCEP-R1 and NCEP-R2, ERA5, and CFSR. Heat fluxes are estimated and based on the use of bulk formulas and thus require the knowledge of several variables such as the wind speed, specific air and surface humidity, air and surface temperatures. Significant differences can exist between the different heat flux products (Bentamy et al., 2017). We therefore use six different products to assess the robustness of our results. The net heat flux (Qnet) can be decomposed into the sum of four components:

$$Q_{net} = Q_{sw} + Q_{lw} + Q_{sh} + Q_{lh} \tag{2.1}$$

where Q_{sw} is the shortwave radiation flux, Q_{lw} is the long-wave radiation flux, and Q_{sh} and Q_{lh} are the turbulent sensible and the latent heat flux, respectively. The latent heat flux can be estimated with the bulk formula (Bentamy et al., 2003):

$$Q_{lh} = L \times \rho_{air} \times C_E \times (Q_s - Q_a) \times U_s \tag{2.2}$$

$$L = 4186.8 \times (597.31 - 0.5625 T_s) \tag{2.3}$$

L is the latent heat of vaporization with a typical value of 2.5×10^6 J/kg, Q_a is the near-surface air specific humidity, U_s is the 10 m wind speed and ρ_{air} is the air density.

$$C_E = 10^{-3} a exp[b(U_{10} + c)] + \frac{d}{U_{10}} + 1 \tag{2.4}$$

The Dalton number, C_E is a function of the wind speed and ranges between 0.0015 and 0.0011 for wind speeds between 2 and 20 m.s^{-1}. With a $=-0.146785$, b$= -0.292400$,

c= -2.206 and d= 1.6112292. Q_s, the saturated surface humidity, has been estimated using the formula:

$$Q_s = \frac{5}{8} \frac{es}{ps - es} \tag{2.5}$$

where es = $T_s^A \times 10^{B+C/T_S}$ with $a = -4.928$, $b = 23.55$, and c= -2937.

2.2.2 Methods

In order to investigate the reasons behind the weakened SST variability in the eastern equatorial Atlantic since the year 2000, the strength of the Bjerknes feedback and the net heat flux damping, are estimated for the time period 1982/01 to 1999/12 and 2000/01 to 2017/12. First, the Bjerknes feedback is estimated via linear regression analysis of (1) western equatorial Atlantic (WAtl) zonal wind stress anomalies (3°S–3°N and 40°W–20° , Figure 2.1) upon Atl3-averaged SSTa (3°S–3°N and 20°W–0° , Figure 2.1), (2) Equatorial thermocline slope anomalies upon WAtl zonal wind stress anomalies and (3) SSTa upon thermocline depth anomalies pointwise in the Atl3 region. The equatorial thermocline slope is computed as the difference between the mean Atl3 23°C isotherm depth (Z_{23}) and WAtl Z_{23}. Second, the net heat flux damping is estimated via the linear regression of net heat flux anomalies upon SSTa in the Atl3 region. Prior to the regressions the linear trend has been removed from all datasets. All analyses are based on monthly-mean anomalies computed by subtracting the climatological monthly mean seasonal cycle calculated separately for each dataset and time period. Equally long periods relative to 2000 are chosen, but taking a longer pre-2000 period does no fundamentally change the results (See Table 2.1).

To support the interpretation of the results the linear recharge oscillator model from Burgers et al. (2005) (hereafter referred to as ReOsc model) is used, which describes the oscillatory behavior of the equatorial Atlantic variability by the interaction of eastern equatorial Atlantic SST and equatorial mean upper ocean heat content:

$$\frac{dT}{dt} = a_{11}T + a_{12}h + \varepsilon_T \tag{2.6}$$

$$\frac{dh}{dt} = a_{21}T + a_{22}h + \varepsilon_h \tag{2.7}$$

where T is the Atl3 SSTa and h is the mean thermocline depth anomalies averaged

over the Equatorial Atlantic region (5°S–5°N, 50°W–20°E, EqAtl, Figure 2.1). The parameters a_{11} and a_{22} represent the damping (or growth rate) of T and h, respectively. a_{12} and a_{21} are the coupling of T to h and h to T, respectively. The tendency equation of T and h are forced by the stochastic noise of T and h, ε_T and ε_h, evaluated as the standard deviation of the residual of the linear regression fit, which can be interpreted as a random noise forcing. It is noted that in this framework, the stochastic forcing terms may contain also nonlinear contributions which still are dependent on the prognostic variables T and h. As this study is focusing on the oceanic and atmospheric processes contributing to the weakened SST variability, the coefficient a_{11} is further decomposed into its oceanic and atmospheric part (Frauen and Dommenget, 2010):

$$a_{11} = a_{11O} + a_{11A} \tag{2.8}$$

$$a_{11A} = \underbrace{a_{12}\lambda C_{\tau T}}_{a_{11wind}} + \underbrace{\frac{C_{fT}}{\gamma}}_{a_{11HF}} \tag{2.9}$$

where $C_{\tau T}$ is the wind stress (Bjerknes) feedback estimated by the linear regression of zonal wind stress in the WAtl box (Figure 2.1) onto T. C_{fT} is the heat flux feedback evaluated as the linear regression of the net atmospheric flux upon T in the Atl3 region. λ and γ are the positive coupling parameter and the ocean mixed layer depth, which are assumed to be constant and amount to 2100 $m^3.N^{-1}$ and 79 $K.m^2.W^{-1}.month^{-1}$, respectively. a_{11O} is the residual of a_{11} when a_{11A} is estimated as in Eq. 2.9, it is expected to be driven by oceanic feedbacks such as the dynamical damping from mean ocean currents and the zonal advective feedback, Ekman feedback and the thermocline feedback as infered from oceanic contributions in the Bjerknes Stability Index analysis (Jin et al., 2006).

Finally, following the approach of Bayr et al. (2014) we compute the zonal stream-function:

$$\psi = 2\pi a \int_0^p u_D \frac{dp}{g} \tag{2.10}$$

where u_D is the divergent component of the zonal wind, a the radius of the earth, p the pressure and g the gravity constant. The zonal wind is averaged between 3°N and 3°S and integrated from the top of the atmosphere to surface.

2.3 Results

2.3.1 Observed changes in interannual variability

Interannual SST variability in the eastern equatorial Atlantic featured a strong change in magnitude around the year 2000 (Figures 2.1, 2.2a). The averaged May-June-July (MJJ) SST standard deviation in the Atl3 region ($3°S - 3°N$, $20°W - 0°$, Figure 2.1) during 1982-1999 was 0.68 ± 0.09 K as derived from the ensemble mean of the nine SST products (Table 2.1), whereas the variability decreased by 31% to 0.47 ± 0.05 K during 2000-2017. In contrast, the averaged November-December-January (NDJ) SST standard deviation in the Atl3 region shows only small changes from 0.45 ± 0.03 K during 1982-1999 to 0.41 ± 0.03 K during 2000-2017. The seasonal evolution of the SST standard deviation along the equator during 1982-1999 depicts a distinct yearly maximum in boreal summer (Figure 2.2b), which is consistent with the seasonally shoaling thermocline depth and maximum surface–subsurface coupling (Keenlyside and Latif, 2007; Harlaß et al., 2015). In November-December (ND), there is a secondary maximum of SST variability, consistent with the findings of Okumura and Xie (2006). The strengthening easterly winds in ND raise the thermocline in the Gulf of Guinea, which reactivates the Bjerknes feedback during this short period. After 2000, the same seasonal pattern of SST variability is observed but with overall reduced variability (Figure 2.2c). Figure 2.2d depicts a maximum of zonal wind variability in April-May-June (AMJ) in the western equatorial Atlantic basin, as measured by the standard deviation of the zonal wind speed anomalies. During 1982-1999, the AMJ WAtl zonal wind speed variability, derived as the ensemble mean of the wind products, amounts to 0.89 ± 0.11 m.s^{-1}, whereas in 2000-2017 the variability decreased to a value of 0.76 ± 0.09 m.s^{-1}. The reduction of the AMJ WAtl wind variability is consistent among the datasets, only NCEP-R1 and NCEP-R2 show a smaller reduction.
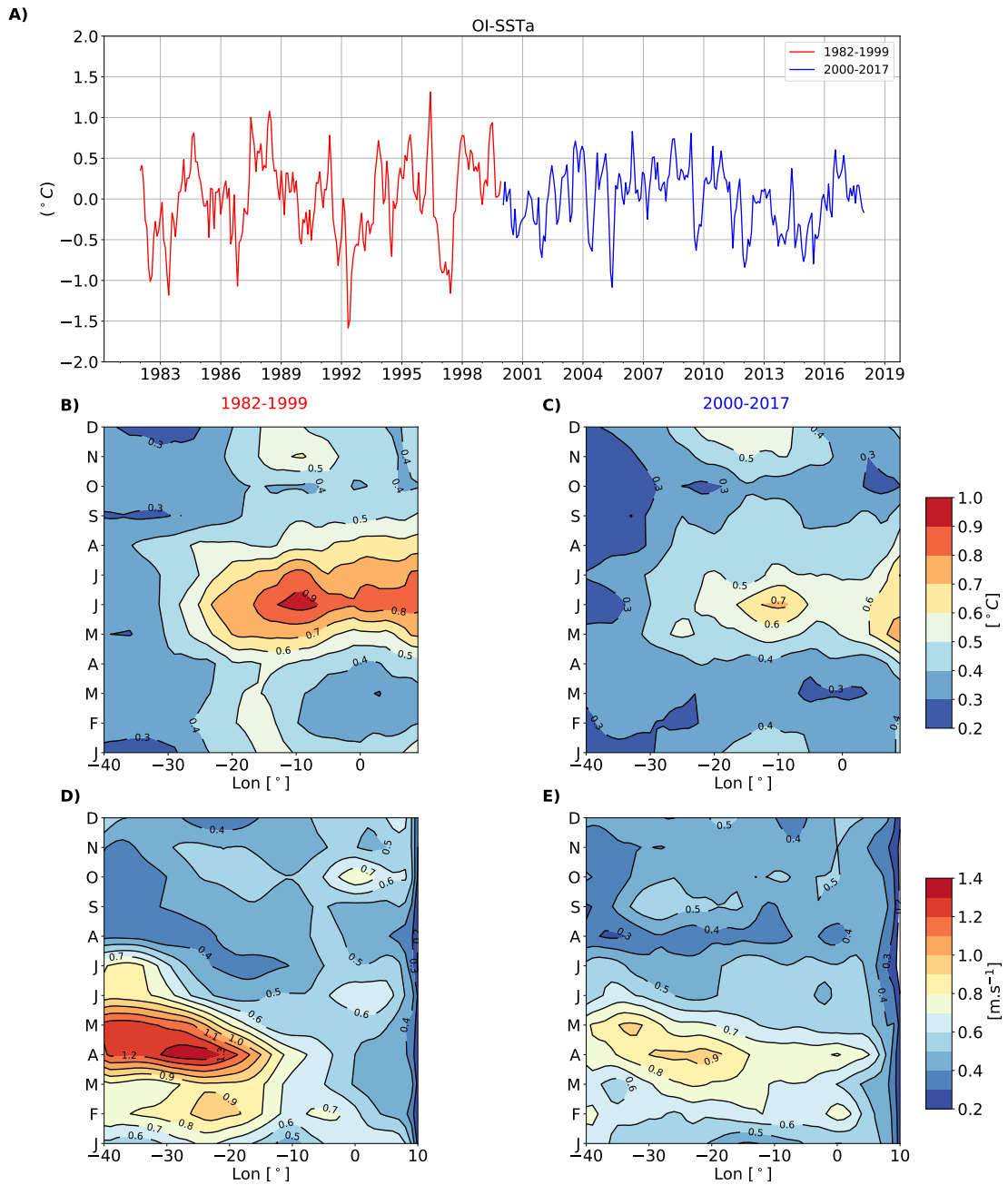
Figure 2.2: (a) Time series of OI-SST anomalies averaged over the Atl3 region (3°S–3°N, 20°W–0°) during 1982-1999 (red) and 2000-2017 (blue). (b, c) Standard deviation of OI-SSTa along the equator and averaged between 3°S and 3°N for the period 1982-1999 and 2000-2017, respectively. (d, e) Standard deviation of ERA-interim zonal wind speed anomalies along the equator averaged between 3°S and 3°N for the period 1982-1999 and 2000-2017, respectively.

Table 2.1: Standard deviation of MJJ (NDJ) SST anomalies averaged over the Atl3 region during 1982-1999 and 2000-2017. The reduction is relative to the first period. EM is the ensemble mean of the SST products.

Product	1960-1999	1982-1999	2000-2017	Reduction (%)
OI-SST	-	0.76 (0.49)	0.54 (0.47)	29 (4.1)
ORA-S4	0.67 (0.50)	0.73 (0.47)	0.52 (0.42)	29 (10.6)
HadI-SST	0.66 (0.50)	0.50 (0.46)	0.34 (0.35)	31 (22.2)
CFSR	-	0.59 (0.43)	0.45 (0.41)	24 (4.6)
ERA5	-	0.72 (0.51)	0.47 (0.42)	35 (17.6)
ERA-interim	-	0.67 (0.44)	0.48 (0.39)	28 (11.3)
OAflux	-	0.65 (0.42)	0.45 (0.38)	32 (9.5)
NCEP-R1	0.67 (0.55)	0.77 (0.42)	0.48 (0.42)	38 (6.6)
NCEP-R2	-	0.76 (0.45)	0.48 (0.42)	37 (6.6)
EM	0.67 ± 0.005 (0.52 ± 0.02)	0.68 ± 0.09 (0.45 ± 0.03)	0.47 ± 0.05 (0.41 ± 0.03)	31 (9)

Table 2.2: Standard deviation of AMJ zonal wind speed anomalies at 10 meters averaged over the WAtl region during 1982-1999 and 2000-2017. The reduction is relative to the first period. EM is the ensemble mean of the wind products.

Wind product	1982-1999	2000-2017	Reduction (%)
ERA-interim	1.04	0.74	28.8
ERA5	0.98	0.78	20.4
CFSR	0.71	0.61	14.1
NCEP-R1	0.84	0.82	2.0
NCEP-R2	0.87	0.87	0.0
EM	0.89 ± 0.11	0.76 ± 0.09	15

2.3.2 Weakened Bjerknes feedback

The Atlantic Niño mode is in part determined by ENSO-like dynamics (Servain et al., 1982; Keenlyside and Latif, 2007; Deppenmeier et al., 2016; Lübbecke and

McPhaden, 2017), in particular by the Bjerknes feedback which can be decomposed into its three components: (1) the zonal wind response to eastern equatorial SSTa, (2) the thermocline slope response to western equatorial wind anomalies and (3) the local response of SSTa to thermocline depth anomalies. In order to understand the pronounced weakening in the SST variability in MJJ after the year 2000 we first calculate the individual components of the Bjerknes feedback separately for the two time periods 1982-1999 and 2000-2017. As the Bjerknes feedback is strongly seasonal, the three components of the Bjerknes feedback are first estimated as a function of the calendar month (Figure 2.3) and then averaged for the relevant seasons (Figure 2.4) via linear regression for the two time periods. The first component is peaking in AMJ (Figure 2.3a) while the second and third components are peaking in MJJ. From Figures 2.2 and 2.3 we decide to focus on MJJ and NDJ when the Bjerknes feedback and interannual SST variability are the highest.
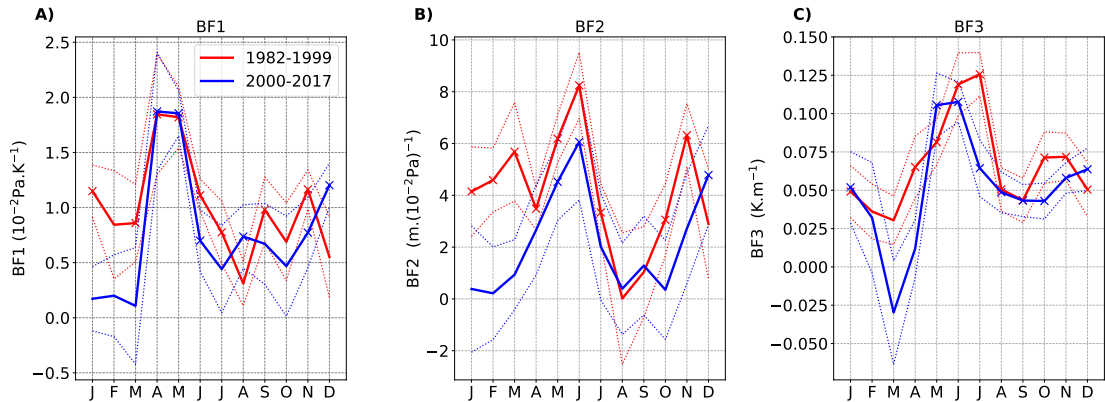
Figure 2.3: Bjerknes feedback components as a function of the calendar months for the period 1982-1999 (red) and 2000-2017 (blue). (a) Zonal wind response to eastern equatorial SST changes. (b) Thermocline slope response to western equatorial surface wind anomalies. (c) Local response of SSTa to thermocline depth anomalies. Crosses indicate that the regressions are significant at the 95%-level according to the Student's t-test. Dotted lines depict the error bars of the regressions.

First, the western zonal wind stress response to eastern equatorial Atlantic SSTa is investigated (Figures 2.4a and 2.4d). Relative to the time period 1982-1999, after 2000 the zonal wind stress response to Atl3 SSTa has weakened by 21% in MJJ and by 24.5% in NDJ. The second component (Figures 2.4b and 2.4e), i.e. the thermocline slope response to western equatorial zonal wind stress anomalies which is driven by

the eastward propagation of equatorial Kelvin waves, has also weakened. Compared to 1982-1999, after 2000 the second component has reduced by 30.2% in MJJ and by 32.7% in NDJ (Figures 2.4b and 2.4e). The third component, i.e. the local response of SSTa to changes in thermocline depth has not experienced any significant change. We note the smaller amount of variance accounted for by the three components since 2000, suggesting that the Bjerknes feedback has become a less important driver of SST variability in the equatorial Atlantic. The same linear regression analysis has also been performed using different products and months. We find that while the regressions are sensitive to the chosen period, the overall general result, i.e. a weakening of the Bjerknes feedback strength, remains the same.

2.3.3   Net heat flux damping

Thermodynamical processes are also known to play an important role in the equatorial Atlantic variability. While their damping effect has been long recognized (e.g. Frankignoul et al. (2002)), they have also been suggested to contribute to the onset of Atlantic Niño events (Nnamchi et al., 2015). The ocean and the atmosphere are coupled through heat fluxes. The turbulent heat exchange, i.e the latent and sensible heat fluxes, allow the ocean to release the heat absorbed from solar radiation. This heat release is responsible for damping the SSTa and hence reducing its variability. The net heat flux damping is the dominant negative feedback in the equatorial Atlantic (Lübbecke and McPhaden, 2013). It is estimated via linear regression of net heat flux anomalies upon SSTa. We use six different heat flux products to get a sense of the uncertainty. Relative to 1982-1999, in 2000-2017 we observe a stronger MJJ net heat flux damping (Table 2.3) with an increase from -16.52 $\pm$ 4.59 W.m^{-2}.K^{-1} to -23.96 $\pm$ 5.92 W.m^{-2}.K^{-1} and from –8.93 $\pm$ 7.44 W.m^{-2}.K^{-1} to -14.57 $\pm$ 8.07 W.m^{-2}.K^{-1} in NDJ as derived from the ensemble mean of the heat flux products.

We decompose the net heat flux into its different components and look separately at the response of each component to the SSTa. The latent heat flux response to SSTa is found to be the most important component with an increase from -13.70 $\pm$ 2.85 W.m^{-2}.K^{-1} to -20.85 $\pm$ 4.67 W.m^{-2}.K^{-1} in MJJ and from -8.14 $\pm$ 1.91 W.m^{-2}.K^{-1} to -11.30 $\pm$ 1.96 W.m^{-2}.K^{-1} in NDJ. The sensible heat flux damping has also increased but is smaller in total numbers (not shown). The stronger net heat flux damping due to
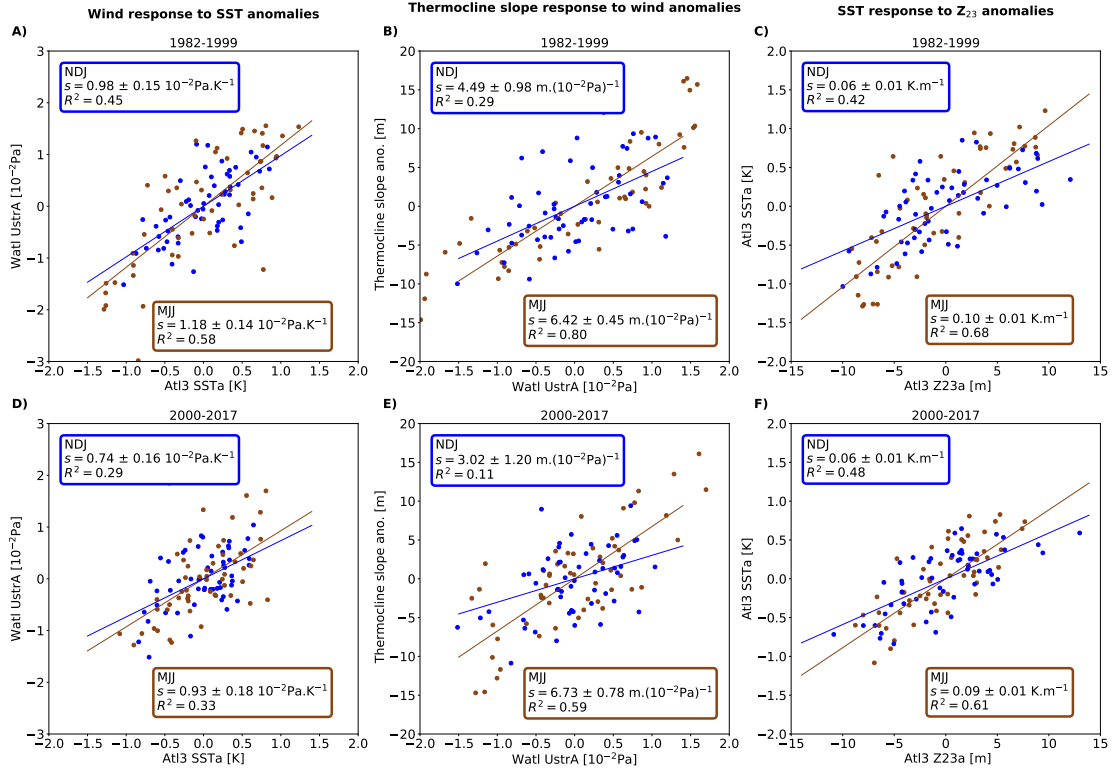
Figure 2.4: Bjerknes feedback components for the equatorial Atlantic for 1982-1999 (upper row) and for 2000-2017 (lower row). (a, d) Linear regression of MJJ Atl3 SST upon MJJ western equatorial Atlantic zonal wind stress anomalies (WAtl, brown) and of November-December-January (NDJ) Atl3 SST upon NDJ Watl wind stress anomalies (dark blue). Linear regression of MJJ (NDJ) WAtl wind anomalies upon MJJ (NDJ) equatorial thermocline slope anomalies (brown and dark blue: b and e, respectively). Linear regression of MJJ (NDJ) Atl3 Z23 anomalies upon MJJ (NDJ) SST anomalies (brown and dark blue: c and f, respectively). Regressions are significant at 95% according to the Student's t-test. S is the slope of the regression line and R^2 is the correlation coefficient squared.

Table 2.3: MJJ Atl3 net heat flux damping (latent heat flux damping) during the periods 1982-1999 and 2000-2017. EM is the ensemble mean of the heat flux products.

Product	1982-1999		2000-2017	
	MJJ	NDJ	MJJ	NDJ
CFSR	-13.43 (-16.17)	1.45 (-8.21)	-16.02 (-17.75)	-2.01 (-8.18)
ERA5	-18.24 (-15.98)	-14.1 (-11.03)	-24.15 (-21.42)	-13.76 (-8.95)
ERA-interim	-16.95 (-12.61)	-16.21 (-6.38)	-23.15 (-17.35)	-22.44 (-12.24)
OAflux	-10.43 (-11.84)	-9.34 (-8.78)	-19.08 (-17.88)	-23.30 (-12.66)
NCEP-R1	-14.96 (-8.86)	-16.1 (-9.27)	-26.68 (-19.89)	-19.61 (-13.1)
NCEP-R2	-25.12 (-16.76)	0.7 (-5.18)	-34.69 (-30.79)	-6.29 (-12.67)
EM	**-16.52 $\pm$ 4.59** **(-13.70 $\pm$ 2.85)**	**-8.93 $\pm$ 7.44** **(-8.14 $\pm$ 1.91)**	**-23.96 $\pm$ 5.92** **(-20.85 $\pm$ 4.67)**	**-14.57 $\pm$ 8.07** **(-11.30 $\pm$ 1.96)**

the latent heat flux is consistent among the datasets (Table 2.3).

Table 2.4: MJJ near-surface specific humidity difference response to Atl3 SST changes for the periods 1982-1999 and 2000-2017. EM is the ensemble mean of the heat flux products.

Product	1982-1999	2000-2017
CFSR	0.50	0.56
ERA5	0.82	0.93
ERA-INT	-	-
OAflux	0.59	0.71
NCEP-R1	0.70	0.76
NCEP-R2	0.59	0.82
EM	**0.64 $\pm$ 0.11**	**0.76 $\pm$ 0.12**

Lloyd et al. (2011) argued that the latent heat flux damping in the equatorial Pacific is mainly driven by near-surface specific humidity difference whereas the winds play only a secondary role. Calculating both the response of the Atl3 zonal wind and the Atl3 near-surface specific humidity difference to Atl3 SSTa, we find that only the latter showed a significant change when comparing the two time periods (Table 2.4),

consistent with the findings by Lloyd et al. (2011) for the Pacific.

Relative to 1982-1999, in 2000-2017 the MJJ Atl3 near-surface specific humidity difference response to SSTa increased (Table 2.4) from 0.64 ± 0.11 g.kg^{-1}.K^{-1} to 0.76 ± 0.12 g.kg^{-1}.K^{-1}. This suggest that the increase in latent heat flux damping is mainly driven by the increased response of the near-surface specific humidity.

2.3.4 Mean state changes

Contemporaneously with the reduced SST variability, the tropical Atlantic mean state has also undergone changes over the past decades. We here investigate the mean state changes to see whether the changes in the Bjerknes feedback and heat flux damping can be related to them.

We observe a sustained positive trend in the SST averaged over the tropical Atlantic basin (20°S–30°N, 60°W–15°E) since 1982 (Figure 2.5a). However, the MJJ SST difference (Figure 2.5b) between 1982-1999 and 2000-2017 mainly depicts a significant warming of about 0.3°C north of the equator but no significant change in the eastern equatorial Atlantic. Figure 2.5c shows the March-April-May (MAM) wind speed difference superimposed on the precipitation difference between the two periods as well as the 5 and 10 mm·day^{-1} precipitation contours as a proxy for the position of the Intertropical convergence zone (ITCZ). Relative to 1982-1999, in 2000-2017 more precipitation is observed over the western African coast and the north-eastern part of Brazil as well as north of the equator pointing to a northward shift of the ITCZ position. The shift of the ITCZ might explain the reduced WAtl wind variability (Zebiak, 1986; Richter et al., 2017). Regarding the winds, a minor intensification of the easterlies is noted over the eastern equatorial Atlantic, which is consistent with a slight shoaling of the thermocline along the equator (Figure 2.5d). The changes in precipitation and wind are not significant and therefore not further discussed. A cooling of 0.3°C of the MJJ ocean temperature from 30°W to 10°E below the thermocline is observed which acts to sharpen the vertical gradient of ocean temperature along the thermocline (Figure 2.5d). Compared to 1982-1999, since 2000 a stronger MJJ net heat flux is observed in the eastern equatorial Atlantic and lower in the western equatorial Atlantic. Although the eastern part of the basin receives more heat no significant warming is observed in MJJ. We hypothesize that the increased easterlies may have enhanced the upwelling along

the equator and balance the heat surplus. Changes in the Walker circulation are represented by the zonal streamfunction (see Section 2.2.2 and eq. (2.10)) in Figure 2.6. Compared to 1982-1999, since 2000 a strengthening and a minor westward shift of the rising branch of the Walker circulation is observed, so that it is situated slightly more over land (Figure 2.6). This can also explain the reduced zonal wind variability in the western equatorial Atlantic and weakened Bjerknes feedback by a similar mechanism that was found in the Pacific: A strengthened and more westward Walker circulation weakens the wind-SST feedback and Bjerknes feedback as this hooks the rising branch of the Walker Circulation over land and therefore hampers the ocean-atmosphere coupling (Bayr et al., 2018, 2019). For the equatorial Pacific, Li et al. (2019) observed a profound shift of the Walker circulation when comparing the periods 1979-1999 and 2000-2017. This westward shift resulted in a significant change of the equatorial Pacific climate variability.

The aforementioned changes in the mean state are hardly significant and can likely not fully explain the weakening of the Bjerknes feedback. Hu et al. (2013), carrying out experiments with the Zebiak-Cane model in the tropical Pacific, found a nonlinear response of ENSO amplitudes to thermocline slope. They found that a too large thermocline slope would hinder warm water zonal migration which is unfavourable for ENSO growth. In our case, however, the larger thermocline tilt as well as the increased zonal winds explain too little variance to account for the 31% reduction of the SST variability.

We conclude that the weakening of the Bjerknes feedback fits to the changes of the background mean state and the reduced zonal wind response to SST anomalies as well as the decreased response of the ocean thermocline slope to wind stress anomalies and thus likely contributed to the reduced SST variability after 2000. We also note here that the enhanced sensitivity of the near-surface humidity difference to SSTa and slightly stronger trade winds along with warmer SSTs may have played a role in enhancing the net heat flux damping through the turbulent heat fluxes.

2.3.5 Verification using the simplest recharge oscillator

The linear recharge oscillator (ReOsc) from Burgers et al. (2005) (see section 2.2) is a tool to diagnose ENSO-like dynamics and used here to corroborate the link between reduced SST variability, weakened Bjerknes feedback and stronger net heat flux
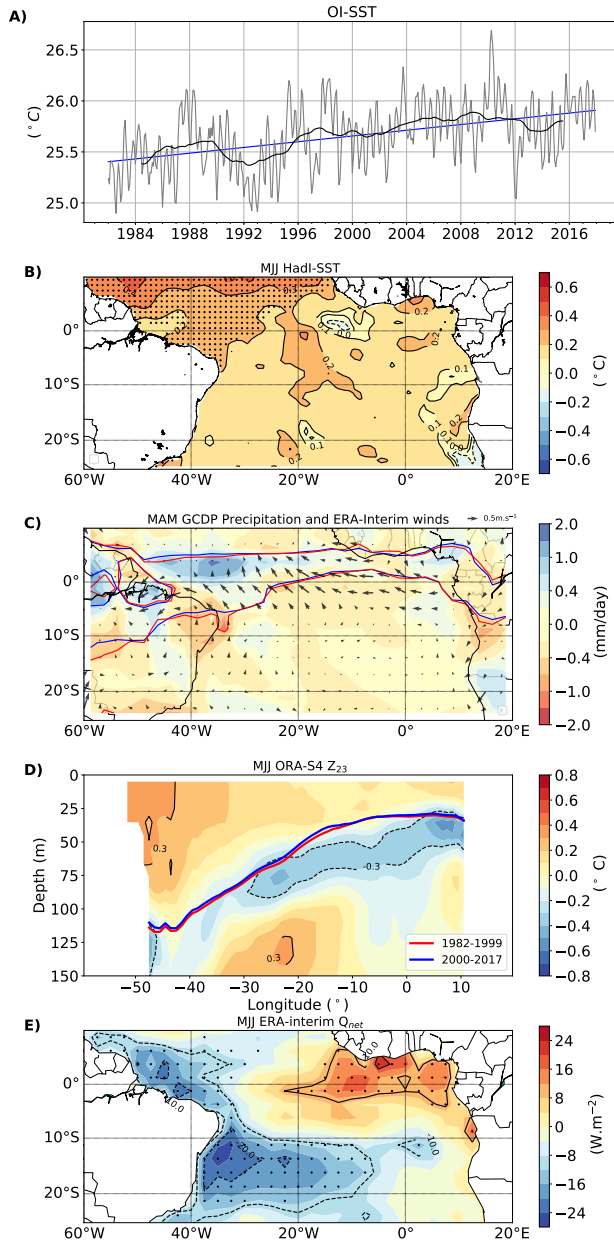
Figure 2.5: (a) Time series of OI-SST averaged over the tropical Atlantic basin (20°S–30°N, 60°W–15°E; gray) the 10 year running mean of SST (black) and the linear trend of SST (blue). Difference between 2000-2017 minus 1982-1999 of (b) MJJ HadI-SST, (c) MAM GPCP precipitation (shading) and ERA-Interim wind speed (shading) as well as the 5 and 10 mm.day^{-1} precipitation contours as a proxy for the ITCZ position in 1982-1999 (red) and 2000-2017 (blue), (d) MJJ ORA-S4 subsurface temperature superimposed by the 23°C isotherm depth as a proxy for thermocline depth during 1982-1999 (red) and 2000-2017 (blue). (e) MJJ ERA-interim net heat flux. Dots indicate that the means are significantly different at 95%-level according to the Welch's t-test.

42
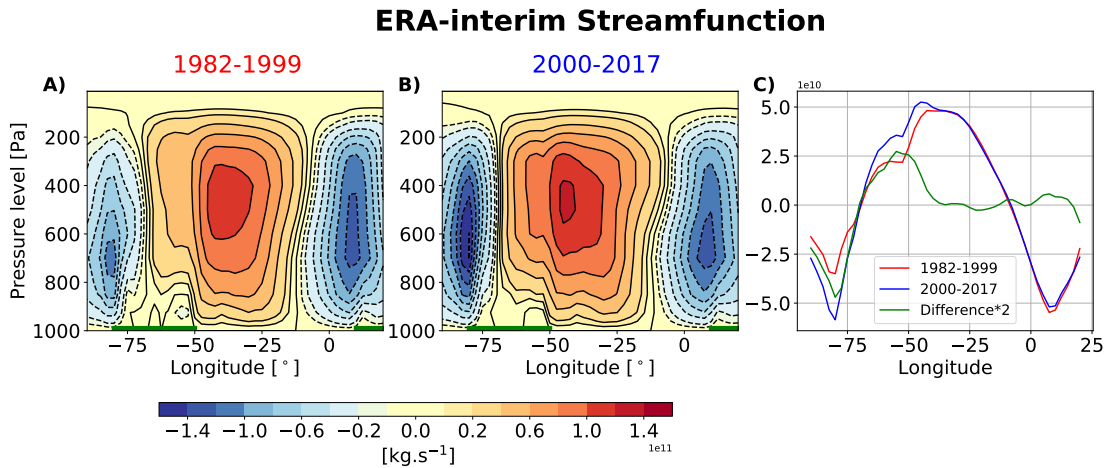
Figure 2.6: (a, b) Zonal ERA-interim streamfunctions representing the Walker circulation computed for the time periods 1982-1999 and 2000-2017, respectively. (c) Vertically integrated zonal streamfunction. Green bold lines at the bottom indicate South America and Africa.

damping during 2000-2017.

Multiple studies have shown that the simple ReOsc model is able to reproduce fundamental aspects of ENSO in the tropical Pacific (Wengel et al., 2018; Vijayeta and Dommenget, 2018) and also the Bjerknes feedback and delayed negative feedback in the tropical Atlantic (Jansen et al., 2009) with the advantage to allow for a decomposition of the ocean and atmosphere contributions to the SST variability. The ReOsc model, however, has limitations, as it does not consider, for example, nonlinearities. Although the equatorial Atlantic variability is overestimated, mainly because of the absence of nonlinearities, the ReOsc model produces a weakening of 50% of the MJJ SST variability from 0.93 during 1982-1999 to 0.46 during 2000-2017 which overestimates but fits to the 31% reduction found with the observations and reanalysis. We consider the tendency equation of Atl3 SSTa (T in eq. (2.6)) and its different components are computed for the two time periods and summarized in Table 2.5.

Consistent with the above results, the ReOsc model displays a stronger damping of T, which changes from -0.27 month^{-1} to -0.46 month^{-1} from 1982-1999 to 2000-2017. Further, the term a_{12}, representing the coupling of SSTa to the thermocline depth, has experienced a strong reduction, from 0.057 K.m^{-1}.month^{-1} to 0.011 K.m^{-1}.month^{-1}, noting that the coupling terms are of minor importance for the strength of SST variability as shown for the Pacific (Wengel et al., 2018). Regarding the stochastic noise

Table 2.5: ReOsc model components of the tendency equation for the MJJ Atl3 SSTa (T) during 1982-1999 and 2000-2017. ORA-S4 was used for T and h, ERA-interim for the wind stress and OAflux for the net heat flux.

Period	a_{11} (1/month)	a_{12} (K/m/month)	ε_T (K/month)
1982-1999	-0.271	0.0574	0.501
2000-2017	-0.456	0.0105	0.385

forcing of T, ε_T, a significant decrease is noted from 0.50 K.month^{-1} during 1982-1999 to 0.39 K.month^{-1} during 2000-2017. This reduction of the stochastic noise forcing is important as Wengel et al. (2018) showed for the Pacific that it can control ENSO amplitude.

In order to disentangle the dynamics behind the stronger damping of T, and using the methodology of Vijayeta and Dommenget (2018) and Dommenget and Vijayeta (2019) that has been applied to the Pacific, the growth rate a_{11} is further decomposed into its oceanic (a_{11O}) and atmospheric (a_{11A}) part (see eq. (2.8) for more details on the separation method).

Table 2.6 summarizes the results of the decomposition. During 1982-1999, the dominant growth rate factor amounting to 1.421 month^{-1} is a_{11wind} which is composed of the coupling of SSTa to local thermocline depth and of the zonal wind to SSTa (eq. (2.9)). The negative feedback, a_{11HF}, which represents the thermal damping, is rather weak -0.196 month^{-1}. The combined atmospheric feedback a_{11A} on T is positive and amounts to 1.224 month^{-1}. In contrast, during 2000-2017, a much weaker atmospheric growth rate is observed with a value of -0.246 month^{-1}.

This strong reduction is the result of two changes: first, a reduction in a_{11wind} component, 0.204 month^{-1} which is due to a combination of the weakened zonal wind response to SSTa ($C_{\tau T}$) and reduced SST-thermocline coupling (a_{12}). The weakened zonal wind sensitivity to SSTa might be related to the slight northward shift of the ITCZ (Figure 2.5c) while the reduced SST-thermocline coupling may be the result of the enhanced vertical gradient of ocean temperature (Figure 2.5d). Second, the stronger thermal damping which has changed from -9.612 W.m^{-2}.K^{-1}during 1982-1999 to -22.03 W.m^{-2}.K^{-1} during 2000-2017. The a_{11O} term becomes less negative from 1982-1999 to 2000-2017, which indicates weaker damping from oceanic processes such as mean

Table 2.6: ReOsc model components of the tendency equation for the Atl3 MJJ SSTa (T) during 1982-1999 and 2000-2017, in which the growth rate of T, a_{11}, has been decomposed into its atmospheric and oceanic part. ORA-S4 was used for T and h, ERA-interim for the wind stress and OAflux for the net heat flux. The units are month^{-1} for the a components, W.m^{-2}.K^{-1} for $C_{f\tau}$ and N.m^{-2}.K^{-1} for $C_{\tau T}$.

Period	a_{11O}	a_{11A}	a_{11HF}	a_{11wind}	$C_{f\tau}$	$C_{\tau T}$
1982-1999	-1.495	1.224	-0.196	1.421	-9.612	0.012
2000-2017	-0.210	-0.246	-0.450	0.204	-22.03	0.009

currents and would lead to an increase in SST variability. However, this effect is over-compensated by the changes of the atmospheric damping. We therefore conclude that atmospheric processes are dominant in driving the variability weakening during these time periods.

2.4   Summary and Discussion

Observational and reanalysis data as well as the linear recharge oscillator model, ReOsc, were used to investigate the multidecadal reduction in interannual MJJ SST variability in the equatorial Atlantic which has considerably weakened from 1982-1999 to 2000-2017. Understanding Equatorial Atlantic SST variability is of great important as it influences climate over the African and American continents and contribute to the variability in the Pacific and Indian Oceans (Lübbecke et al., 2018). The major feedbacks determining the MJJ SST anomalies (SSTa) in the equatorial Atlantic have been estimated to obtain insight into the dynamics underlying the reduction in equatorial Atlantic interannual SST variability. First, we analyzed the positive Bjerknes feedback. The western equatorial Atlantic zonal wind stress response to eastern equatorial Atlantic SSTa has reduced during the latter period, and this reduction might be at least partly linked to the slight northward shift of the ITCZ position observed when comparing the mean boreal spring situations of 1982-1999 and 2000-2017. A northward shift of the mean deep convection could lead to a reduced wind sensitivity to SSTa (Zebiak, 1986; Richter et al., 2017). Similarly, the thermocline response to western zonal wind stress anomalies has weakened during boreal summer. The surface-subsurface coupling did

not exhibit a significant change.

Overall, the Bjerknes feedback weakened but the weakening cannot be fully attributed to the mean state changes which are rather weak. We did not find significant changes in the mean thermocline depth and zonal wind as found by Hu et al. (2013) for the Pacific, where a stronger thermocline tilt consistent with stronger trade winds and enhanced Walker circulation was observed after the year 2000 explaining the weakened variability on the equatorial Pacific Ocean. A cooling of the subsurface ocean temperature is found between 30°W and 10°E which enhances the vertical gradient of temperature and may help to reduce the surface-subsurface coupling. The mean tropical Atlantic MJJ SST underwent a significant warming of 0.2-0.3 K north of the equator but not much on the equator.

Second, we analyzed the net heat flux damping, the dominant negative feedback on SSTa over the equatorial Atlantic (Lübbecke and McPhaden, 2013). The net heat flux damping has strongly increased during 2000-2017, which is mostly due to the stronger latent heat flux response to SSTa and found to be the result of a larger response of the air-surface specific humidity difference response to SSTa.

The linear recharge oscillator (ReOsc) allowed us to linearly decompose the ocean and atmosphere contributions to the SST variability. The results of the ReOsc show that the weakened SST variability in the eastern equatorial Atlantic is mainly due to a stronger atmosphere damping after 2000. Changes in oceanic damping are overcompensated by atmospheric processes. Besides, the MJJ stochastic forcing of the SSTa has also reduced since 2000, which might influence the amplitude of the Atlantic zonal mode as Wengel et al. (2018) showed that the stochastic forcing has an impact on ENSO amplitude. However, studying the link between the stochastic forcing and the SST variability in the equatorial Atlantic would need further research. The possibility to decompose the stochastic forcing into a state-dependent and state-independent part is noted (Levine et al., 2016), which is however beyond the scope of this paper.

Tokinaga and Xie (2011) studied the weakening of the equatorial Atlantic cold tongue during 1950-2009. Using the 20°C isotherm for the thermocline depth, they found a deepening trend of the thermocline along with a relaxation of the equatorial trade winds in the eastern Atlantic and a basin-wide warming with a local maximum in the cold tongue region. They concluded that these mean state changes together with

enhanced atmospheric convection were responsible for the reduced SST variability in the equatorial Atlantic. As shown by Castaño-Tierno et al. (2018), the use of the 20°C isotherm as a proxy for thermocline depth might impact the assessment of the air-sea coupling as the 20°C isotherm is too deep and therefore less sensitive to changes in surface temperatures and winds. Our study shows no significant change in the trade winds, during the analysis period, or at least no weakening, which is consistent with the findings of Servain et al. (2014). The different wind trends found in different studies, depending on the exact region, time period and wind product, highlights the multi-decadal variability as well as the uncertainty of wind datasets. It is known that reanalysis datasets have large biases in the tropical Atlantic (Huang et al., 2007) that may overshadow the mean state changes from one period to the other and increase the uncertainty on the ocean-atmosphere feedbacks (Kumar and Hu, 2012). However, the use of several datasets allows to show the robustness of our results.

Other possible sources for multidecadal changes in the equatorial Atlantic interannual variability can be of remote origin. The El Niño/Southern Oscillation (ENSO), the dominant mode of interannual variability in the Pacific Ocean, is suggested to influence Atlantic variability in various ways (Latif and Grötzner, 2000; Chang et al., 2006). Similarly to the equatorial Atlantic, the equatorial Pacific also has experienced a weakening in variability during the last two decades (Hu et al., 2013, 2017; Li et al., 2019), raising the question whether the two phenomena are connected. The connection between ENSO and the Atlantic Niño mode is, however, complicated (see Cai et al. (2019) for a review) and directed both from the Pacific to the Atlantic (Enfield and Mayer, 1997; Latif and Grötzner, 2000; Chang et al., 2006; Lübbecke and McPhaden, 2013) and from the Atlantic to the Pacific (Jansen et al., 2009; Rodríguez-Fonseca et al., 2009; Ding et al., 2012). Wang (2017) showed a weakened interannual variability in the contrast in rainfall between the eastern equatorial Pacific and equatorial Atlantic since 2000. This weakening was associated with the weakened interannual variability in the inter-Pacific-Atlantic zonal SST gradient and in the associated equatorial cross-South American wind linking the two ocean basins since 2000. This study shows the importance of the influences from the Pacific on the variability of the equatorial Atlantic via Pacific-Atlantic interactions. Hence, the relationship between the weakened variability in both the equatorial Atlantic and Pacific around the year 2000 will need to

be investigated further.

Finally, the Atlantic Multidecadal Oscillation (AMO) might have also played a role in the SST variability change in the equatorial Atlantic. Recently, Martín-Rey et al. (2018) showed that during a negative phase of the AMO, the equatorial Atlantic SST variability is enhanced by more than 150% in boreal summer. Wang and Zhang (2013) showed that the warm phase of AMO corresponds to a strengthening of the Atlantic meridional overturning circulation (AMOC) while Svendsen et al. (2014) showed that a weakening of the AMOC could enhance the equatorial Atlantic variability. Hence a positive phase of the AMO might tend to weaken the equatorial Atlantic variability. In the early 1990s, the AMO changed phase from negative to positive, which could have contributed to the relative weakening of the equatorial Atlantic SST variability.

2.5   Acknowledgements

Chapter 3

Origin of weakened interannual sea surface temperature variability in the Southeastern Tropical Atlantic Ocean

Chapter 2 revealed that relative to 1982-1999, during 2000-2017 the interannual SST variability in May-June-July in the eastern equatorial Atlantic has reduced by 31%. As introduced in Chapter 1 the eastern equatorial Atlantic and Angola-Benguela area are strongly connected. Hence it may well be that the interannual SST variability in the southeastern tropical Atlantic also has undergone a reduction since 2000. This is the topic of Chapter 3.

The candidate designed the original study, carried out all the analyses, produced all the figures and authored the manuscript from the first draft to the final published version.

Abstract

Observations and reanalysis products are used to investigate the substantial weakening in the southeastern tropical Atlantic sea surface temperature (SST) variability since 2000. Relative to 1982-1999, the March-April-May SST variability in the Angola-Benguela area (ABA) has decreased by more than 30%. Both equatorial remote forcing and local forcing are known to play an important role in driving SST variability in the ABA. Compared to 1982-1999, since 2000, equatorial remote forcing had less influence on ABA SSTs, whereas local forcing has become more important. In particular, the robust correlation that existed between the equatorial zonal wind stress and the ABA SSTs has substantially weakened, suggesting less influence of Kelvin waves on ABA SSTs. Moreover, the strong correlation linking the South Atlantic Anticyclone and the ABA SSTs has reduced. Finally, multidecadal surface warming of the ABA could also have played a role in the weakening of the interannual SST variability.

3.1   Introduction

The tropical Atlantic Ocean sea surface temperatures (SSTs) have warmed substantially over the last decades (Tokinaga and Xie, 2011; Servain et al., 2014; Vizy and Cook, 2016) and particularly in the southeastern tropical Atlantic. In association with the basin-wide warming, which is most pronounced in boreal summer reducing the annual cycle through a positive ocean–atmosphere feedback, a strong reduction of the equatorial Atlantic SST variability was reported by Tokinaga and Xie (2011) over the period 1950-2009. However, multidecadal variability is large. Nnamchi et al. (2020) found that SSTs during the satellite era 1979–2018 exhibit a warming hole over the equatorial Atlantic cold tongue region in boreal summer. This lack of surface warming denotes an 11% amplification of the mean SST annual cycle in that region. Recently, Prigent et al. (2020a), using observations and reanalysis products, found that the equatorial Atlantic interannual SST variability in May-June-July has reduced by 31% during 2000-2017 relative to 1982-1999. Interannual SST variability in the equatorial Atlantic and Angola-Benguela area (ABA) are strongly connected (Reason et al., 2006; Hu and Huang, 2007; Lübbecke et al., 2010). Hence, it may well be that the SST variability in the southeastern tropical Atlantic also has undergone a reduction since 2000, which is

the topic of this study.

SSTs along the coasts of Namibia and Angola are characterized by a strong seasonal cycle, with warmest SSTs in March-April-May (MAM), modulated by variability from subseasonal to decadal time scales (Bachèlery et al., 2020). The main features of interannual SST variability over the ABA (8°E-to the coast; 10°S-20°S, blue box Figures 3.1a and 3.1b) are warm and cold events, the so-called Benguela Niños and Benguela Niñas (Shannon et al., 1986), respectively. Anomalous surface temperatures along the coasts of Angola and Namibia, typically lasting for a few months and peaking in MAM, impact the regional climate (Hansingo and Reason, 2009; Rouault et al., 2003, 2007; Lutz et al., 2013; Koseki and Imbol Koungue, 2021) as well as marine ecosystems and fisheries (Gammelsrød et al., 1998; Binet et al., 2001; Bachèlery et al., 2016a, 2020).

Such events are mainly driven by two mechanisms: (1) remote forcing from the equatorial Atlantic and (2) local atmospheric forcing. The remote forcing is associated with the fluctuations of the trade winds over the western and central parts of the equatorial Atlantic, triggering eastward propagating equatorial Kelvin waves (EKWs). When reaching the West African coast, part of the energy of the EKWs is transmitted poleward along the West African coast (Polo et al., 2008) as coastally trapped waves (CTWs; Clarke (1983)), which affect local stratification, SST, alongshore currents and biogeochemical conditions (Rouault, 2012; Rouault et al., 2018; Bachèlery et al., 2016b, 2020; Illig et al., 2018b,a; Illig and Bachèlery, 2019). Bachèlery et al. (2020) showed in an ocean modeling study that remote forcing from the equatorial Atlantic explains around 50% (70%) of the interannual SST (sea level anomaly) variability between 10°S and 20°S along the West African coast. Richter et al. (2010) showed, using observations and a coupled general circulation model, that Benguela Niños also can be forced by weakened local alongshore winds related to the strength of the South Atlantic Anticyclone (SAA). Moreover, Lübbecke et al. (2019) have demonstrated that the warm event of 2016 off Angola and Namibia was generated by a combination of local processes, that is, reduction of alongshore winds and local upwelling, anomalous heat fluxes, freshwater input, and meridional advection.

Predicting SSTs in the ABA is challenging. Two predictors have been suggested: (1) an index based on SAA strength (Lübbecke et al., 2010), and (2) an index based on

EKW activity (Imbol Koungue et al., 2017). Both approaches would allow to predict Benguela Niño and Benguela Niña events at 1 to 2 months lead time. In this study, we document a marked reduction of the interannual SST variability in the ABA since 2000. Possible links to remote forcing from the equatorial Atlantic and to the SAA and implications for the predictability of Benguela Niños and Benguela Niñas are discussed.

3.2 Data and methods

3.2.1 Data

Ocean reanalysis

Three ocean reanalysis SST products with monthly resolution are used: (1) Climate Forecast System Reanalysis Version 1 and 2 (CFSR, Saha et al. (2014)) available at $0.5°$ horizontal resolution and spanning the period from January 1979 to August 2019. (2) European Centre for Medium-range Weather Forecast (ECMWF) Re-Analysis 5 (ERA5, Hersbach et al. (2020)) available at $0.25°$ horizontal resolution for the period January 1979 to January 2020. (3) Ocean Reanalysis System version 4 (ORA-S4, Balmaseda et al. (2013)) from the ECMWF available at $1°$ horizontal resolution and spanning the period January 1958 to December 2017. Wind stress and sea level pressure (SLP) are taken from ERA5. The $20°$C isotherm depth (Z_{20}) is taken from ORA-S4.

Observations

Observational SST products used are (1) Hadley Centre Sea Ice and Sea Surface Temperature data set version 1.1 (HadI-SST, Rayner (2003)) available at $1°$ horizontal resolution for the period January 1870 to December 2019. (2) Centennial in situ Observation-Based Estimates SST (COBE-SST, Ishii et al. (2005)) available at $1°$ horizontal resolution and spanning the period January 1891 to December 2019. (3) Optimum Interpolation SST Version 2 (OI-SST, Reynolds et al. (2007)) available at $0.25°$ horizontal resolution for the period September 1981 to December 2019. Table S1 in the supporting information provides an overview of the datasets and variables used.

3.2.2 Methods

In order to investigate the changes in the interannual SST variability in the ABA since 2000, we compare the periods January 1982 to December 1999 and January 2000 to December 2017. The year 2000 was chosen as the year of separation because major shifts occurred around this year both in the tropical Atlantic (Prigent et al., 2020a) and tropical Pacific (McPhaden, 2012; Hu et al., 2013, 2017, 2020; Lübbecke and McPhaden, 2014; Li et al., 2019). All analyses use monthly-mean anomalies computed by subtracting the climatological monthly-mean seasonal cycle derived separately for each data set and period. Prior to all analyses, linear trends calculated over the entire period 1982-2017 were removed.

3.3 SST variability

The magnitude of the interannual SST variability in the southeastern tropical Atlantic, as measured by the standard deviation, has undergone a strong multidecadal reduction (Figure 3.1a). The time series of the SST anomalies (SSTa) averaged over the ABA (Figure 3.1b) exhibits a clear change in character from the pre-2000 period to the post-2000 period. The seasonal cycle of the standard deviation of the SSTa in the ABA exhibits a distinct maximum in MAM (Figure 3.1c), when most of the Benguela Niños/Niñas occur (Imbol Koungue et al., 2017, 2019). However, the standard deviations during 2000-2017 are much smaller. There is still considerable interannual variability after 2000 but major events are fewer and SST fluctuations less persistent (Figure 3.1d).

While the MAM SST in the ABA has warmed by 0.3 K from 1982-1999 to 2000-2017 (Figure S1a), the meridional gradient of MAM SST in the ABA remained nearly constant (Figure S1b). Vizy et al. (2018) showed a poleward trend of the Angola Benguela Frontal Zone (ABFZ), which could have influenced the ABA SST variability as the area of variability would shift with it. However, the observed reduction in SST variability occurred over a relatively large region. While the reduction is significant mainly to the north of the ABFZ, it extends almost along the whole Angolan and Namibian coasts (Figure 3.1a). Therefore, the reduction is not likely associated with a poleward displacement of the ABFZ.
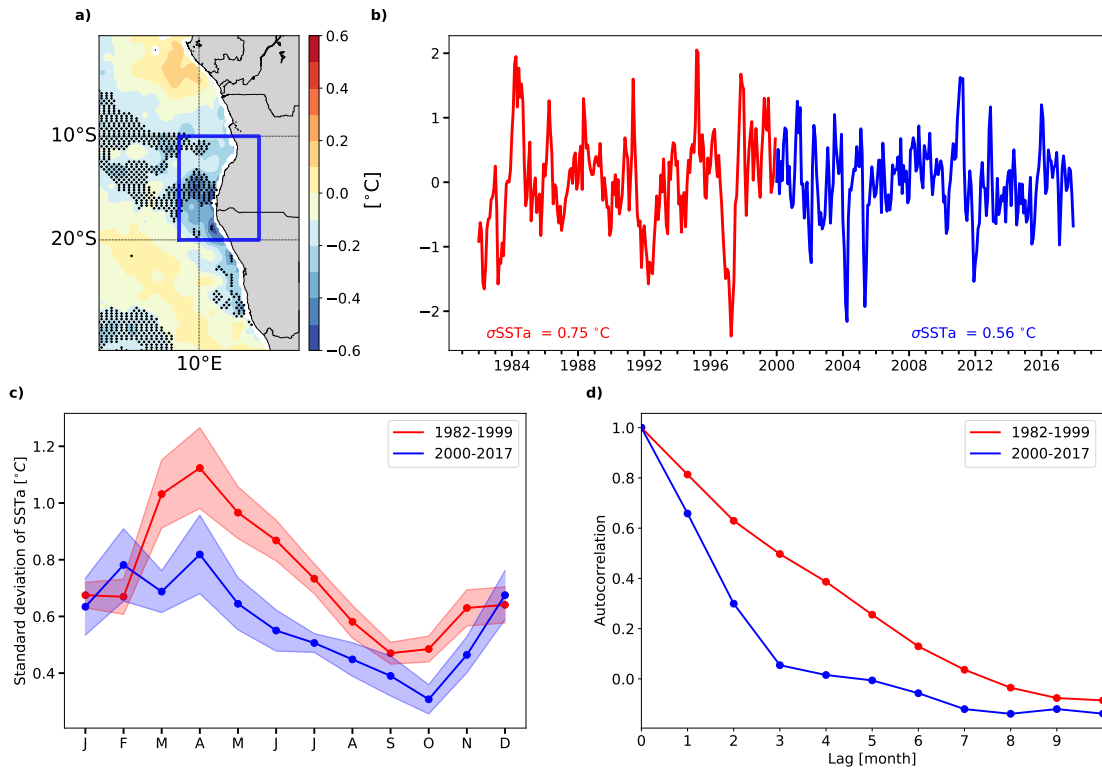
Figure 3.1: (a) Difference of MAM SSTa standard deviation between 2000-2017 and 1982-1999 from ERA5. Dots indicate where the standard deviations between the two periods are significantly different at the 95%-level according to a Welch's t-test. (b) Time series of monthly ABA-averaged ERA5 SST anomalies. (c) Ensemble mean standard deviation of ABA-averaged SSTa as function of the calendar month during 1982-1999 (red) and 2000-2017 (blue). The six SST products used are indicated in Table S1. (d) Autocorrelation function of the monthly ABA SSTa during 1982-1999 (red) and 2000-2017 (blue).

The standard deviation of SSTa in the ABA calculated over all calendar months has weakened by 22.3%, from 0.74 ± 0.05 K in 1982-1999 to 0.58 ± 0.07 K in 2000-2017. Strongest reduction occurred in MAM (Table 3.1). The MAM standard deviation was 1.08 ± 0.13 K during 1982-1999 and decreased by 30.5% to 0.75 ± 0.11 K during 2000-2017 (Table 3.1).

	1982-1999		2000-2017		Reduction (%)	
Product	All month	MAM	All month	MAM	All month	MAM
CFSR	0.75	1.15	0.64	0.83	15	28
ERA5	0.75	1.10	0.56	0.80	25	27
HadI-SST	0.72	0.91	0.48	0.63	33	31
COBE-SST	0.64	0.90	0.48	0.58	25	36
OI-SST	0.78	1.23	0.66	0.84	16	32
ORA-S4	0.78	1.18	0.63	0.84	20	29
EM	0.74 ± 0.05	1.08 ± 0.13	0.58 ± 0.07	0.75 ± 0.11	22.3 ± 6.2	30.5 ± 3

Table 3.1: Standard deviation of the ABA-averaged SSTa (K) for the periods 1982-1999 and 2000-2017. EM denotes the ensemble mean of all products (Table S1).

3.4 Relative roles of equatorial and local forcing

During 1982-1999, the ABA SSTa are mainly linked to zonal wind stress fluctuations in the western equatorial Atlantic, as shown by linear regression on ABA SSTa (Figures 3.2a and S2a). Equatorial zonal wind stress fluctuations can generate EKWs that propagate eastward along the equator. At the West African coast, part of the EKW energy is transmitted poleward as CTWs which can trigger coastal warm/cold events (Illig et al., 2004; Florenchie et al., 2003, 2004; Lübbecke et al., 2010; Imbol Koungue et al., 2017, 2019; Bachèlery et al., 2020). In contrast, during 2000-2017 (Figures 3.2b and S2b), the link between western equatorial zonal wind stress fluctuations and coastal SSTa is considerably weaker, which is consistent with the reduced equatorial wind stress variability described in Prigent et al. (2020a). Instead, relatively large regression coefficients are found in the southeastern tropical Atlantic close to the West African coast (Figure 3.2b), suggesting that the role of local meridional wind stress fluctuations in driving interannual SST variability in the ABA has increased. This is further supported by the strengthened link between ABA SSTa and near-coastal wind-stress curl anomalies along the Angolan and Namibian coasts when comparing 1982-1999 (Figure 3.2c) to 2000-2017 (Figure 3.2d). We also observe a magnitude maximum of

the regression coefficients around 20°S and 20°W (Figure 3.2b) which, however, is not statistically significant at 95% according to a Student's t-test.
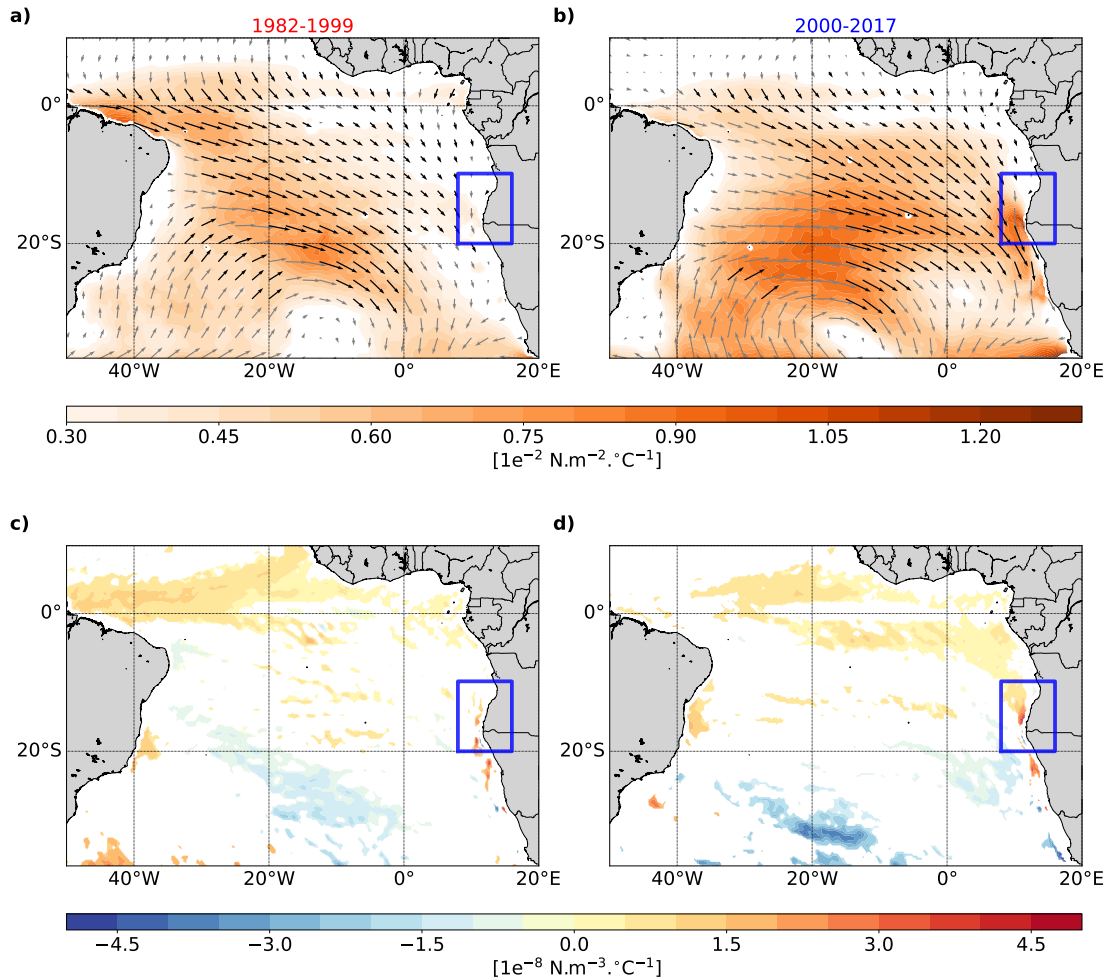
Figure 3.2: The vectors represent the regressions of detrended ERA5 wind stress anomalies on ERA5 ABA-averaged (8°E to the coast, 20°S-10°S; blue box) SSTa with winds leading by one month for (a) 1982-1999 and (b) 2000-2017. Regressions have been calculated for each wind stress component separately. The color shading depicts the magnitude of the vectors. Black (grey) arrows indicate pointwise significant (not significant) regressions for both components at the 95% level according to a Student's t-test. (c, d) Regression coefficients of detrended ERA5 wind-stress curl anomalies on ERA5 ABA-averaged SSTa with the wind-stress curl anomalies leading by one month during 1982-1999 and 2000-2017, respectively. Displayed regressions are significant at the 95% level according to the Student's t-test.

We next examine the impact of the equatorial zonal wind stress on thermocline depth. Variability in the latter serves here to assess the role of EKW activity (Im-

bol Koungue et al., 2017).
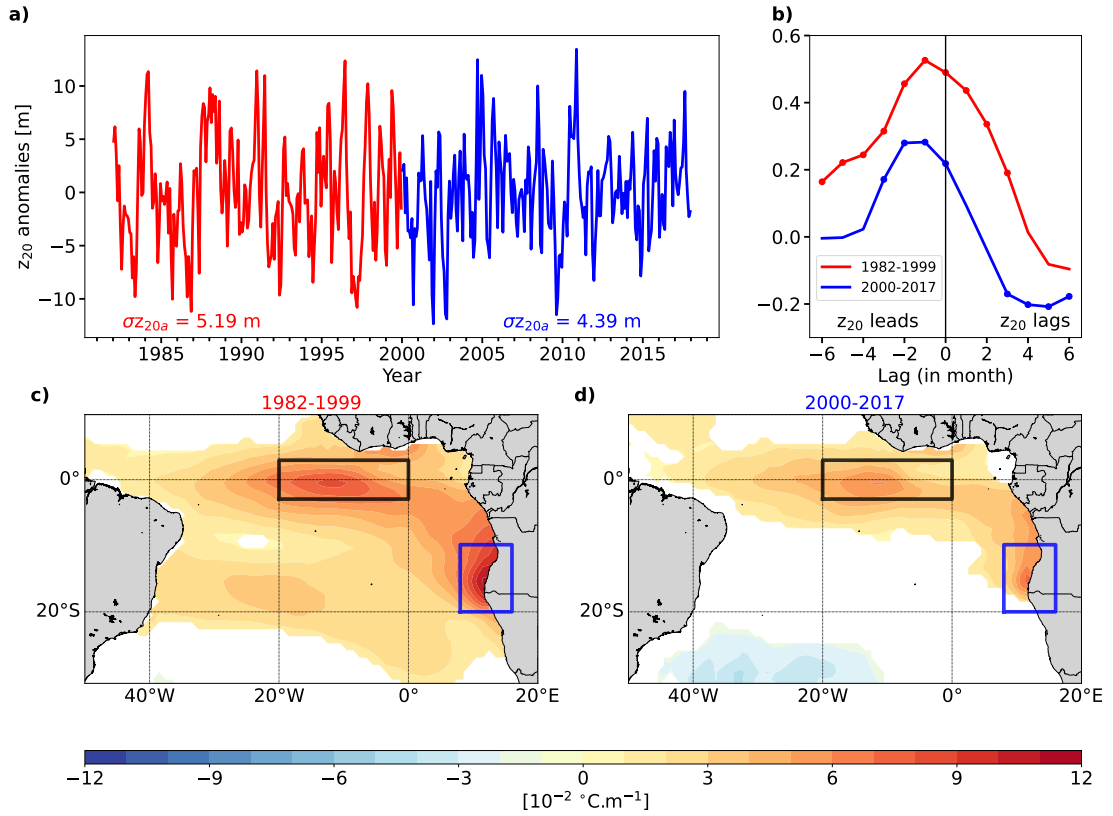
Figure 3.3: Time series of monthly ATL3 ORA-S4 20°C isotherm depth anomalies (z_{20a}). (b) Cross correlation of monthly ATL3 z_{20a} and ABA SSTa for 1982-1999 (red) and 2000-2017 (blue). Dots indicate correlations that are significant at the 95% level. (c,d) Regression coefficients of the detrended ORA-S4 SSTa on ATL3 ORA-S4 z_{20a} with the z_{20a} leading by one month during (c) 1982-1999 and (d) 2000-2017. Only statistically significant regressions at the 95% level are shown. Statistical significance is assessed by the Student's t test.

The standard deviation of the thermocline depth anomalies (z_{20a}) in the ATL3 box (20°W-0°, 3°N-3°S; Figure 3.3a) has reduced by 15.4% from 5.19 m during 1982-1999 to 4.39 m during 2000-2017. Further, the relationship between ATL3 z_{20a} and ABA SSTa also has markedly weakened after 2000 (Figure 3.3b). In fact, during 1982-1999, the ATL3 z_{20a} was leading ABA SSTa by one month with a correlation of 0.52 whereas the correlation at the same lead-time dropped to 0.28 during 2000-2017. These results suggest that after 2000 the importance of remote equatorial forcing of ABA SSTa by EKWs has substantially reduced. Consistent with this, the major warm event

of 2016 resulted from a combination of different local processes (Lübbecke et al., 2019). The results shown in Figure 3.3b also imply that an index based on equatorial Atlantic oceanic variability has become a less skillful predictor for the ABA SST variability after 2000: while the shape of the cross-correlation function remained unchanged, the magnitude of the correlations has dropped considerably.

The link between the ABA SSTa and the equatorial ocean dynamics can be estimated by regressing the SSTa on the (detrended) ATL3 z_{20a} taken one month earlier. This link has weakened at the equator from 1982-1999 (Figure 3.3c) to 2000-2017 (Figure 3.3d), especially between 20°W to 5°E and along the West African coast between 5°S and 20°S. This again suggests that after 2000, equatorial thermocline displacement anomalies have less impact on the ABA SSTs. However, reanalysis products are known to exhibit large biases in the tropical Atlantic region (Tchipalanga et al., 2018; Kumar and Hu, 2012; Huang et al., 2007). High-resolution ocean models forced by the history of observed wind stress could be a way out of this dilemma.

Lübbecke et al. (2010) showed that western equatorial Atlantic zonal wind stress variations are linked to the variations of the strength of the SAA. Later, Lübbecke et al. (2014) demonstrated that this link is facilitated through the wind power. Richter et al. (2010) also highlighted the importance of the SAA on the development of warm events off the Angolan and Namibian coasts.
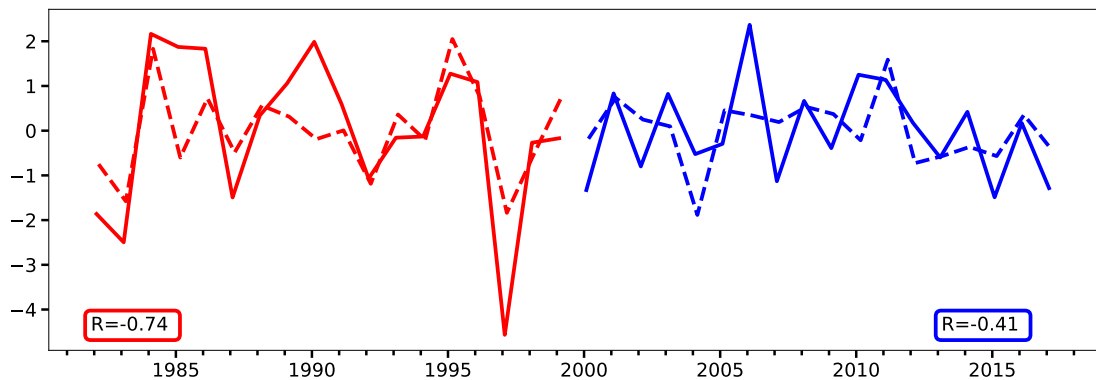
Figure 3.4: Time series of interannual anomalies of February SAA index (SLP (hPa) averaged over 40°S to 20°S and 30°W to 10°W; inverted, full line) and March ABA SST (°C, dashed line) from ERA5 during 1982-1999 (red) and 2000-2017 (blue).

In agreement with Lübbecke et al. (2010), the fluctuations of the strength of the SAA in austral summer during 1982-1999 have been well anticorrelated with the subsequent

austral fall ABA SSTs with a correlation coefficient of -0.74 (Figure 3.4). However, over the period 2000-2017, the correlation coefficient dropped to -0.41. No major shift in the SAA position was found that could explain the diminishing correlation between March ABA SSTa and February SLPa from 1982-1999 (Figure S3a) to 2000-2017 (Figure S3b). Moreover, since 2000 a weaker relationship between the SLP-anomaly field and ABA SSTa is evident in the regression maps (Figures S3c and S3d). Hence, the ABA SSTs during 2000-2017 are less influenced by the variations in the strength of the SAA than during 1982-1999. The reason for this weaker relationship is unclear and beyond the scope of this paper.

3.5   Discussion and conclusions

This study documents a multidecadal reduction in the interannual SST variability in the ABA during 2000-2017 relative to 1982-1999. The interannual SST variability in the ABA has reduced in the annual mean by 22.3% during 2000-2017 relative to 1982-1999, with the strongest reduction amounting to 30.5% in March-April-May (MAM). The reduced interannual SST variability in the ABA goes along with a smaller influence of remote forcing by equatorial wind stress variability. The zonal wind stress variability over the western equatorial Atlantic diminished during the recent decades, as reported by Prigent et al. (2020a). Lower zonal wind stress variability tends to reduce EKW activity that is an important driver of SST in the ABA. This by itself enhances the relative importance of the local atmospheric forcing through near-coastal meridional wind stress and wind stress curl, if the local factors remain unchanged. However, the quantification of the relative importance of the local and remote wind stress forcing over the last decades remains a challenge due to limited data. Ocean modelling would be an alternative and additionally allow disentangling the contribution of each equatorial baroclinic mode to ABA SST variability.

Another factor that could have contributed to the reduced interannual SST variability in the ABA is the multidecadal surface warming in the region. In MAM, the season of the largest interannual SST variability, the SST in the ABA has warmed by 0.3 K when comparing the pre-2000 period to the post-2000 period. This is consistent with Vizy and Cook (2016) who investigated multidecadal changes in the southeastern tropi-

cal Atlantic over the period 1982-2013 and found significant SST warming trends along the Angolan/Namibian coasts of 0.5 K-1.5 K per 32 years. This multidecadal surface warming was associated with an increased net heat flux from the atmosphere and reduced coastal upwelling. The surface warming and concurrent subsurface cooling (Figures S4a and S4b) might have reduced surface-subsurface coupling in the post-2000 period. There is a shoaling of the stratification maximum in the ABA since 2000 (Figure S4b), which would support a larger sensitivity of the mixed layer to local forcing. Due to large biases in reanalysis products and limited observations (Tchipalanga et al., 2018; Kumar and Hu, 2012; Huang et al., 2007), large uncertainties remain regarding the potential influence of multidecadal changes in stratification on the interannual SST variability in the ABA.

Although some major remotely forced Benguela Niño/Niña events occurred after 2000, Table S1 and Table S2 from Imbol Koungue et al. (2019) indicate a smaller number relative to previous decades. Over the period 1982-2015, out of eight (six) warm (cold) events only two (one) took place after 2000. However, over the same time period, out of 15 (7) moderate warm (cold) events 7 (5) occurred between 2000 and 2015. This illustrates that relative to 1982-1999, since 2000 fewer remotely forced major and more moderate events occurred in the ABA.

Numerous other potential factors could have contributed to the reduced SST variability in the ABA. One of them might be the interdecadal shift of El Niño/Southern Oscillation (ENSO) that occurred around 2000 (McPhaden, 2012; Hu et al., 2013, 2017, 2020; Lübbecke et al., 2014). This shift featured a decrease in ENSO variability, an increase in ENSO frequency (Hu et al., 2013, 2020) as well as a profound westward shift of the Walker Circulation in the equatorial Pacific (Li et al., 2019). The latter might have altered ENSO teleconnections, and thus, could have contributed to the weakened SST variability in the tropical Atlantic. However, the influence of the multidecadal shift in ENSO on the tropical Atlantic SST requires further analyses.

Finally, our results may have implications for the predictability of Benguela Niño/Niña events. In particular, the strong link between equatorial thermocline displacements and ABA SSTa during 1982-1999 has significantly weakened since 2000. In addition, we show that the strong link between the fluctuations in SAA strength and ABA SSTa observed during the pre-2000 period (Lübbecke et al., 2010) has diminished considerably

during the post-2000 period. This raises the question as to whether predictors based on equatorial variables or the SAA strength are still useful to forecast Benguela Niño/Niña events.

3.6 Acknowledgements and Data

3.7 Supplementary material

Table S1: Information on the datasets used and their sources. U-stress and V-stress are the zonal and meridional wind stress. SLP is the sea level pressure, SST is the sea surface temperature, T is the temperature and S is the salinity.

Product	Resolution (lon x lat x lev)	Time period	Variable used	Reference
CFSR	720 x 361	1979/01 - 2019/08	SST	Saha et al. (2013)
ERA5	1440 x 720	1979/01 - 2020/01	SST, U-stress, V-stress, SLP	Hersbach et al. (2020)
HadI-SST	360 x 180	1870/01 - 2019/12	SST	Rayner (2003)
COBE-SST	360 x 180	1891/01 - 2019/12	SST	Ishii et al. (2005)
OI-SST	1440 x 720	1981/09 - 2019/12	SST	Reynolds et al. (2007)
ORA-S4	360 x 180 x 42	1958/01 - 2017/12	SST, T, S	Balmaseda et al. (2013)
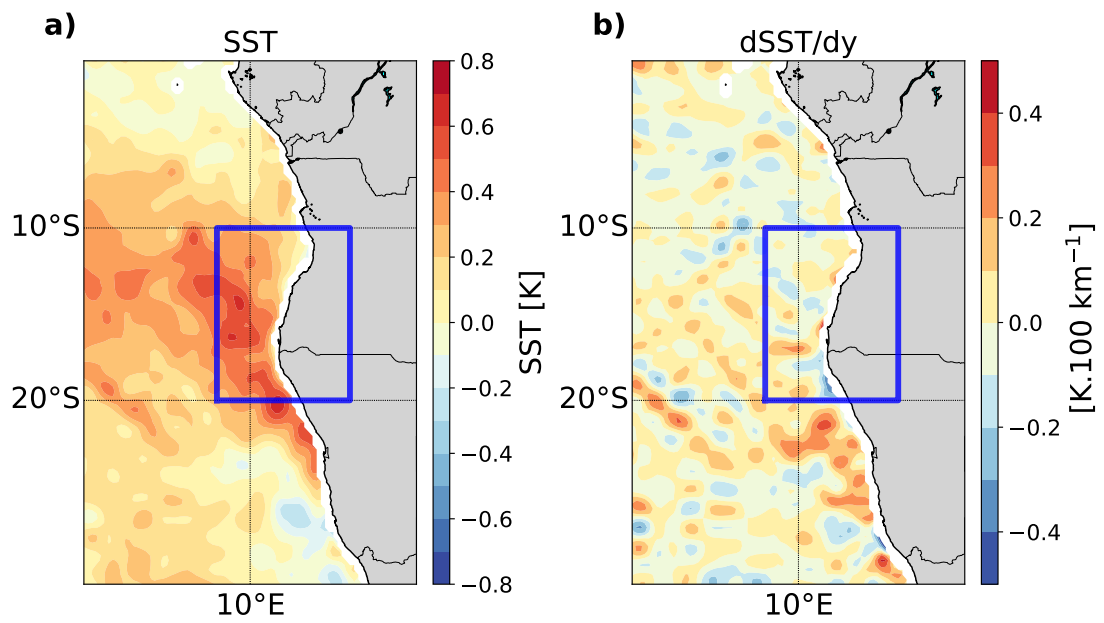
Figure S1: (a) Difference of ERA5 MAM SST, 2000-2017 minus 1982-1999. (b) Difference of ERA5 MAM meridional gradient of SST, 2000-2017 minus 1982-1999.
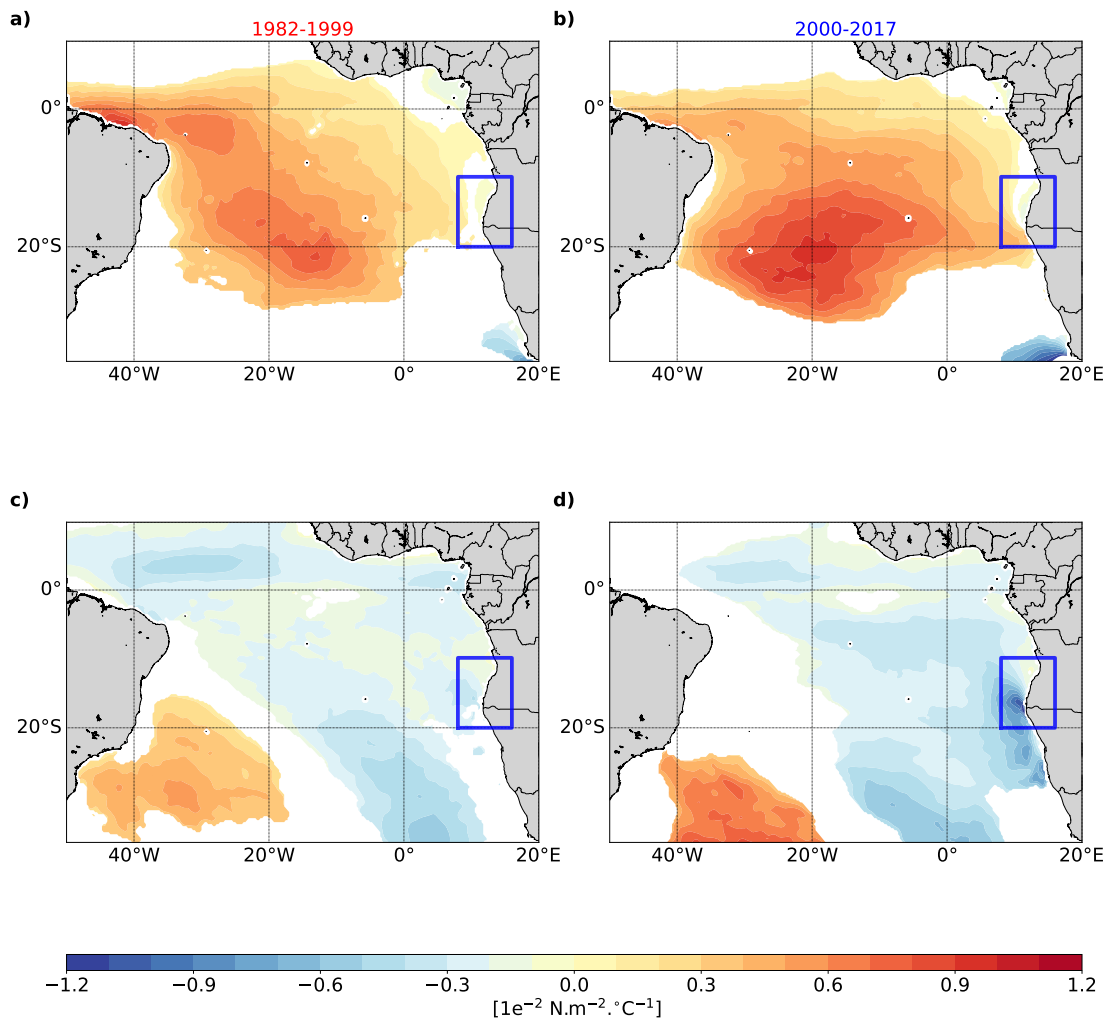
Figure S2: Regression of detrended ERA5 zonal wind stress anomalies on ERA5 SSTa averaged over the ABA with winds leading by one month for (a) 1982-1999 and (b) 2000-2017. Regression of detrended ERA5 meridional wind stress anomalies on ERA5 SSTa averaged over the ABA with winds leading by one month for (c) 1982-1999 and (d) 2000-2017. The color shading depicts the slope of the regressions. Displayed values are significant at the 95% level according to a Student's t-test.
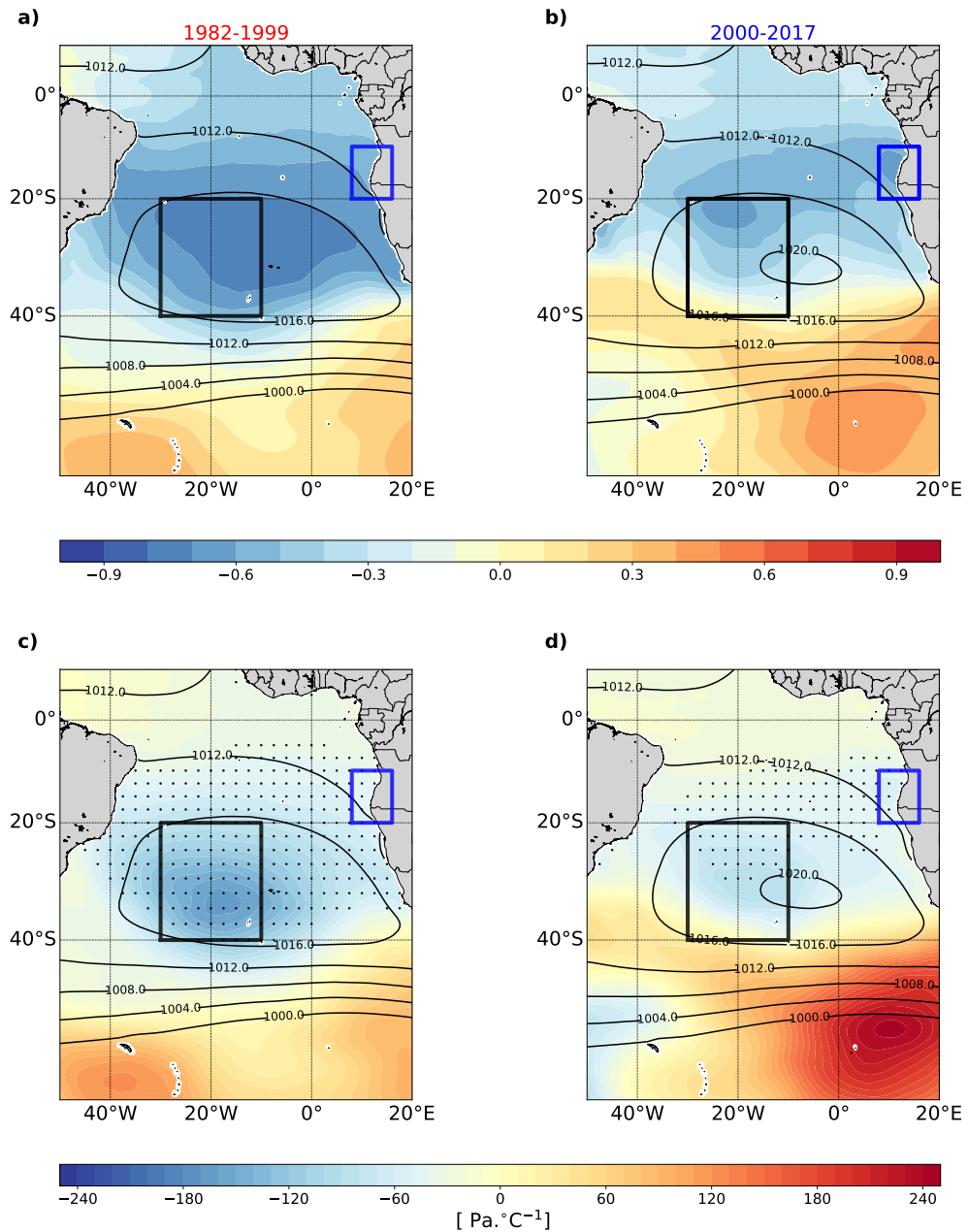
Figure S3: (a, b) Correlation coefficients between detrended ERA5 February SLPa and March ERA5 ABA-averaged SST anomalies for the periods 1982-1999 and 2000-2017, respectively. (c, d) Regressions of detrended ERA5 mean February SLPa on March ERA5 ABA-averaged SSTa during 1982-1999 and 2000-2017, respectively. The color shading depicts the slope of the regressions. Dots indicate significance at the 95% level according to a Student's t-test. Black contours are the mean SLP in hPa. The black box represents the SAA-index region (40°S, 20°S; 30°W, 10°W), and the blue box the ABA-index region (20°S, 10°S; 8°E, 16°E).
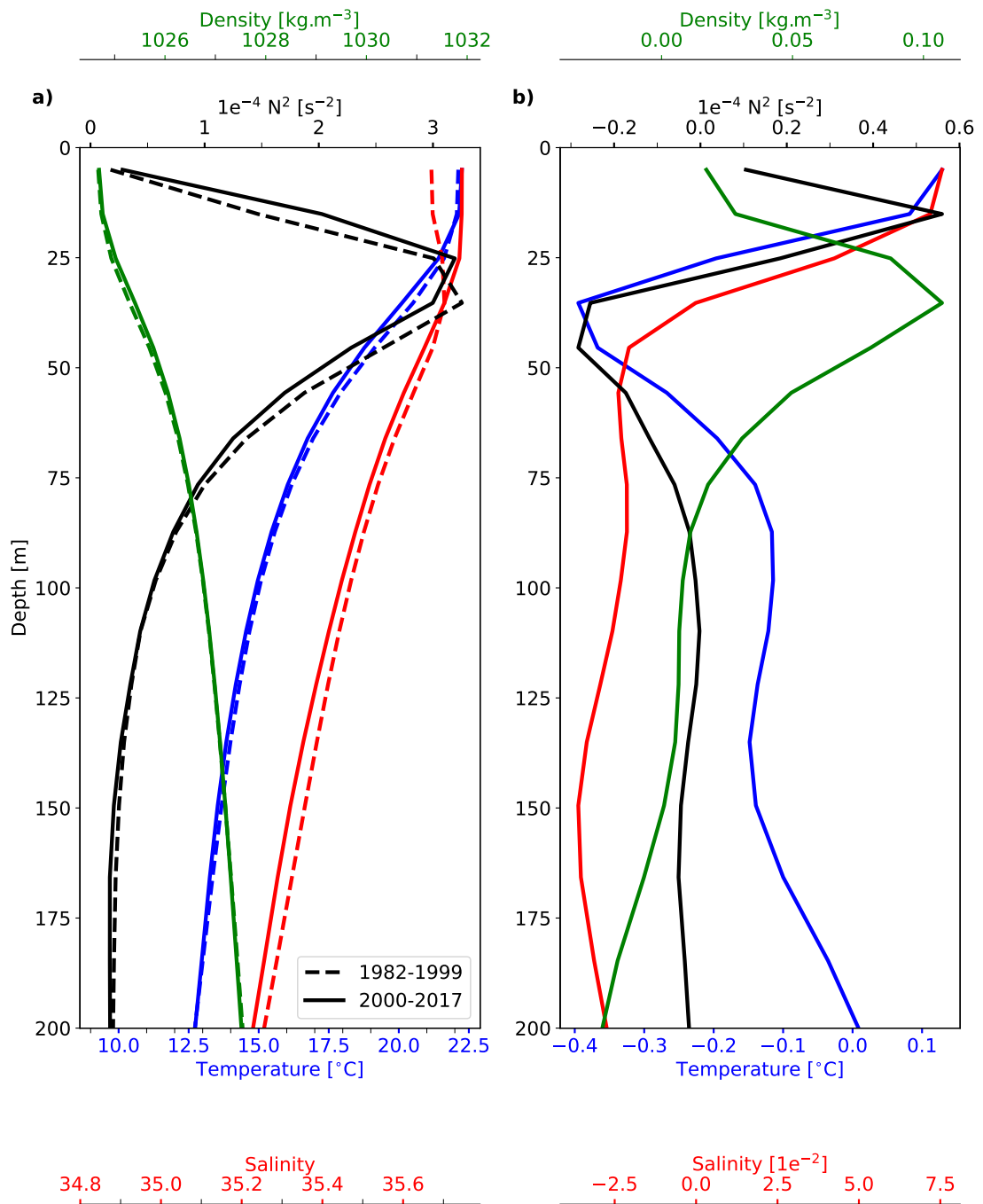
Figure S4: (a) ORA-S4 temperature (blue), salinity (red), Brunt-Väisälä frequency squared (black) and density (green) profiles averaged over the ABA for the periods 1982-1999 (dashed lines) and 2000-2017 (full lines). (b) Difference, 2000-2017 profiles minus 1982-1999 profiles.

Chapter 4

Weakening of the Atlantic Niño variability under global warming

Chapters 2 and 3 revealed that during recent decades the southeastern tropical and eastern equatorial Atlantic interannual SST variability experienced multidecadal changes. In the following chapter, we investigate the future projection of the interannual SST variability in the eastern equatorial Atlantic using a global CMIP5 and CMIP6 coupled models.

> Citation: Crespo, L. R., **Prigent, A.**, Keenlyside, K., Koseki, S., Svendsen, L., Richter, I., & Sánchez-Gómez, E. (In preparation). Weakening of the Atlantic Niño variability under global warming

The candidate contributed to all the analyses, produced all the figures and participated to the drafting of the manuscript.

Abstract

The Atlantic Niño is one of the most important tropical patterns of interannual climate variability, with major regional and global impacts. How global warming will influence the Atlantic Niño has been hardly explored, because of large climate model errors. We show for the first time that state-of-the-art climate models robustly predict a weakening of Atlantic Niños in response to global warming. This is primarily because subsurface and surface temperature variations decouple as the upper equatorial Atlantic Ocean warms. The weakening is predicted by most ($> 80\%$) models following the highest emission scenarios in the Coupled Model Intercomparison Project Phases 5 and 6 considered here. These indicate a reduction in variability by the end of the century of 12-17%, and as much as 30% when accounting for model errors. Weaker Atlantic Niño variability will have major consequences for global climate and the skill of seasonal predictions.

4.1   Introduction

The Atlantic Niño phenomenon exhibits many similarities to the stronger El Niño/ Southern Oscillation (ENSO; McPhaden et al. (2006); Timmermann et al. (2018)) in the Pacific. The eastern equatorial Atlantic is anomalously warm, surface trade winds relax and rainfall shifts equatorward during positive Atlantic Niño (Keenlyside and Latif, 2007; Lübbecke et al., 2018; Zebiak, 1993) events. The sea surface temperature (SST) anomalies in the equatorial cold tongue can reach 1.5ºC and thermocline (20°C isotherm) depth anomalies can exceed 30 m in boreal summer when the events peak. Opposite conditions are found during negative events. Coupled ocean-atmosphere interactions— Bjerknes positive and delayed negative feedbacks —similar to those in the Pacific can explain most Atlantic Niño variability, but other mechanisms can contribute substantially to equatorial SST anomalies (Lübbecke et al., 2018; Richter et al., 2013). The Atlantic Niño has significant impacts on the climate (Hirst and Hastenrath, 1983; Nobre and Shukla, 1996; Gu and Adler, 2004) and marine biogeochemistry (Boyd et al., 1992; Chenillat et al., 2021) in the tropical Atlantic sector, on ENSO (Rodríguez-Fonseca et al., 2009; Ding et al., 2012; Polo et al., 2015; Martín-Rey et al., 2015; Exarchou et al., 2021), and extra-tropical climate (García-Serrano et al., 2008; Haarsma and

Hazeleger, 2007; Losada et al., 2012; Mohino and Losada, 2015).

Recent studies have shown a weakening of the Atlantic Niño variability in the last decades (Tokinaga and Xie, 2011; Prigent et al., 2020a; Silva et al., 2021). The changes in eastern equatorial Atlantic SST variability have been attributed to the combined effect of a weakening of the Bjerknes feedback (Prigent et al., 2020a) (BF) and increased heat flux damping (Prigent et al., 2020a; Silva et al., 2021), and to a basin-wide warming related to climate change (Tokinaga and Xie, 2011). These studies used observational and reanalysis datasets to investigate changes in the SST variability during the historical period.

Extensive analysis of the projections from the Coupled Model Intercomparison Project (CMIP) indicate that ENSO events will become stronger under global warming, but large uncertainties exist (Collins et al., 2010; DiNezio et al., 2012; Kim et al., 2014; Cai et al., 2014, 2015). Large climate model biases in the tropical Atlantic sector (Li and Xie, 2012; Richter et al., 2012, 2014; Richter and Tokinaga, 2020) have discouraged the climate community from carrying out similar in-depth assessment of climate change in the area. However, we will show that such biases do not preclude a more robust assessment of global warming impacts on Atlantic Niño variability than has been achieved in the Pacific.

4.2 Weakened variability of the equatorial Atlantic SST

To investigate how the SST variability in the eastern equatorial Atlantic will change under global warming, we use historical simulations and the future highest emission scenario simulations from the CMIP5 (Taylor et al., 2012) and CMIP6 (Eyring et al., 2016) archives. The comparison between the historical (1950-99) and future scenario (2050-99) periods in the CMIP models shows that the SST variability in the eastern equatorial Atlantic sector in June-July-August (JJA) is reduced in the majority of the CMIP models (33 out of 40). The reduction is statistically significant at the 95% level in most of the models (23 out of 33) and there is no statistically significant increase in variability in any model (Figure 4.1a and table 4.1). The multi-model ensemble mean of CMIP5 (CMIP6) shows a reduction of the SST variability of 12% (17%) in the future scenario simulation with respect to the historical simulation (Table 4.1). The surface

zonal winds in the western Atlantic sector also show a reduced future variability in May-June-July (MJJ) season in the CMIP5 and CMIP6 models with only 4 out of 40 models showing increased variability, although not statistically significant (Figure 4.1d and table 4.1). The ensemble mean of the standard deviation of the MJJ zonal wind anomalies (UAS hereafter) is reduced by 14% in CMIP5 and by 18% in CMIP6, which corresponds very well to the amplitude of the reduction in JJA SST variability (Table 4.1). The reduction of the zonal surface winds in the western equatorial Atlantic is consistent with a more stratified atmosphere in a future warmer climate (Maloney and Xie, 2013).

The reduction of the standard deviation in both SST and UAS is more pronounced and localized in the ensemble mean of CMIP6 (Figures 4.1c and 4.1f) than in CMIP5 (Figures 4.1b and 4.1e. The weakening of the standard deviation of the MJJ zonal winds in the western equatorial Atlantic is followed by a weakening of the eastern equatorial Atlantic JJA SST variability in both CMIP5 (Figures 4.1b and 4.1e) and CMIP6 (Figures 4.1c and 4.1f) ensemble means, suggesting that the reduced wind variability may be the cause of the reduced SST variability. However, the linear regression between the two variables explains only 32% of the variance (Figure S1 in Section 4.9). Consequently, there are other mechanisms that play an important role in the reduction of the standard deviation of the SST in the eastern equatorial Atlantic.

4.3 Weakened ocean-atmosphere coupling

We explore the relative importance of the dynamical and thermodynamical drivers of the future changes in the SST, through the BF components and the net heat flux damping (Methods). The basin-wide weakening of the SST variability and winds in the future scenario simulation might be related to a weakening of the BF. The changes in variability in CMIP5 and CMIP6 are rather similar and therefore, we will consider all CMIP models together in this section.

Both ensemble means of CMIP5 and CMIP6 models show a small change of the first component of the BF (i.e. the linear regression of MJJ ATL4 zonal winds anomalies on the JJA ATL3 SSTa). A majority of the CMIP models agrees on a decrease of the first component of the BF; 29 out of 40 models (Figure 4.2a). The second component of the

Table 4.1: List of CMIP5 and CMIP6 models used in this study (first column). Standard deviation of the JJA ATL3-averaged SST anomalies and the MJJ ATL4-averaged UAS anomalies (second column) in brackets, during 1950-1999 and 2050-2099. The reduction is relative to the 1950-1999 period. ENS is the multi-model ensemble mean of the CMIP5 and CMIP6. A F-test was applied to the JJA SST variability (MJJ UAS variability) to determine if the change in variability is significant at the 95% level (fourth column). JJA ATL3-averaged SST change (fifth column), defined as the difference of the 2050-2099 mean minus the 1950-1999 mean.

| No. | Models | ATL3 JJA SST variability [K] (ATL4 MJJ UAS variability [m.s^{-1}]) | | | | ATL3 JJA SST Change [K] |
		1950-1999	2050-2099	Reduction [%]	F-test	
0	ACCESS-CM2	0.54 (1.26)	0.38 (0.96)	30 (24)	Yes (Yes)	3.52
1	ACCESS-ESM1-5	0.68 (1.07)	0.53 (0.76)	22 (29)	Yes (Yes)	3.14
2	BCC-CSM2-MR	0.31 (0.50)	0.28 (0.46)	10 (8)	No (No)	2.18
3	CAMS-CSM1-0	0.39 (0.87)	0.28 (0.58)	28 (31)	Yes (Yes)	0.8
4	CanESM5	0.54 (0.70)	0.34 (0.35)	37 (44)	Yes (Yes)	3.96
5	EC-Earth3	0.63 (1.02)	0.69 (1.09)	-10 (-7)	No (No)	2.49
6	EC-Earth3-Veg	0.65 (0.95)	0.60 (1.02)	8 (-7)	No (No)	2.50
7	GFDL-ESM4	0.54 (0.74)	0.52 (0.66)	4 (11)	No (No)	2.27
8	INM-CM4-8	0.34 (0.49)	0.26 (0.40)	24 (18)	Yes (Yes)	2.23
9	INM-CM5-0	0.36 (0.50)	0.27 (0.45)	25 (10)	Yes (No)	2.04
10	IPSL-CM6A-LR	0.68 (0.79)	0.52 (0.65)	24 (18)	Yes (Yes)	3.56
11	MIROC6	0.51 (0.89)	0.32 (0.79)	37 (11)	Yes (No)	2.77
12	MPI-ESM1-2-HR	0.56 (0.81)	0.35 (0.53)	38 (35)	Yes (Yes)	1.81
13	MPI-ESM1-2-LR	0.32 (0.88)	0.35 (0.75)	-9 (15)	No (No)	1.68
14	MRI-ESM2-0	0.7 (1.10)	0.59 (0.97)	16 (12)	Yes (Yes)	3.36
15	NESM3	0.37 (0.72)	0.39 (0.56)	-5 (22)	No (Yes)	2.34
	ENS	**0.51 ± 0.14** (**0.83 ± 0.21**)	**0.42 ± 0.13** (**0.68 ± 0.22**)	**17 ± 13** (**18 ± 14**)		**2.70 ± 0.58**
16	ACCESS1-0	0.41 (0.60)	0.29 (0.61)	29 (-2)	Yes (No)	3.07
17	ACCESS1-3	0.52 (0.81)	0.50 (0.73)	4 (10)	No (No)	3.16
18	CMCC-CESM	0.46 (1.15)	0.69 (1.26)	-50 (-10)	No (No)	2.51
19	CMCC-CMS	0.38 (0.76)	0.37 (0.72)	3 (5)	No (No)	3.02
20	CMCC-CM	0.37 (0.62)	0.35 (0.57)	5 (8)	No (No)	2.75
21	CNRM-CM5	0.23 (0.75)	0.22 (0.71)	5 (5)	No (No)	2.11
22	CSIRO-Mk3-6-0	0.46 (0.52)	0.33 (0.30)	28 (42)	Yes (Yes)	2.59
23	GFDL-CM3	0.81 (0.99)	0.69 (0.87)	15 (12)	No (No)	2.99
24	GFDL-ESM2M	0.90 (1.51)	0.97 (1.41)	-8 (7)	No (No)	2.36
25	GISS-E2-H-CC	0.31 (0.78)	0.28 (0.54)	10 (31)	No (Yes)	1.91
26	GISS-E2-H	0.35 (0.58)	0.27 (0.51)	23 (12)	Yes (No)	2.16
27	GISS-E2-R-CC	0.22 (0.48)	0.19 (0.39)	14 (19)	Yes (Yes)	1.98
28	GISS-E2-R	0.24 (0.49)	0.19 (0.46)	21 (6)	Yes (No)	1.91
29	HadGEM2-CC	0.82 (1.07)	0.60 (0.91)	27 (15)	Yes (Yes)	3.41
30	IPSL-CM5A-LR	0.48 (0.50)	0.45 (0.47)	6 (6)	No (No)	3.83
31	IPSL-CM5A-MR	0.44 (0.51)	0.38 (0.43)	14 (16)	Yes (Yes)	3.70
32	IPSL-CM5B-LR	0.31 (1.19)	0.32 (0.91)	-3 (24)	No (Yes)	2.08
33	MIROC-ESM-CHEM	0.33 (0.37)	0.26 (0.30)	21 (19)	Yes (Yes)	3.27
34	MIROC-ESM	0.37 (0.36)	0.27 (0.30)	27 (17)	Yes (Yes)	3.25
35	MIROC5	0.63 (1.22)	0.41 (0.75)	35 (39)	Yes (Yes)	3.10
36	MPI-ESM-LR	0.43 (0.74)	0.34 (0.55)	21 (26)	Yes (Yes)	2.80
37	MPI-ESM-MR	0.48 (0.67)	0.36 (0.59)	25 (12)	Yes (No)	2.76
38	MRI-CGCM3	0.52 (0.90)	0.4 (0.87)	23 (3)	Yes (No)	2.43
39	NorESM1-M	0.43 (1.02)	0.49 (0.90)	-14 (12)	No (No)	1.77
	ENS	**0.45 ± 0.18** (**0.77 ± 0.29**)	**0.40 ± 0.18** (**0.67 ± 0.28**)	**12 ± 18** (**14 ± 12**)		**2.54 ± 0.79**

71
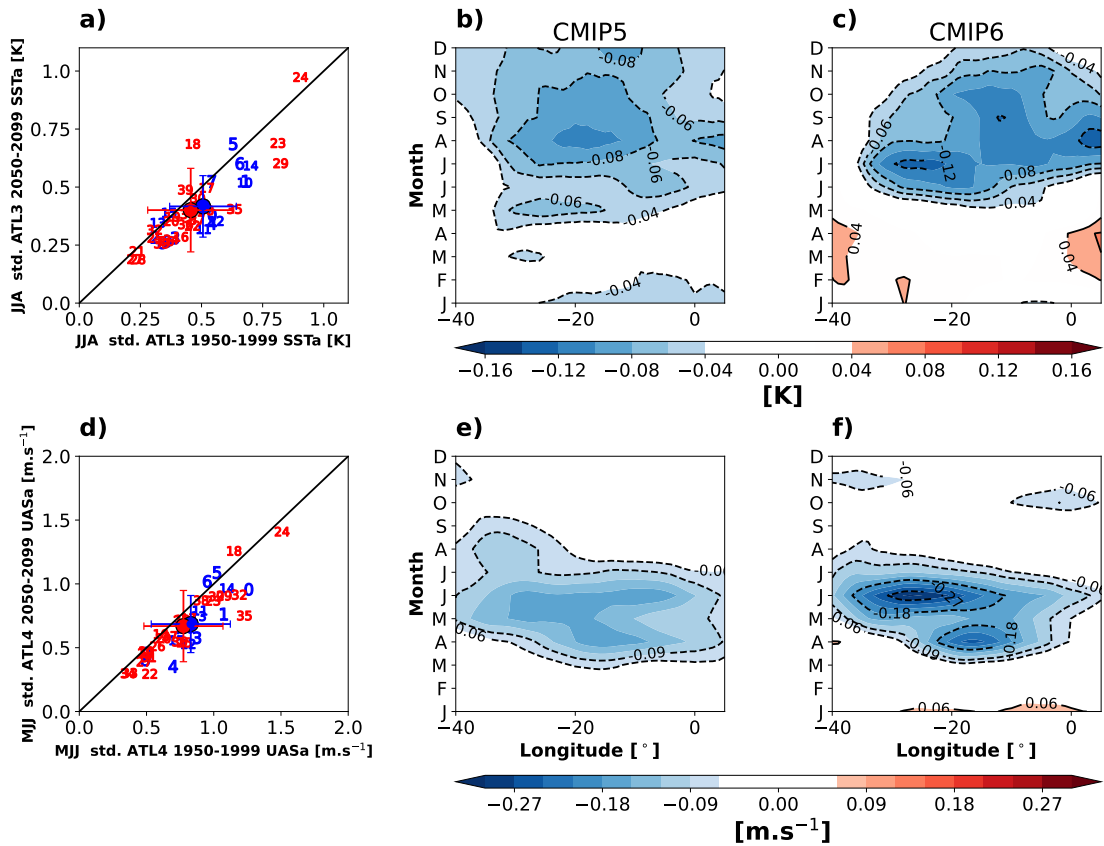
Figure 4.1: Weakening of the eastern equatorial Atlantic SST variability. (a) Scatter plot of the JJA average standard deviation of the SST anomalies (SSTa) for the historical period (1950-99) in the x axis against the standard deviation of SSTa for the scenario period (2050-99) in the y axis. The black line represents the no-change line and is added for easier interpretation. Difference between the means of the 2050-2099 and the 1950-1999 periods standard deviation of the SST anomalies for the ensemble mean of CMIP5 (b) and CMIP6 (c) models, along the equator and averaged between 3°S and 3°N. Same as (b) and (c) for the surface zonal wind anomalies of the CMIP5 (e) and CMIP6 (f) models, along the equator and averaged between 3°S and 3°N. (d) Scatter plot of the MJJ average standard deviation of the UASa for the historical period (1950-99) in the x axis against the standard deviation of UASa for the scenario period (2050-99) in the y axis. The black line represents the no-change line and is added for easier interpretation. The blue (red) numbers correspond to the CMIP6 (CMIP5) models listed in Table 4.1. The blue (red) circle shows the ensemble mean of CMIP6 (CMIP5) models.

BF, the thermocline zonal slope response to western equatorial wind anomalies, shows a small reduction for 26 in 40 CMIP models (Figure 4.2b). The change in the second BF component shows slightly less inter-model agreement than the first component of the BF with 26 out of 40 CMIP models showing a decrease of the second component of the BF. The third component of the BF, that accounts for the local response of SSTa to thermocline depth anomalies in the ATL3 region, shows the most consistent changes; with 30 out of 40 CMIP models showing a reduction of the third BF component. Both the CMIP5 and the CMIP6 multi-model ensemble means show a reduction in the strength of this relation in the future climate simulations (Figure 4.2f).

The change of the third BF component between historical and future simulations is strongly related to the change in ATL3 JJA SST variability between the two periods, with an explained variance of 61% when considering all CMIP models (Figure 4.2f). Contrastingly, the changes in the first and second components of the BF explain only little variance of the change in SST variability, 19% and 18%, respectively. Therefore, the reduced sensitivity of SST to local changes in thermocline depth dominates the reduction of SST variability in the eastern equatorial Atlantic in the future scenario. However, the majority of the CMIP models largely underestimates the strength of this part of the feedback in historical simulations (Figure 4.2c), a flaw already present in CMIP5 models (Deppenmeier et al., 2016) that still persists in the latest CMIP6 generation. Therefore, the CMIP models might underestimate the future reduction of SST variability.
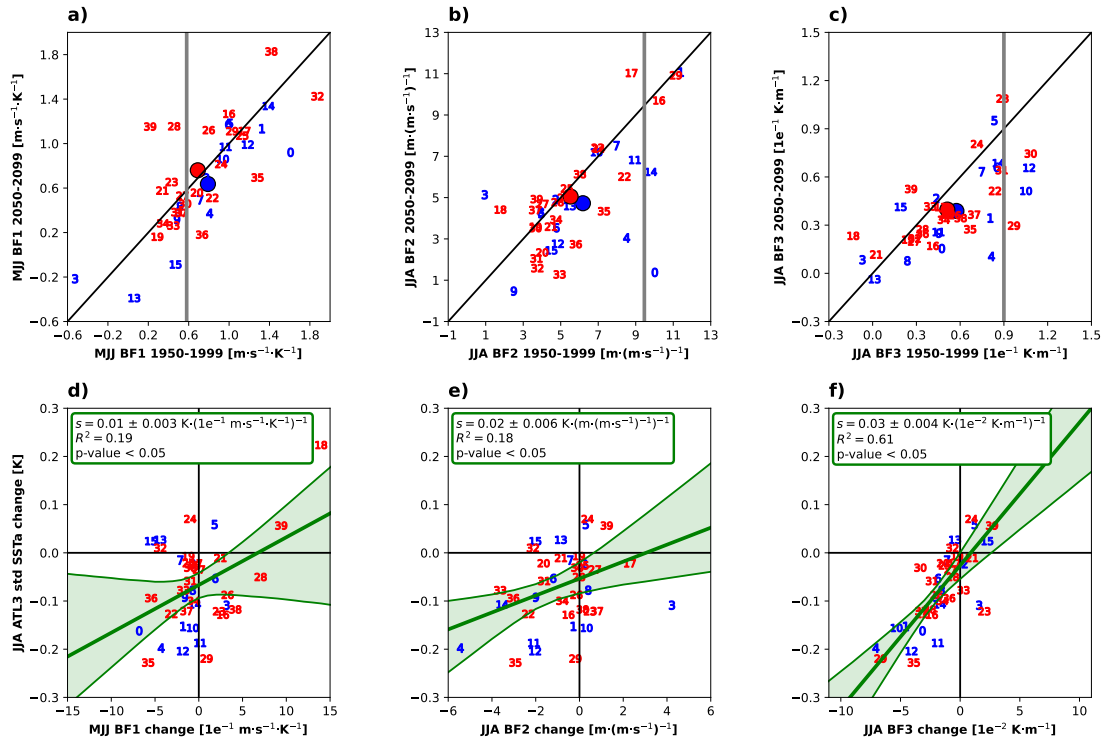
Figure 4.2: Dynamical drivers of the weakening of the SST variability. Changes between the historical and future scenario in the strength of the Bjerknes feedback (BF) components. (a) First component of the BF is the linear regression of ATL4 MJJ UAS anomalies against the JJA ATL3 SSTa. (b) Second component of the BF as the linear regression of ATL4 JJA UAS anomalies on the thermocline slope depth anomalies (i.e. z20 in ATL3 minus z20 in ATL4). (c) Third component of BF computed as the linear regression of ATL3 JJA SSTa onto the JJA ATL3 Z20 anomalies. The blue and red dots are the ensemble mean of the CMIP6 and CMIP5 ensemble, respectively. Linear regression between the change in JJA SSTa variance and the change in BF components (d, e, f). The change here is defined as the difference of the mean of the scenario period (2050-99) minus the mean of the historical period (1950-99). The vertical grey lines represent an estimation of the three components of the BF (a, b and c) from observation and reanalysis datasets. The green shading depicts the 95% confidence interval of the linear regression. The confidence interval is obtained by taking the 2.5th and 97.5th percentile of the distribution of the linear regressions of the 10000-time resampled datasets.

4.4 Future mean changes of the tropical Atlantic SST

The strength of the third component of the BF is linked to the strength of climatological upwelling and vertical temperature stratification (Ding et al., 2015). In particular, a weaker feedback can result from the weaker upwelling of relatively warmer subsurface waters. Despite a large intermodel spread, the SST change between historical and future scenario simulations shows a robust warming of the equatorial Atlantic cold tongue consistent with a weakening of the third BF component (Table 4.1). The future scenario simulations of CMIP5 and CMIP6 models present a warming of the JJA season in the eastern equatorial Atlantic of 2.54 ± 0.79 K and 2.70 ± 0.58 K, respectively. The multimodel ensemble mean of the CMIP5 and CMIP6 models show a warming of 2 K to 3 K in the tropical Atlantic sector between the historical and the future scenario simulations (Figures 4.3a and 4.3b). The spatial patterns of the future warming rate in the multimodel ensemble mean of both CMIPs are rather similar and show a strong zonally homogeneous warming along the equatorial band. The surface trade winds are projected to weaken in most of the tropical Atlantic in CMIP5 and CMIP6, coinciding with the warming pattern (Figures 4.3a and 4.3b). In the CMIP6 ensemble mean, the weakening of the surface trade winds is particularly strong in the eastern equatorial Atlantic and north of 10ºN (Figure 4.3b). Weaker equatorial trade winds will weaken equatorial upwelling, and thereby contribute to a weaker third component of the BF.

The vertical section of the difference between future scenarios and historical simulations of the equatorial Atlantic Ocean temperature clearly shows a stronger warming of the upper ocean, from the surface down to about 50 meters in the eastern equatorial Atlantic, and 70 meters in the western equatorial Atlantic in the CMIP5 ensemble mean (Figure 4.3c). The warming of the upper levels is rather zonally homogeneous in both CMIP5 and CMIP6. However, this is not the case for the deeper levels where the eastern equatorial Atlantic is warming faster than the western side of the basin; this warming pattern could be related to changes in oceanic circulation associated with the subtropical cells and AMOC (Chang et al., 2008). The strong warming of the upper levels in the ensemble mean of both CMIP generations leads to a deeper thermocline in the future scenario (Figures 4.3c and 4.3d). As the thermocline gets deeper the coupling between the thermocline and the SST gets weaker, because the stratification at the base of the mixed layer becomes weaker. In other words, the variability in the SST is less sensitive

to the variability of the thermocline, in agreement with the previously shown weakening of the third component of the BF (Figure 4.2c). The reduction of the SST variability could also be affected by changes in the thermodynamical coupling between the ocean and the atmosphere. However, we find that in the CMIP models the thermodynamical mechanism is not relevant for explaining the change in the SST variance between the future climate and the historical climate periods (Figure S2).

4.5   Impact of model biases

Coupled general circulation models show large biases in the tropical Atlantic region (Li and Xie, 2012; Richter et al., 2012, 2014; Richter and Tokinaga, 2020; Exarchou et al., 2018; Voldoire et al., 2019) and in particular, a warm SST bias in JJA in the eastern equatorial Atlantic, where projected changes in SST variability are largest. We explore to what extent our findings are affected by the model biases in the region. We find that the models with smaller bias have a stronger reduction of the SST variability (Figure 4.4a), a stronger reduction of the third component of the Bjerknes feedback (i.e., the thermocline feedback) (Figure 4.4b) and a larger SST change between future scenario and historical (Figure 4.4c). This is consistent with a previous study using different versions of the same climate model (Park and Latif, 2020). Therefore, biases in the models seem to suppress the reduction of the SST variability in a future warmer climate through a reduction of the weakening of the thermocline feedback. In light of these relationships, the reduction of future SST variability might indeed be larger than shown in this study if the models were unbiased and the reduction of the thermocline feedback were better captured.
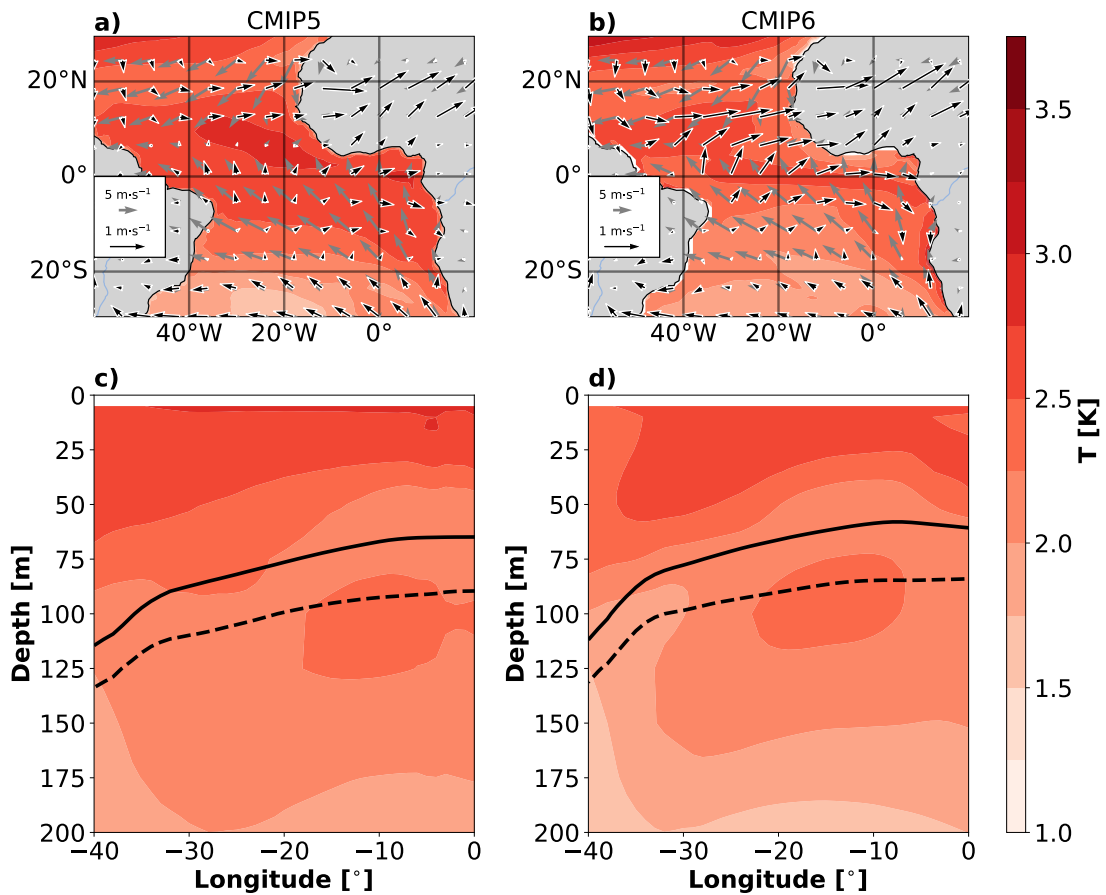
Figure 4.3: Mean state changes in the equatorial Atlantic. (Top row) Difference between future scenario and historical simulations of JJA SST (in shading) and JJA surface winds (black arrows) for the multi-model ensemble means of (a) CMIP5 and (b) CMIP6. The grey arrows depict the mean historical surface winds. The units are °C and m.s^{-1} for SST and for surface winds, respectively. (Bottom row) Vertical section of the difference in ocean temperature between future scenario and historical simulations for (c) CMIP5 and (d) CMIP6 multi-model ensemble means for June-July-August average. The black solid (dashed) line represents the depth of the 20°C isotherm, for the climatological mean of the historical (future scenario) period. The temperature has been latitudinally averaged from 3°S to 3°N. The periods taken for the historical and the future scenario simulations are 1950-99 and 2050-99, respectively.
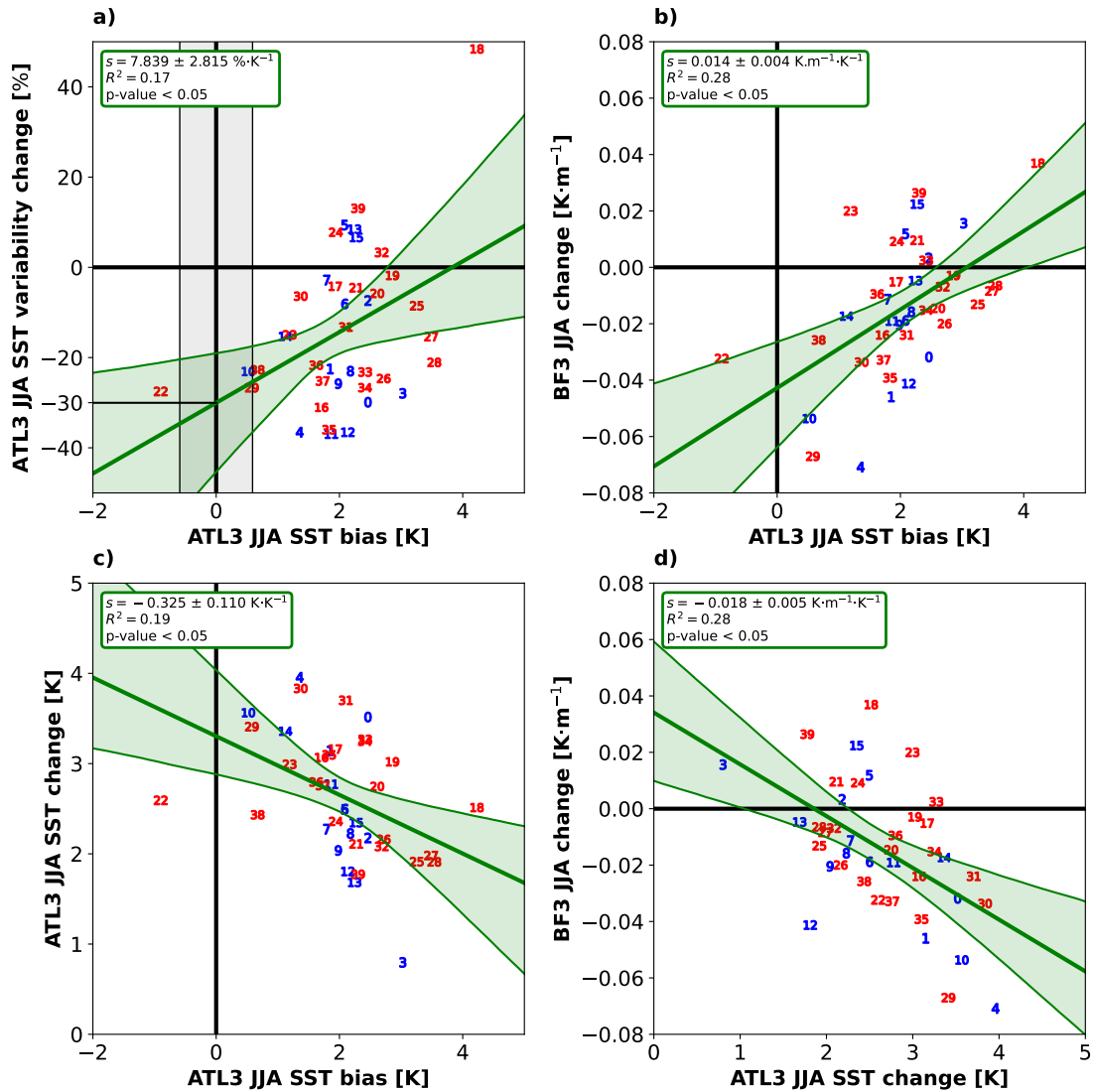
Figure 4.4: Impact of model biases. (a) Scatter plot of the JJA ATL3-averaged SST bias and relative SST variability change $((\sigma_{2050-2099} - \sigma_{1950-1999})/\sigma_{1950-1999})$. The SST bias is estimated as the difference between detrended model SST and detrended HadI-SST over the period 1950-1999. The grey shading around 0 K bias is $\pm$ the standard deviation of the detrended ATL3-averaged JJA HadI-SST over the period 1950-1999. (b) Scatter plot of JJA ATL3-averaged SST bias and BF3 change. (c) Scatter plot of JJA ATL3-averaged SST bias and mean SST change. (d) Scatter plot of JJA ATL3-averaged mean SST change and BF3 change. The change here is defined as the difference of the mean of the scenario period (2050-99) minus the mean of the historical period (1950-99). The green shading depicts the 95% confidence interval of the linear regression. The confidence interval is obtained by taking the 2.5th and 97.5th percentile of the distribution of the linear regressions of the 10000-time resampled datasets.

78

4.6 Concluding remarks

We show that the eastern equatorial Atlantic SST variability is projected to weaken under global warming, based on a comparison of historical and future highest emission scenario simulations of the CMIP5 and CMIP6 models. Similarly, the variability of the zonal surface wind in the western equatorial Atlantic will also weaken but explains only up to 32% the reduction in eastern equatorial interannual SST variability. Instead, the weakening of the third component of the Bjerknes feedback, the so-called thermocline feedback, explains up to 61% of the change in the SST variance. We find that in a warmer future climate the upper-layer of the ocean will become deeper and equatorial trade winds weaken. This together leads to a weakening of the thermocline feedback, because the thermocline decouples from the SST variability. This mechanism is remarkably different to the driving mechanisms of climate change in the equatorial Pacific, where the changes in the zonal SST gradient under greenhouse forcing are most relevant (Collins et al., 2010; Heede et al., 2020, 2021). However, in contrast to our findings in the Atlantic, the models in the Pacific show little agreement on the sign of the change in SST gradient (Heede et al., 2021).

The future weakening of the boreal summer SST variability in the eastern equatorial Atlantic shows large agreement across model ensembles of both CMIP generations. Moreover, the weakening of SST variability is found in the multi-model ensemble mean of all future scenarios (Figures S3 and S4), and in the majority of the individual models, and therefore we are rather confident in the robustness of our results.

The future weakening of the SST could be interpreted as an amplification of the already observed weakening in the recent decades that has been attributed to a weakening of the Bjerknes feedback and a stronger thermal damping (Prigent et al., 2020a; Silva et al., 2021). The role of the Bjerknes feedback in the CMIP models is a key for the weakening in SST variability. However, the CMIP models do not show any significant relationship between changes in the surface net heat fluxes and changes in the SST variability. Furthermore, the biases present in the CMIP models affect the amplitude of the SST variability. The weakening of the SST variability in the future is stronger in the models with less SST biases. Reducing the biases in the models should increase the reliability of the climate projections in the tropical Atlantic sector and greatly improve our assessment of climate change in the region.

4.7   Methods

Data. We use monthly mean model outputs obtained from the two latest CMIP international exercises: CMIP5 (Taylor et al., 2012) and CMIP6 (Eyring et al., 2016). We use the following fields from the CMIP models: sea surface temperature (SST), zonal surface wind anomalies (UASa), surface heat fluxes and the ocean potential temperature to derive the depth of the 20°C isotherm depth to use it as a proxy of the thermocline depth (z20 hereafter). In addition, we use the SST from the Optimum Interpolation SST analysis version 2 (OI-SST Reynolds et al. (2007)) available at 1° by 1° horizontal resolution for the period 1981/12 to 2019/12; the temperature from Ocean Reanalysis System Version 4 (ORA-S4, Balmaseda et al. (2013)) from the European Centre for Medium-range Weather forecast (ECMWF) available at 1° by 1° horizontal resolution for the period 1958/01 to 2017/12; and the zonal wind speed from ECMWF Re-Analysis (ERA)-interim (Dee et al., 2011) available at 0.5° by 0.5° horizontal resolution for the period 1979/01 to 2018/12 were used to estimate the three components of the Bjerknes feedback over the period 1982/01-2017/12. We investigate future climate changes in the equatorial Atlantic using the emissions future scenarios, rcp26, rcp45, rcp60, rcp85 and ssp126, ssp245, ssp370, ssp585, for CMIP5 and CMIP6, respectively. The climate models used in this study are listed in Table 4.1. All model data has been interpolated to a common horizontal 1° × 1° grid.

Statistical metrics. We use the standard deviation of the June-July-August (JJA) SST anomalies (SSTa) and the May-June-July (MJJ) zonal surface wind anomalies (UASa) as metrics to investigate the changes in variability between the simulated historical and future climate periods. The season JJA (MJJ) is chosen for the SST (UAS) variability as it is the season of largest SST (UAS) variability in CMIP5 and CMIP6 models. For this analysis we use the 50-year periods January 1950 to December 1999 and January 2050 to December 2099 for the historical and scenario simulations, respectively. We calculate the monthly anomalies by subtracting the seasonal cycle evaluated on each time period. We remove all linear trends prior to this analysis.

Quantification of dynamical ocean-atmosphere feedbacks. We compute the three components of the Bjerknes feedback that involve SST, thermocline depth and zonal surface winds to explore the potential dynamical drivers of the future changes in the SST variability (Lübbecke and McPhaden, 2017). The three components of the Bjerk-

nes feedback are estimated through linear regression of (1) western equatorial Atlantic (3°S-3°N, 40°W-20°; ATL4) zonal wind stress anomalies upon eastern equatorial Atlantic (3°S-3°N, 20°W-0°N; ATL3), (2) equatorial thermocline slope anomalies regressed onto ATL4 zonal wind stress anomalies and (3) SSTa in ATL3 upon thermocline depth anomalies in ATL3. The equatorial thermocline slope is computed as the difference between the mean z20 in ATL3 and ATL4.

4.8   Acknowledgements

4.9 Supplementary material
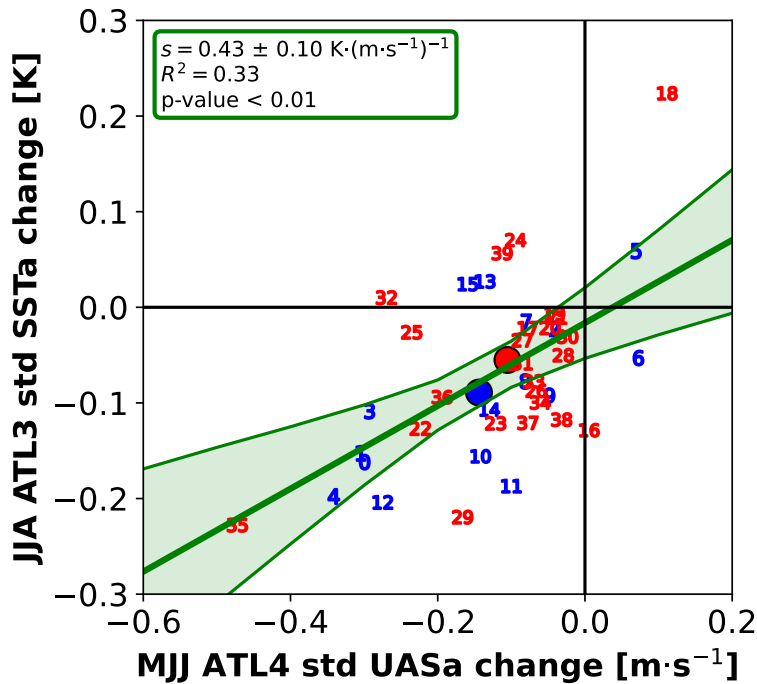
Figure S1: Linear regression between the change of the ATL3-averaged JJA SST variability and the change in ATL4-averaged MJJ UAS variability. The change is defined as the difference of the mean of the scenario period (2050-99) minus the mean of the historical period (1950-99). CMIP6 (CMIP5) models are presented with blue (red) numbers and the ensemble mean with a circle of the corresponding colour. The green shading depicts the 95% confidence interval of the linear regression. The confidence interval is obtained by taking the 2.5th and 97.5th percentile of the distribution of the linear regressions of the 10000-time resampled datasets.
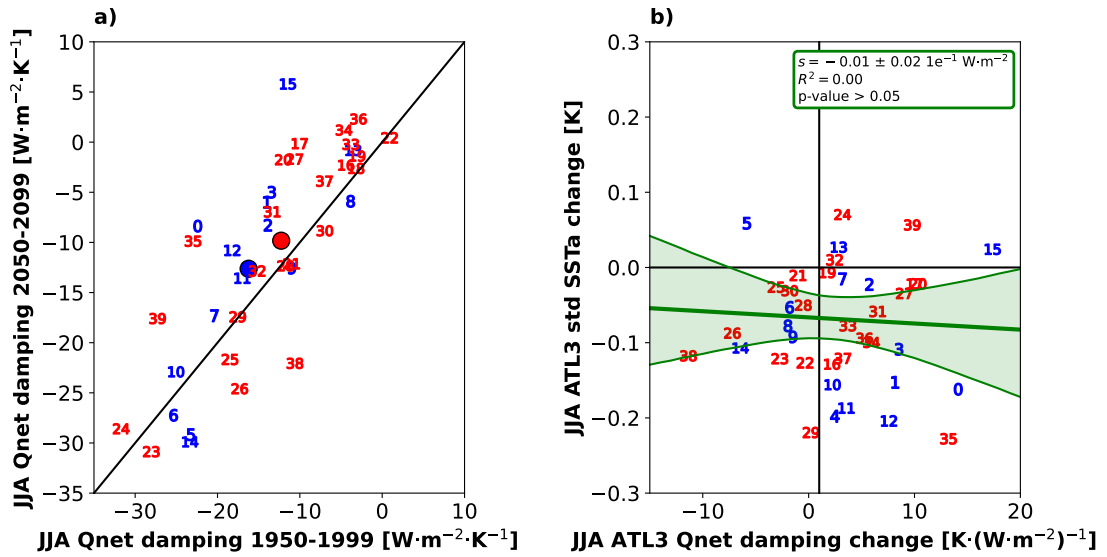
Figure S2: (a) Scatter plot of the ATL3 averaged JJA thermal damping for the historical period (1950-99) in the x axis against the ATL3 averaged JJA thermal damping for the scenario period (2050-99) in the y axis. Transparent numbers denote the models which exhibit a non-significant linear regression for either the historical or future period. The blue and dots represent the ensemble mean of the CMP6 and CMIP5 ensembles, respectively. The black line represents the no-change line and is added for easier interpretation. The green shading depicts the 95% confidence interval of the linear regression. The confidence interval is obtained by taking the 2.5th and 97.5th percentile of the distribution of the linear regressions of the 10000-time resampled datasets.
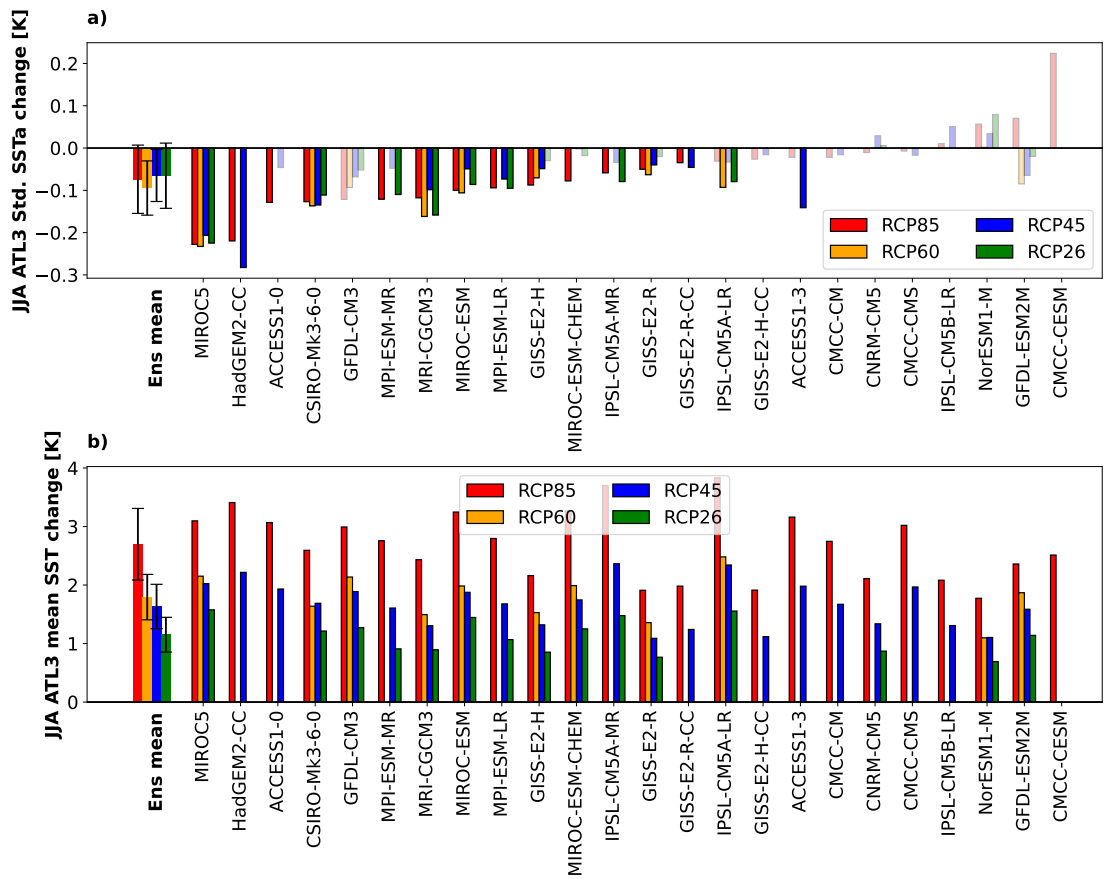
Figure S3: (a) Histogram representing the JJA ATL3-averaged SST variability change, i.e. 2050-2099 minus 1950-1999, for the following CMIP5 scenarios: RCP26 (green), RCP45 (blue), RCP60 (orange) and RCP85 (red). (b) same as (a) but for the JJA ATL3-averaged mean SST change. The ensemble means (Ens mean on the histogram) were evaluated only with the models that are common to the four scenarios. Light coloured bars indicate that the change in JJA ATL3-averaged SST variability is not significant at 95% according to the F-test.
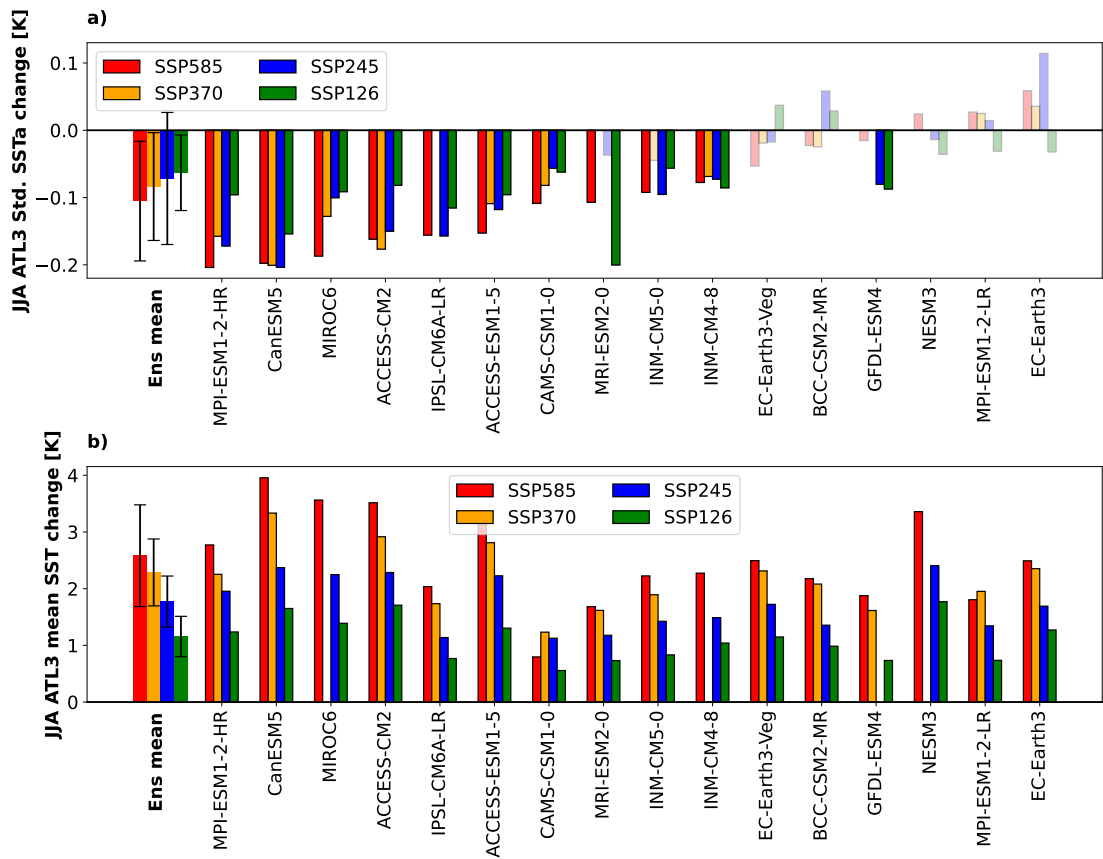
Figure S4: (a) Histogram representing the JJA ATL3-averaged SST variability change, i.e. 2050-2099 minus 1950-1999, for the following CMIP6 scenarios: SSP126 (green), SSP245 (blue), SSP370 (orange) and SSP585 (red). (b) same as (a) but for the JJA ATL3-averaged mean SST change. The ensemble means (Ens mean on the histogram) were evaluated only with the common models of the four scenarios. Light coloured bars indicate that the change in JJA ATL3-averaged SST variability is not significant at 95% according to the F-test.

Chapter 5

Future weakening of southeastern Tropical Atlantic Ocean interannual SST variability in a nested coupled model

Chapter 4 revealed that the eastern equatorial Atlantic interannual SST variability is projected to decrease in 80% of the 40 CMIP5 and CMIP6 models considered. As the eastern equatorial Atlantic and the ABA are strongly connected, future projections of interannual SST variability in the ABA may also weakened. As CMIP5 and CMIP6 models suffer from strong biases in the southeastern tropical Atlantic (Richter and Tokinaga, 2020), the global coupled model FOCI with enhanced oceanic resolution is used in Chapter 5 to investigate the future projections of the interannual SST variability in the ABA.

Citation: **Prigent, A.**, Imbol Koungue, R. A., Lübbecke, J. F., Brandt, P., Bayr, T., Harlaß, J., & Latif, M. (Under revision at Journal of Climate). Future weakening of southeastern Tropical Atlantic Ocean interannual SST variability in a nested coupled model.

The candidate designed the original study, carried out all the analyses, produced all the figures and authored the manuscript from the first draft to the submitted version.

Abstract

A coupled ocean-atmosphere model with an embedded high-resolution nest in the tropical Atlantic Ocean is used to investigate future changes in the southeastern tropical Atlantic interannual sea surface temperature (SST) variability in response to anthropogenic global warming. In the model, the Angola-Benguela Area (ABA) is among the regions in the tropical Atlantic that exhibit the largest surface warming. Relative to 1970-1999, the SST variability in the ABA during the peak season, May-June-July (MJJ), decreases by about 24% during 2070-2099 under the worst-case scenario of the Shared Socioeconomic Pathway 5-8.5 (SSP5-8.5). The MJJ interannual temperature variability weakens along the Angolan and Namibian coasts in the top 40 m of the ocean. This reduction appears to be due to a smaller temperature response to thermocline-depth variations, i.e. a weaker thermocline feedback. The weaker thermocline feedback is found where the thermocline deepens the most. Our model results suggest that the trend towards a weakening of the interannual SST variability in the ABA observed during the recent decades could persist in the future under a worst-case global warming scenario.

5.1   Introduction

The southeastern tropical Atlantic sea surface temperatures (SSTs) are marked by a strong seasonal cycle with warmest SSTs in March-April-May (MAM). The variations in the amplitude and phase of the seasonal cycle give rise to SST variability on various timescales, from subseasonal to decadal (Bachèlery et al., 2020; Imbol Koungue and Brandt, 2021). The extreme warm and cold events occurring off the coasts of Angola and Namibia, more precisely in the Angola Benguela Area (ABA, 10°S-20°S, within 2° off the coast), the so-called Benguela Niños and Niñas (Shannon et al., 1986), are the main features of the interannual SST variability. These events, typically peaking in MAM and lasting a few months, impact the regional climate (Rouault et al., 2003; Hansingo and Reason, 2009; Imbol Koungue et al., 2019; Koseki and Imbol Koungue, 2021), as well as marine ecosystems and fisheries (Bachèlery et al., 2016a; Binet et al., 2001; Gammelsrød et al., 1998).

Benguela Niños are mainly driven by two forcing mechanisms: (1) remote equato-

rial and (2) local atmospheric forcing. The remote equatorial forcing is associated with fluctuations of the trade winds over the western and central equatorial Atlantic, triggering equatorial Kelvin waves (EKWs, Illig et al. (2004)). EKWs propagate eastward to the West African coast (Polo et al., 2008), where a part of their energy is transmitted poleward as coastal trapped waves (CTWs, Clarke (1983); Illig et al. (2018b,a)). These CTWs, when reaching the Angolan and Namibian coasts, affect the SST, near-coastal stratification, currents and biogeochemical conditions (Bachèlery et al., 2016b, 2020; Illig and Bachèlery, 2019; Rouault, 2012; Rouault et al., 2018). The local atmospheric forcing includes alongshore wind modulations related to the strength of the South Atlantic anticyclone (Richter et al., 2010). These alongshore wind anomalies also trigger CTWs at the eastern boundary of the tropical Atlantic and modify the local currents (Junker et al., 2017). Lübbecke et al. (2019) showed that the reduction of the alongshore winds and associated local upwelling combined with other local processes such as anomalous heat fluxes, freshwater input and meridional advection can also generate an extreme warm event as the one in 2016.

The tropical Atlantic Ocean SST exhibits a marked multidecadal variability. Tokinaga and Xie (2011) reported a strong reduction of the eastern equatorial Atlantic interannual SST variability over the period 1950-2009, which was associated with an enhanced warming trend of the SST in this region. More recently, Prigent et al. (2020a) found that relative to the period 1982-1999, the eastern equatorial Atlantic interannual SST variability in May-June-July (MJJ) during 2000-2017 has decreased by 31%. Consistent with the strong connection between the equatorial Atlantic and the ABA (Reason et al., 2006; Lübbecke et al., 2010; Illig et al., 2020), Prigent et al. (2020b) reported a 30.5% reduction of the MAM interannual SST variability in the ABA during 2000-2017 relative to 1982-1999. As the ABA can be expected to continue to warm during this century due to anthropogenic global warming (Bakun et al., 2015; Wang et al., 2015), the question arises how the interannual SST variability in the ABA will change in the future. In this study, we address this question utilizing two ensembles of a coupled model with a high-resolution nest in the tropical and Southern Atlantic Ocean. The paper is organized as follows: the data and methods are described in section 5.2. The future changes in the interannual SST variability of the ABA are presented in section 5.3, and the underlying mechanisms are analyzed in section 5.4. The mean-state changes and

their influences on the interannual variability are discussed in section 5.5. Section 5.6 provides a brief summary and a discussion of the main findings.

5.2 Data, methodology and model verification

5.2.1 Data

Model description and experiments

Here we use the FOCI model (Flexible Ocean Climate Infrastructure; Matthes et al. (2020)) which is composed of the atmospheric model ECHAM6.3 (Stevens et al., 2013) coupled to the NEMO3.6 (Madec et al., 2017) ocean model using the OASIS3-MCT coupler (Valcke, 2013). The atmospheric component is the T63L95 setting of ECHAM6 with approximately $1.8° \times 1.8°$ horizontal resolution, 95 vertical hybrid sigma-pressure levels and the top at 0.01 hPa. The version of the ocean component is NEMO-ORCA05 (Biastoch et al., 2008) with a horizontal resolution of $0.5° \times 0.5°$ and 46 z-levels in the vertical. A high-resolution ocean nest (INALT10X; Schwarzkopf et al. (2019)) with horizontal resolution enhanced to $1/10°$ in the tropical and Southern Atlantic as well as the western Indian Ocean (70°W to 70°E, 63°S to 10°N) is embedded in the ocean via a two-way nesting approach. The nest enables, for example, enhanced representation of equatorial Kelvin and coastal trapped waves. Six out of the ten model runs used in this study include interactive chemistry in the atmosphere simulated by the Model for Ozone and Related Chemical Tracers (MOZART3, Kinnison et al. (2007)) and implemented in ECHAM6 (ECHAM6-HAMMOZ; Schultz et al. (2018). Temporal variations in solar radiation follow the CMIP6 recommendations provided by the SOLARIS-HEPPA project (Matthes et al., 2017). The model runs with and without interactive chemistry in the atmosphere yield very similar results with respect to tropical Atlantic climatology and variability. The future-scenario runs of FOCI (future ensemble hereafter) used here are forced by the Shared Socioeconomic Pathway 5-8.5 (SSP5-8.5, O'Neill et al. (2016)), representing the high end of the range of the future scenarios that can be considered as a worst-case scenario with a very strong increase of atmospheric greenhouse gas concentrations. The CO_2-concentration at the end of the simulations in 2100 amounts to 1135 ppm. More information on the FOCI configuration can be

90

found in Matthes et al. (2020). The results from the scenario ensemble are compared to an ensemble of four historical simulations (historical ensemble hereafter) that employ observed external forcing for the period 1951-2013. Finally, the last 1000 years of a 1500-year long preindustrial control run are used to estimate the internal variability of multidecadal SST-variability trends in the FOCI model. The preindustrial control run, however, was performed without the nest. The preindustrial control run is initialized with the PHC2.1 climatology (Steele et al., 2001) for temperature and salinity. The FOCI experiments used in this study are listed in Table 5.1.

Table 5.1: Simulations with the FOCI model used in this study. The historical ensemble consists of four and the future ensemble of six simulations. MOZART3 denotes interactive atmospheric chemistry. INALT10X indicates the use of the oceanic nest with a resolution of 1/10°. SSP5-8.5 indicates that the run is forced by the SSP5-8.5 future scenario.

Run	Time period	Configuration
FOCI1.13-II005	1951-2013	T63L95 + MOZART3 + INALT10X, Historical
FOCI1.14-II006	1951-2013	T63L95 + MOZART3 + INALT10X, Historical
FOCI1.14-II007	1951-2013	T63L95 + MOZART3 + INALT10X, Historical
FOCI171-JH015	1951-2013	T63L95 + INALT10X, Historical
FOCI1.14-II010	2014-2099	T63L95 + MOZART3 + INALT10X, SSP5-8.5
FOCI1.14-II011	2014-2099	T63L95 + MOZART3 + INALT10X, SSP5-8.5
FOCI1.14-SW128	2014-2099	T63L95 + MOZART3 + INALT10X, SSP5-8.5
FOCI1.14-JH027	2014-2099	T63L95 + INALT10X, SSP5-8.5
FOCI1.14-JH037	2014-2099	T63L95 + INALT10X, SSP5-8.5
FOCI1.14-JH039	2014-2099	T63L95 + INALT10X, SSP5-8.5
FOCI1.3-SW038	1850-3349	T63L95, preindustrial control run under 1850 climate conditions, initialized from an ocean at rest and PHC2.1 climatology (Steele et al., 2001) for temperature and salinity

Observational and reanalysis datasets, and CMIP6 models

For model comparison, we use the fifth generation of the European Centre for Medium-range Weather Forecast (ECMWF) atmospheric reanalysis (ERA5; Hersbach et al. (2020)), with $0.25° \times 0.25°$ horizontal resolution that is available for January 1950 to December 2020. We also use the SST from the Hadley Centre Sea Ice SST data set Version 1.1 (HadISST; Rayner (2003)), with $1° \times 1°$ horizontal resolution that is available for January 1870 to December 2020.

Fifteen models from the Coupled Model Intercomparison Project phase 6 (CMIP6; Eyring et al. (2016); see Table S1 in section 5.7) are used to compare the performance of FOCI in simulating the tropical Atlantic SST mean-state, seasonal cycle and interannual variability. The corresponding preindustrial control runs are used to estimate the internal variability of multidecadal SST-variability trends in the CMIP6 models. Prior to all analyses, the data from the CMIP6 models were interpolated onto a $1° \times 1°$ horizontal grid.

5.2.2   Methodology

Definition of anomalies

In order to calculate the future changes in interannual SST variability, we compare the results of the future ensemble with that from the historical ensemble using the periods January 1970 to December 1999 and January 2070 to December 2099. Two methods were applied to compute the SST anomalies: (1) monthly-mean anomalies are computed by subtracting the climatological monthly-mean seasonal cycle derived separately for the periods 1970-1999 and 2070-2099. Prior to the computation, the linear trend estimated over each 30-year period was removed; (2) the monthly-mean anomalies were computed by subtracting a detrended 31-year moving climatological monthly-mean seasonal cycle. The two methods yield very similar results and method (1) has been applied below, except in section 5.5 where method (2) is applied. For the computation of the vertical sections, the output of the ocean-model output at $0.5°$ horizontal resolution has been used.

Thermocline definition

Two commonly used proxies for the thermocline depth in the tropical Atlantic are used in this study: (1) the 20°C isotherm depth (Z20) and (2) sea surface height (SSH). Z20 allows us to assess the thermocline feedback over the vertical. As Z20 in the south-eastern tropical Atlantic may occasionally outcrop during the year leading to gaps in the Z20 time series, only the regression coefficients obtained from a local Z20 time series that is at least two third of the length of the local temperature time series are considered when regressing the temperature upon Z20 anomalies. In the equatorial Atlantic, the variability in the Z20 and the depth of the maximum vertical temperature gradient are quite well correlated (~ 0.52). However, along the West African coast, the depth of the maximum vertical temperature gradient is much shallower than the Z20, and therefore the two variables are hardly correlated (~ -0.19). Nevertheless, we decided to use the Z20 as a proxy for thermocline depth, because the change in temperature variability matches well with the reduced temperature response to Z20 variations (see section 5.4). Using SSH allows us to investigate the thermocline feedback horizontally, as in previous studies (e.g. Keenlyside and Latif (2007)), because SSH is independent of outcropping. Further, Z20 and SSH variations are highly correlated (~ 0.81) over the equatorial Atlantic (20°W-0°; 1°S-1°N).

5.2.3 Model verification

A common problem in coupled models is the warm SST bias along the West African coast and over the eastern and central equatorial Atlantic (e.g. Richter (2015)). The ensemble mean SST biases in the CMIP6 (Figure 5.1a) and FOCI ensemble (Figure 5.1b) have been quantified relative to HadISST over the period 1970-1999. Compared to the CMIP6 ensemble mean, the FOCI ensemble exhibits a reduced SST bias off the West African coast (Figure 5.1c). Yet, a considerable SST bias remains (Figure 5.1b). The remaining bias could be partly due to the coarse atmospheric resolution (approximately 1.8°×1.8°), causing a misrepresentation of the near-coastal low-level winds (Harlaß et al., 2018; Kurian et al., 2021). Both ensembles simulate a realistic phase of the SST annual cycle (Figure 5.1d), but too warm SSTs throughout the calendar year.
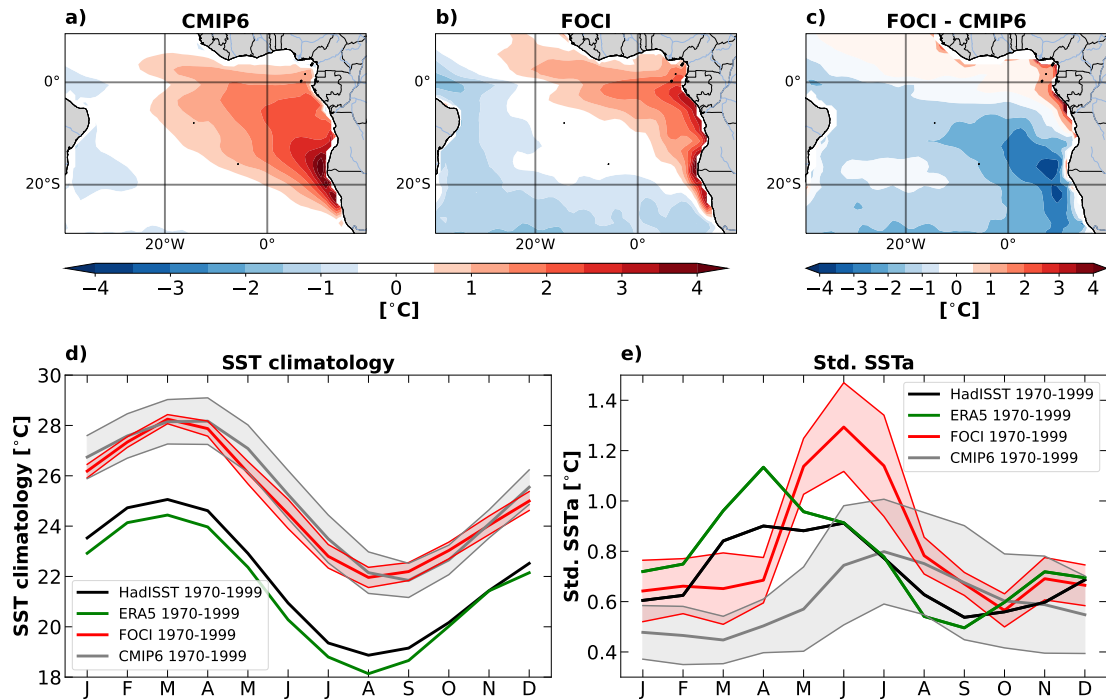
Figure 5.1: Simulation of SST. (a) CMIP6 ensemble mean minus HadISST (1970-1999), (b) FOCI ensemble mean minus HadISST (1970-1999). (c) FOCI (b) minus CMIP6 (a). (d) ABA-averaged SST climatology 1970-1999 calculated from the FOCI ensemble (red line) and the CMIP6 ensemble (grey line). The black (green) line represents HadISST (ERA5). (e) Same as (d) but for the ABA-averaged interannual SST variability expressed by the standard deviations. The red and grey shadings represent the ensemble spreads, defined as $\pm$ 1 standard deviation of each ensemble.

State-of-the-art coupled models are known to underestimate and misrepresent the seasonality of the interannual SST variability in the ABA (Richter and Tokinaga, 2020). The CMIP6 and FOCI ensembles both fail to simulate a realistic seasonality of the ABA-averaged interannual SST variability (Figure 5.1e). A lag of two to three months in the peak of the ABA-averaged SST variability is common in the models (Richter and Tokinaga, 2020). The bias in timing, however, may be reducible when enhancing the atmospheric resolution (Harlaß et al., 2018). We note the strong peak in the standard deviation in early boreal summer in FOCI.

Empirical Orthogonal Function (EOF) analysis is applied to the SST anomalies (SSTa) from FOCI (Figure 5.2a) and HadISST (Figure 5.2b) over the tropical Atlantic (40°W-20°E, 30°S-10°N) for the period 1970-1999. The first EOF (EOF1) calculated from the FOCI historical ensemble (Figure 5.2a), accounting for 25% of the variance,

agrees well with the EOF1 from HadISST (Figure 5.2b) which explains 42% of the variance.
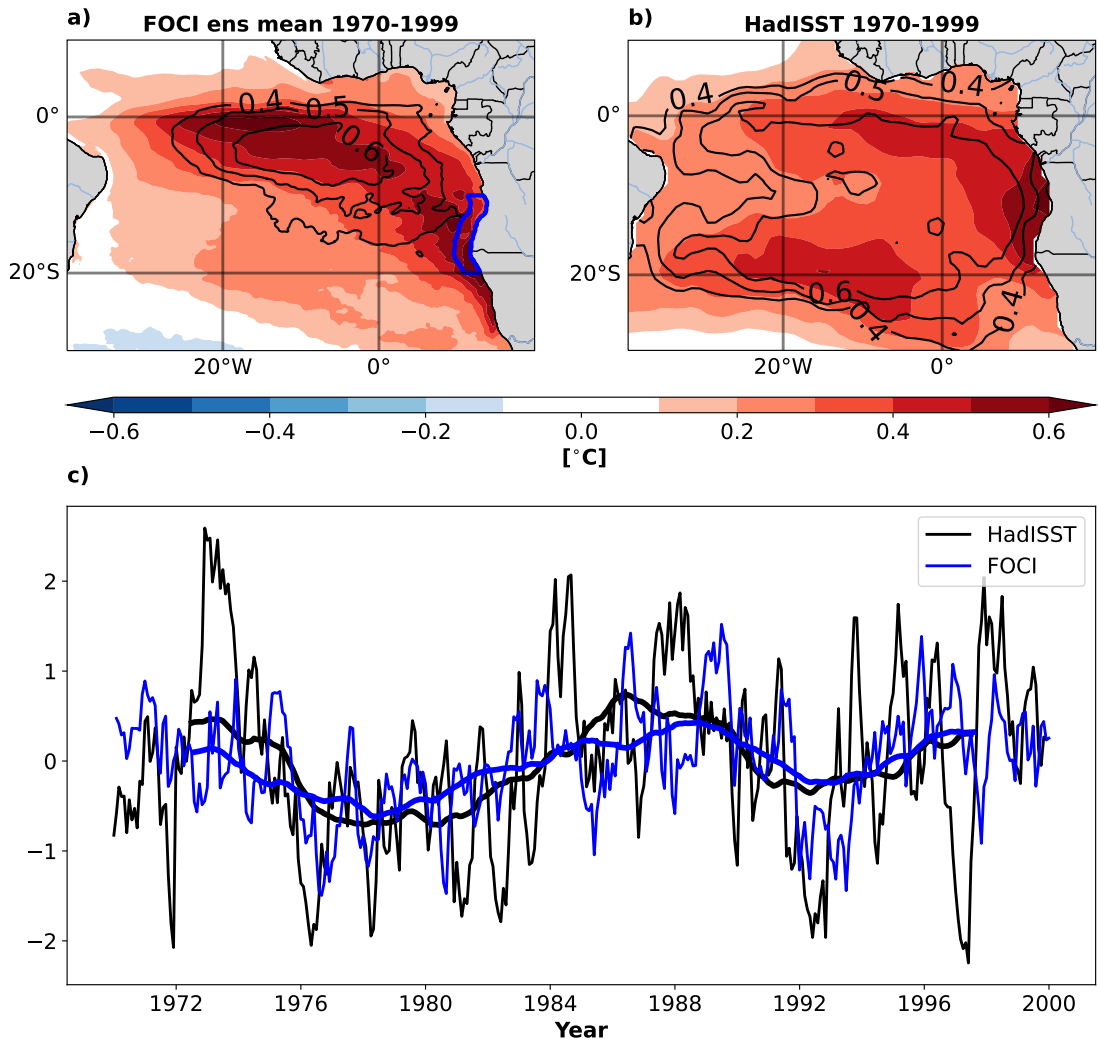
Figure 5.2: (a) EOF1 of the SST anomalies over the tropical Atlantic (40°W-20°E, 30°S-10°N) during 1970-1999 calculated from the FOCI historical ensemble. (b) Same as (a) but from HadISST. Black contours represent the variance explained locally by EOF1. (c) First principal component (PC1) from FOCI (blue) and HadISST (black). The thick black and blue lines are the 5-year running means.

There is high variability in the equatorial Atlantic and along the Angolan and Namibian coasts from 10°S to 20°S (the ABA is denoted by the blue contour in Figure 5.2a), which is the focus of this study. The variance explained locally by EOF1 indicates that it is more concentrated in the equatorial region in FOCI than in HadISST. The corresponding leading principal components (PC1s) (Figure 5.2c) exhibit a correlation of 0.85 on decadal time scale, as estimated by the correlation between the 5-year running

means, which suggests that external forcing plays a role in the long-term variability.

5.3 SST variability changes

The southeastern tropical Atlantic Ocean exhibits a strong warming in response to the rising CO_2-concentration, with the strongest rise in SST in the ABA (Figures 5.3a and 5.3b). Relative to 1970-1999, the annual mean (MJJ) SST has increased by 3.36 $\pm$ 0.40°C (2.82 $\pm$ 0.6°C) in the ABA during 2070-2099. The ABA-averaged inter-annual SST variability experiences an overall reduction during 2070-2099 relative to 1970-1999 (Figure 5.3b), with the strongest reduction in May-June-July (MJJ), i.e. the peak phase of the variability in the model. When considering all calendar months, the standard deviation of the ABA-averaged interannual SST anomalies (SSTa) amounts to 0.80 $\pm$ 0.08°C during 1970-1999 and 0.63 $\pm$ 0.03°C during 2070-2099, corresponding to a reduction of 21.2%. In MJJ, the standard deviation of the ABA-averaged SSTa amounts to 1.19 $\pm$ 0.15°C during 1970-1999 and 0.90 $\pm$ 0.05°C in 2070-2099, corresponding to a reduction of 24.4%. In FOCI, the seasonal cycle of the standard deviation of the ABA SSTa during 1970-1999 exhibits a prominent peak in MJJ (Figure 5.3b). In observations, the peak in variability occurs in March-April-May (MAM) that is associated with the Benguela Niños/Niñas (Imbol Koungue et al., 2017). Figure 5.3c depicts the differences in the standard deviation of SSTa in MJJ between the ensemble means of the future and the historical simulations. The differences exhibit a cold-tongue like pattern of reduced interannual SST variability with largest declines amounting to about -0.3°C in the ABA and central equatorial Atlantic.
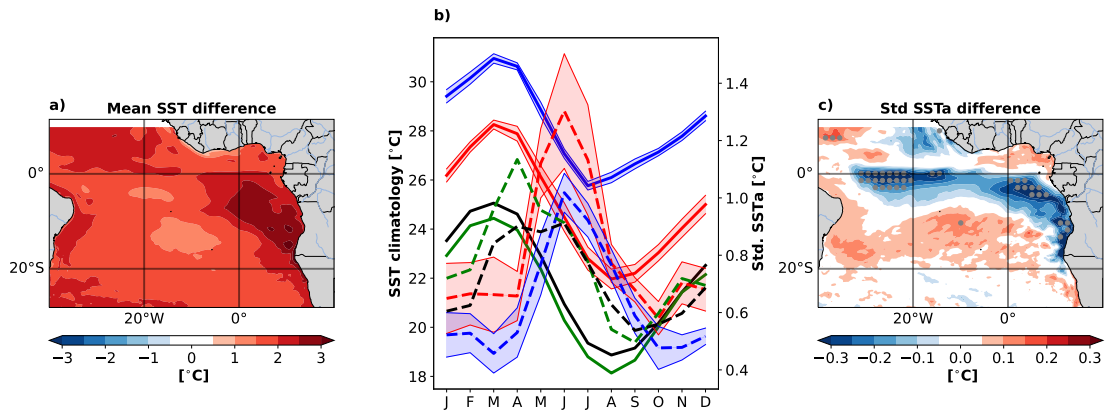
Figure 5.3: CO$_2$-forced response in the FOCI model. (a) Difference between mean MJJ SST between 2070-2099 and 1970-1999. (b) ABA-averaged SST climatology (solid lines) as a function of the calendar month during 1970-1999 (red) and 2070-2099 (blue), and from HadISST and ERA5 during 1970-1999 (black and green, respectively). Ensemble-mean standard deviation of ABA-averaged SSTa (dashed lines) as a function of the calendar month during 1970-1999 (red) and 2070-2099 (blue), and from HadISST and ERA5 during 1970-1999 (black and green, respectively). The blue and red shadings represent the ensemble spread, defined as $\pm$ 1 standard deviation of each ensemble. (c) Difference in the standard deviations of the MJJ SSTa between 2070-2099 and 1970-1999.

Changes in temperature variability are not restricted to the surface. The MJJ inter-annual temperature variability has changed in the top 200 m along the equator and the Southwest African coast. During 1970-1999, strong interannual variability was located near the mean Z20, reaching the surface at the equator between 30°W and 10°W (Figure 5.4a) and along the Southwest African coast between 10°S and 20°S (Figure 5.4b). During 2070-2099, the interannual variability is weaker along the equator at the position of the mean Z20 (Figures 5.4c and 5.4e). Along the Southwest African coast, the interannual variability has weakened in the top 35 m but increased between 35 m and 55 m in the latitude range 0°-15°S (Figures 5.4d and 5.4f).
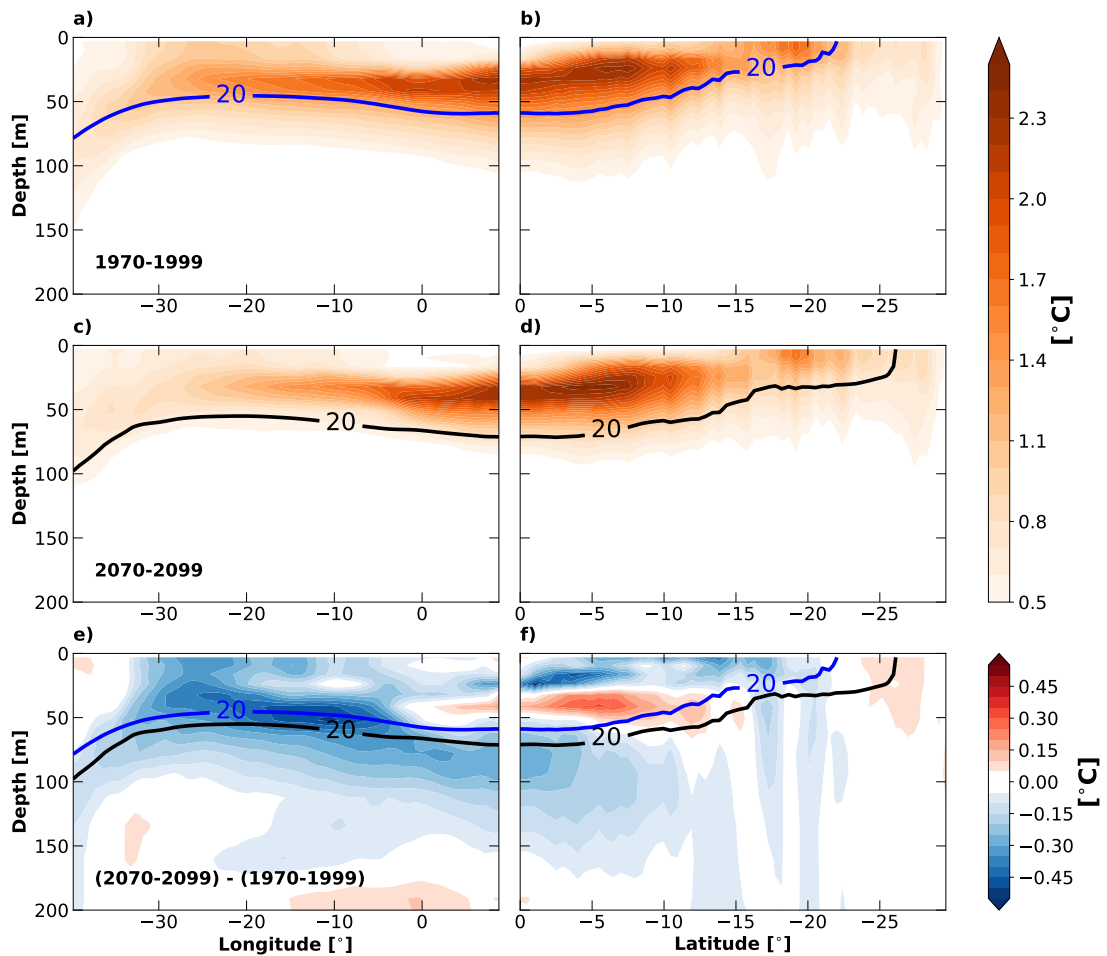
Figure 5.4: Changes in interannual temperature variability in the upper 200 m. (a, b) Vertical sections of the standard deviation of the detrended temperature anomalies in MJJ during 1970-1999 along the equator (averaged between 1°S-1°N) and along the Southwest African coast (averaged within a 2° band), respectively. (c, d) same as (a, b), but for the period 2070-2099. (e, f) Differences between the standard deviations during the two epochs, calculated as 2070-2099 (c, d) minus 1970-1999 (a, b). The blue (black) solid line is the position of the depth of the mean 20°C isotherm (Z20) during 1970-1999 (2070-2099). Small values (≤ 0.5°C) of MJJ temperature variability are in white in (a, b) and (c, d).

5.4 Mechanisms reducing the SST variability

5.4.1 Role of remote and local atmospheric processes

Both equatorial zonal wind stress and local meridional wind-stress fluctuations are known to be important drivers of interannual SST variability in the ABA (Lübbecke et al., 2010; Richter et al., 2010). Equatorial zonal wind stress fluctuations can trigger EKWs that propagate eastward along the equator. When reaching the West African coast the wave energy will be partly reflected as westward propagating Rossby waves. A substantial part of the energy will be transmitted poleward as CTWs (Polo et al., 2008). Downwelling (upwelling) CTWs can trigger warm (cold) events in the ABA by deepening (shoaling) the thermocline (Bachèlery et al., 2020; Illig et al., 2004; Imbol Koungue et al., 2017, 2019; Lübbecke et al., 2010; Imbol Koungue and Brandt, 2021).

Relative to 1970-1999, the link between western/central equatorial wind stress and ABA SSTs has become slightly less important during 2070-2099 (Figures 5.5a and 5.5b). In contrast, we observe a strengthened link between ABA SSTa and (1) the near-coastal wind-stress (Figures 5.5a and 5.5b) and (2) near-costal wind-stress curl anomalies (Figures 5.5c and 5.5d) during 2070-2099 relative to 1970-1999, suggesting that the role of the local wind-stress fluctuations in driving interannual SST variability in the ABA has increased.
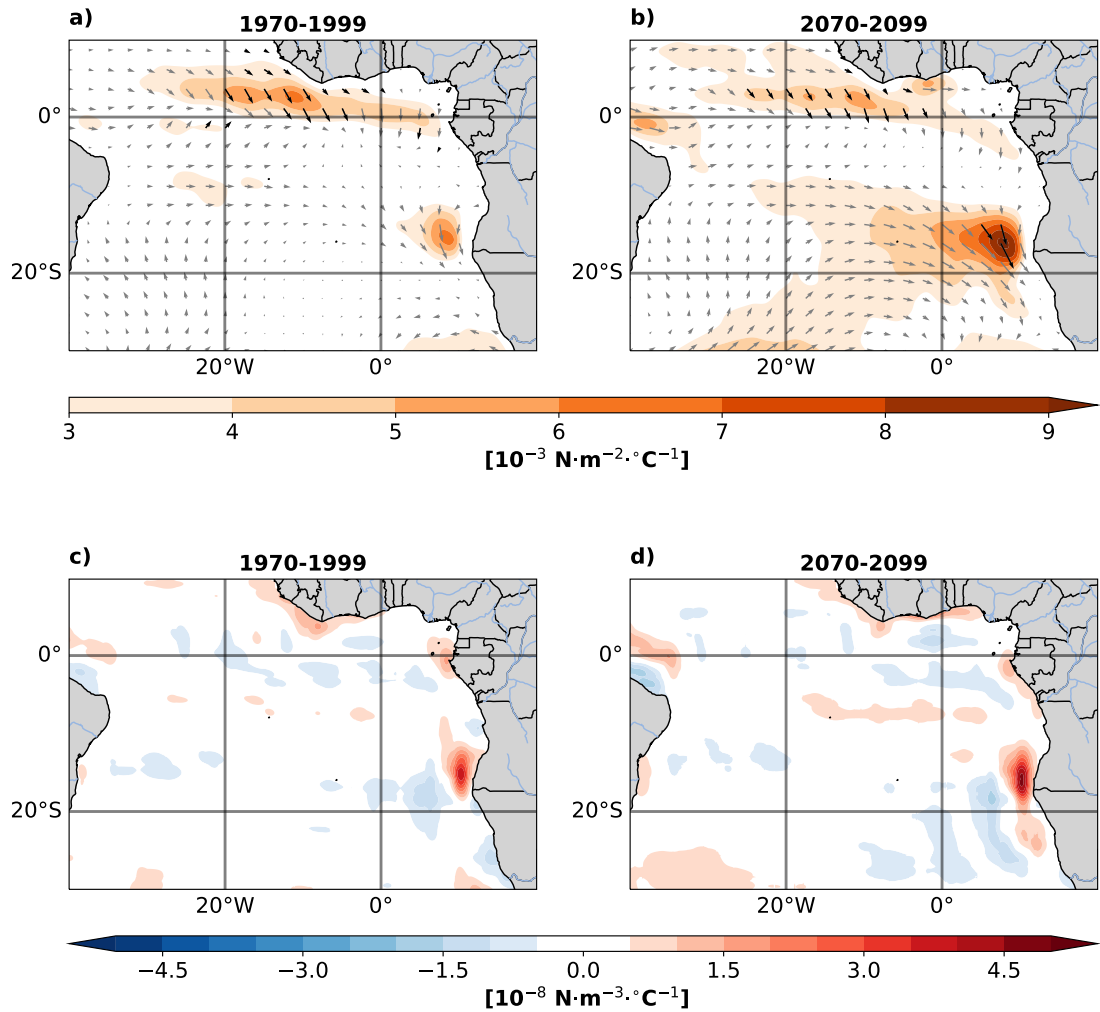
Figure 5.5: Influence of wind-stress and wind-stress curl anomalies in MJJ. (a, b) Regressions of detrended wind-stress anomalies on ABA-averaged SSTa. (a) 1970-1999 and (b) 2070-2099. Regressions have been calculated for each wind-stress component separately. Black (grey) arrows indicate pointwise significant (not significant) regressions for both components at the 95% level. Color shading depicts the magnitude of the vectors. (c, d) Regressions of wind-stress curl anomalies on ABA-averaged SSTa. (c) 1970-1999 and (d) 2070-2099. Displayed regressions are significant at the 95% level. Significance is assessed by the Student's t test.

5.4.2   Role of the thermocline feedback

Surface/subsurface coupling plays an important role in driving interannual SST variability in the ABA (Imbol Koungue et al., 2017; Bachèlery et al., 2020). To examine the coupling between ABA SSTa and thermocline-depth variations, termed thermocline

feedback, we pointwise regressed the SSTa on the SSH anomalies. The latter serve here as a proxy for thermocline-depth variations. During 1970-1999, large regression coefficients are observed at the equator between 30°W and 10°W and along the Southwest African coast from 10°S to 20°S where the thermocline is relatively shallow (Figure 5.6a). We observe a similar pattern but with smaller regression coefficients, particularly in the ABA, during 2070-2099 (Figure 5.6b). The smaller regression coefficients illustrate a reduction of the SST response to thermocline perturbations (Figure 5.6c). The thermocline feedback in the ABA, as estimated in this manner, has reduced by 21.4%, from 30.45 ± 2.56 °C·m^{-1} during 1970-1999 to 23.92 ± 2.18 °C·m^{-1} during 2070-2099. Noteworthy, the regions of reduced thermocline feedback are collocated with the regions where the Z20 has deepened the most (Figure 5.6c).
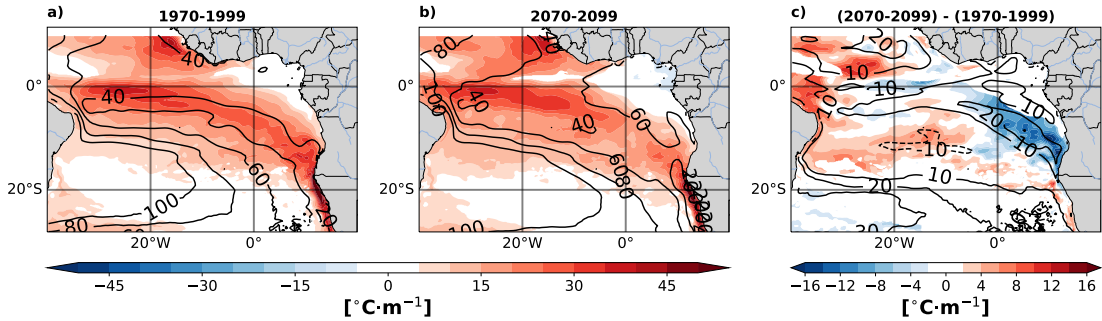
Figure 5.6: Pointwise regression coefficients of SST anomalies on the SSH anomalies (serving as proxy for thermocline-depth variations) in MJJ during (a) 1970-1999, (b) 2070-2099, and (c) their differences. Black contours in (a) and (b) indicate the mean Z20 in MJJ, and in (c) the change in Z20 between the two periods. Displayed values are significant at 95% according to the Student's t-test. The data have been detrended prior to the analyses. Only regressions with values larger than ± 5 °C·m^{-1} are plotted in (a) and (b).

We next examine the regressions of the temperature anomalies upon the Z20 anomalies at the equator and along a 2° band along the Southwest African coast (Figure 5.7). The Z20 is used here as a proxy for the thermocline depth (see section 5.2.2). During 1970-1999, the co-variability between temperature and Z20 anomalies (Figures 5.7a and 5.7b) is strong within about ± 40 m of the mean Z20 (blue bold line). In the central equatorial Atlantic (30°W-10°W), where the thermocline is shallow, large regression coefficients also appear at and just below the base of the mixed layer (blue dashed line),

which illustrates the thermocline feedback effectiveness (Dewitte et al., 2013). Along the West African coast, large regression coefficients appear at the base of the mixed layer in the region 0°S-17°S and above the base in the region 17°S-20°S. We note that south of 22°S (26°S), no regression coefficients can be calculated as the thermocline outcrops during 1970-1999 (2070-2099). During 2070-2099 (Figures 5.7c and 5.7d), the temperature response to thermocline-depth variations has weakened between the base of the mixed layer and Z20 along the equator, and near the base of the mixed layer along the West African coast (Figures 5.7e and 5.7f). This suggests a reduction of the effectiveness of the thermocline feedback during 2070-2999 relative to 1970-1999. In addition, there is a deepening of the mean Z20 along the equator and Southwest African coast, consistent with Figure 5.6. Furthermore, the increased (decreased) response of the temperature anomalies to Z20-variations is co-located with the increased (decreased) interannual temperature variability (Figures 5.7e and 5.7f; thin black contours). Bachèlery et al. (2020), using model experiments, showed that equatorially forced CTWs explains up to 70% of the 0-200 m integrated temperature fluctuations in the ABA. This supports our result that the reduced interannual SST variability in 2070-2099 is mainly driven dynamically by the reduced SST/temperature response to thermocline-depth variations. Further, Figure 5.6 suggests that the weaker thermocline feedback is due to the deepening of the mean Z20, linking the change in the interannual variability to the mean-state changes.
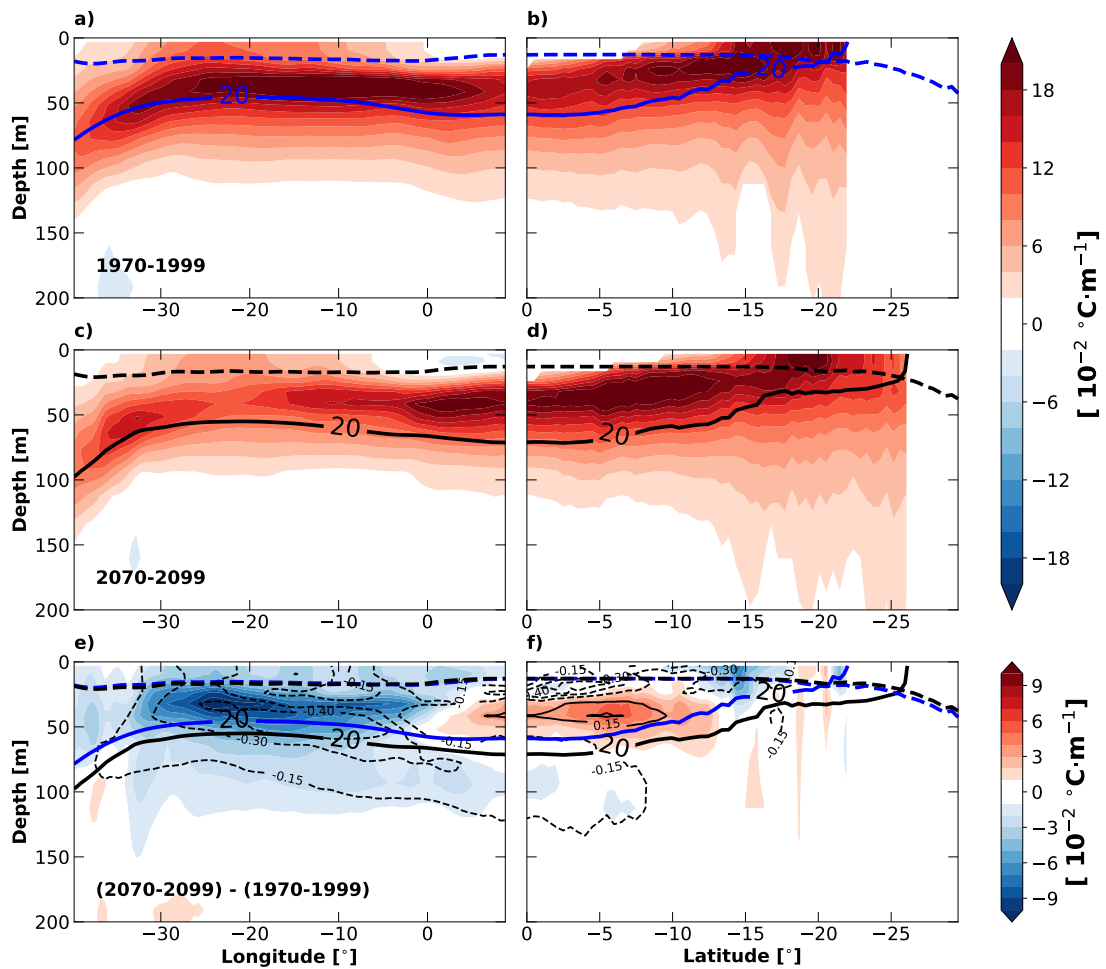
Figure 5.7: Role of thermocline-depth variations on upper-ocean temperature. (a, b) Regression coefficients in the upper 200 m of temperature upon Z20 anomalies (serving as proxy for thermocline-depth variations) in MJJ during 1970-1999 at the equator (40°W-9°E; 1°S-1°N) and along a 2° band along the Southwest African coast, respectively. (c, d) same as (a, b) but for the period 2070-2099. (e, f) Differences between the two periods. The blue (black) bold solid line is the mean depth of the 20°C isotherm (Z20) during 1970-1999 (2070-2099). The blue (black) dashed thick line represents the mean mixed layer depth during 1970-1999 (2070-2099). Black contours in (e, f) represent the change in MJJ temperature variability with dashed (solid) contours showing a decrease (increase) in variability during 2070-2099 relative to 1970-1999. Displayed values are significant at 95% according to the Student's t-test. The data have been detrended prior to the analyses. Only regressions with values larger than $\pm\, 2 \times 10^{-2}\,°\text{C·m}^{-1}$ are plotted in (a) and (b).

5.5 Mean-state changes

We next examine in more detail the mean-state changes in MJJ along the equator and at the Southwest African coast. Figures 5.8a to 5.8c depict the warming pattern during 2070-2099 relative to 1970-1999 in the top 200 m. Largest warming ($> 2.5°C$) occurs in the top 50 m in the eastern equatorial Atlantic and between $0°S$ and $20°S$ along the Southwest African coast.
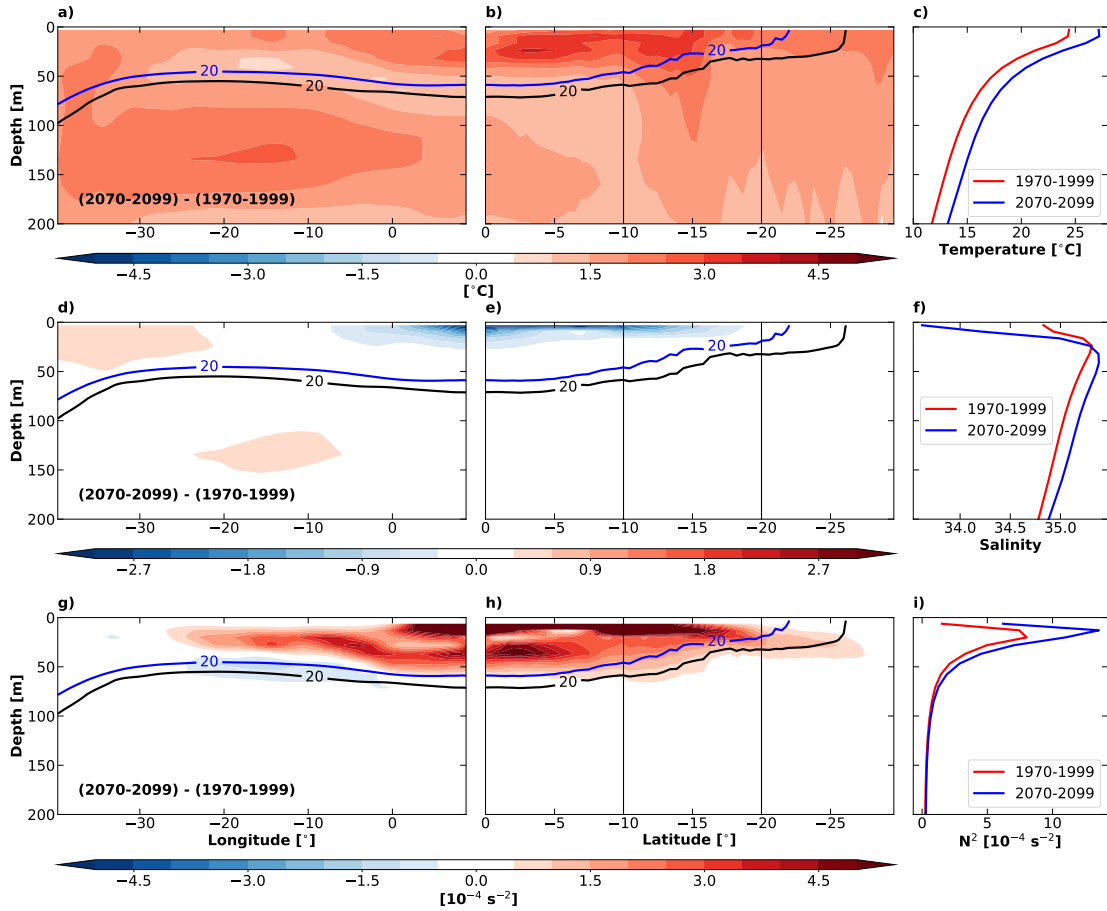
Figure 5.8: Mean-state changes. (a, b) Upper-ocean (0-200 m) temperature differences in MJJ between 2070-2099 and 1970-1999 at the equator (40°W- 9°E; 1°S-1°N) and along a 2° band along the Southwest African coast (30°S-0°), respectively. (d, e) Same as (a, b), but for the salinity. (g, h) Same as (a, b), but for the Brunt-Väisälä frequency (N^2). (c, f, i) are the ABA-averaged temperature, salinity and N^2 profiles for 1970-1999 (red) and 2070-2099 (blue). The ABA is denoted by the black vertical lines in b, e, f.

In these regions, the ocean in the top 25 m also is becoming fresher (Figures 5.8d to 5.8f). The surface freshening could be the result of the increased precipitation over

the eastern tropical Atlantic during 2070-2099 relative to 1970-1999 (Figure 5.9). This result is consistent with Park and Latif (2020), who used the Kiel Climate Model, a predecessor of the FOCI system, with a coarse-resolution ocean model ($2° \times 0.5°$ in the equatorial Atlantic) coupled to ECHAM5 at two different resolutions (T42L31 and T255L62). The temperature (Figure 5.8e) and salinity ((Figure 5.8f) changes act to increase the stratification from the surface to the mean Z20 (Figures 5.8g to 5.8i), favoring a weaker thermocline feedback and thus supporting reduced SST variability in the ABA.
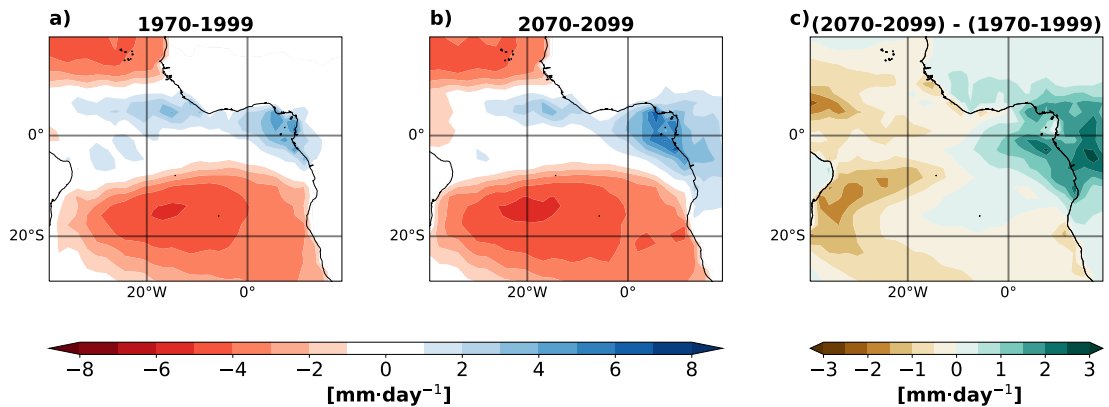
Figure 5.9: Mean-state change in the modeled surface-freshwater flux. (a) Mean precipitation minus evaporation during 1970-1999. (b) Same as (a), but for 2070-2099. (c) Differences between the two periods.

5.6 Summary and discussion

In this study, we compared two ensembles performed with the climate model FOCI, which employs a high-resolution nest in its oceanic component, to investigate potential future changes in the interannual SST variability over the southeastern tropical Atlantic Ocean, in particular the ABA. One ensemble is a set of historical simulations, the other a set of simulations forced by the SSP5-8.5 scenario. The ABA-averaged interannual SST variability in MJJ weakens by 24.4%, from $1.19 \pm 0.15°C$ during 1970-1999 to 0.90 ± 0.05 °C in 2070-2099. Further, the interannual temperature variability has reduced in the top 35 m along the Southwest African coast between $0°$ and $20°$S while it increased between 35 m and 50 m depth.

Both local atmospheric and remote equatorial forcing are known to drive interan-

nual SST variability in the ABA. The link between the western/central equatorial wind stress and ABA SSTs has slightly weakened during 2070-2099 relative to 1970-1999. In contrast, the impact of the local alongshore wind stress and near-coastal wind stress curl on ABA SSTs has strongly increased. Thus, the local atmospheric wind-stress forcing becomes a more important driver of the interannual SST variability in the ABA in FOCI under strongly increased CO_2-concentrations. Regarding the local thermodynamic processes, the net heat-flux damping as well as the cloud cover-SST feedback do not exhibit large changes (not shown). Thus, it is unlikely that they have significantly contributed to the weakened interannual SST variability over the ABA.

The reduced interannual SST/upper-ocean temperature variability off the coasts of Angola and Namibia during 2070-2099 relative to 1970-1999 goes along with a smaller SST/upper-ocean temperature response to thermocline-depth variations, i.e. a weaker thermocline feedback. Moreover, the regions of reduced thermocline feedback are co-located with the regions where the mean Z20 deepens the most, supporting that the weakened thermocline feedback is driven by the mean-state changes. In fact, the ABA experienced the strongest SST warming over the tropical Atlantic Ocean, amounting to $2.82 \pm 0.6°C$ in MJJ when comparing the period 2070-2099 with 1970-1999. The subsurface temperatures in the top 50 m from $0°S$ to $15°S$ also exhibit a substantial warming, supporting weaker surface/subsurface coupling. While the 30-year running mean of the ABA-averaged SST in MJJ shows a strong increasing trend during the 21st century (Figure 5.10, red line), the 30-year running standard deviation of the ABA-averaged SST anomalies in MJJ (Figure 5.10, blue line) displays a downward trend. Over the 90-year period 1981-2071, the trend in SST variability amounts to -0.023 $°C·decade^{-1}$ (Figure 5.10, black line). This decline in the ABA-averaged interannual SST variability is superimposed by a pronounced multidecadal variability, as shown by selected 30-year trends (Figure 5.10).
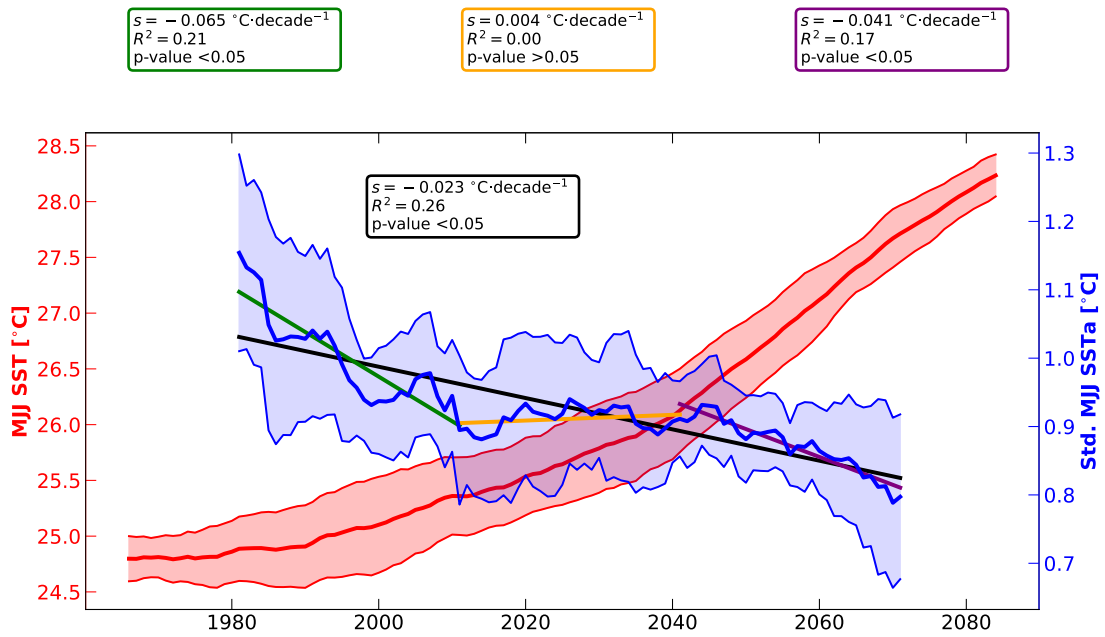
Figure 5.10: ABA-averaged model SST in MJJ. (a) 30-year running mean SST (red line) and 30-year running standard deviation of the SST anomalies (blue line). The shadings represent the ensemble spread, defined as $\pm$ 1 standard deviation (σ) of each ensemble.

In order to evaluate the significance of the forced trends, we use the internal variability estimated from the preindustrial control runs of the FOCI model and of the CMIP6 models. We note, however, that the control run of FOCI was condcuted with a model version without the nest in the tropical and South Atlantic. Distributions of 90-year and 30-year trends in ABA-averaged MJJ-SST variability were computed from the FOCI (Figures 5.11a and 5.11b, respectively) and CMIP6 control runs (Figures 5.11c and 5.11d, respectively). The trends derived from the FOCI-future ensemble are within the range of the trends simulated in the preindustrial control runs, suggesting that the trends in the externally forced simulations could be due to internal variability.
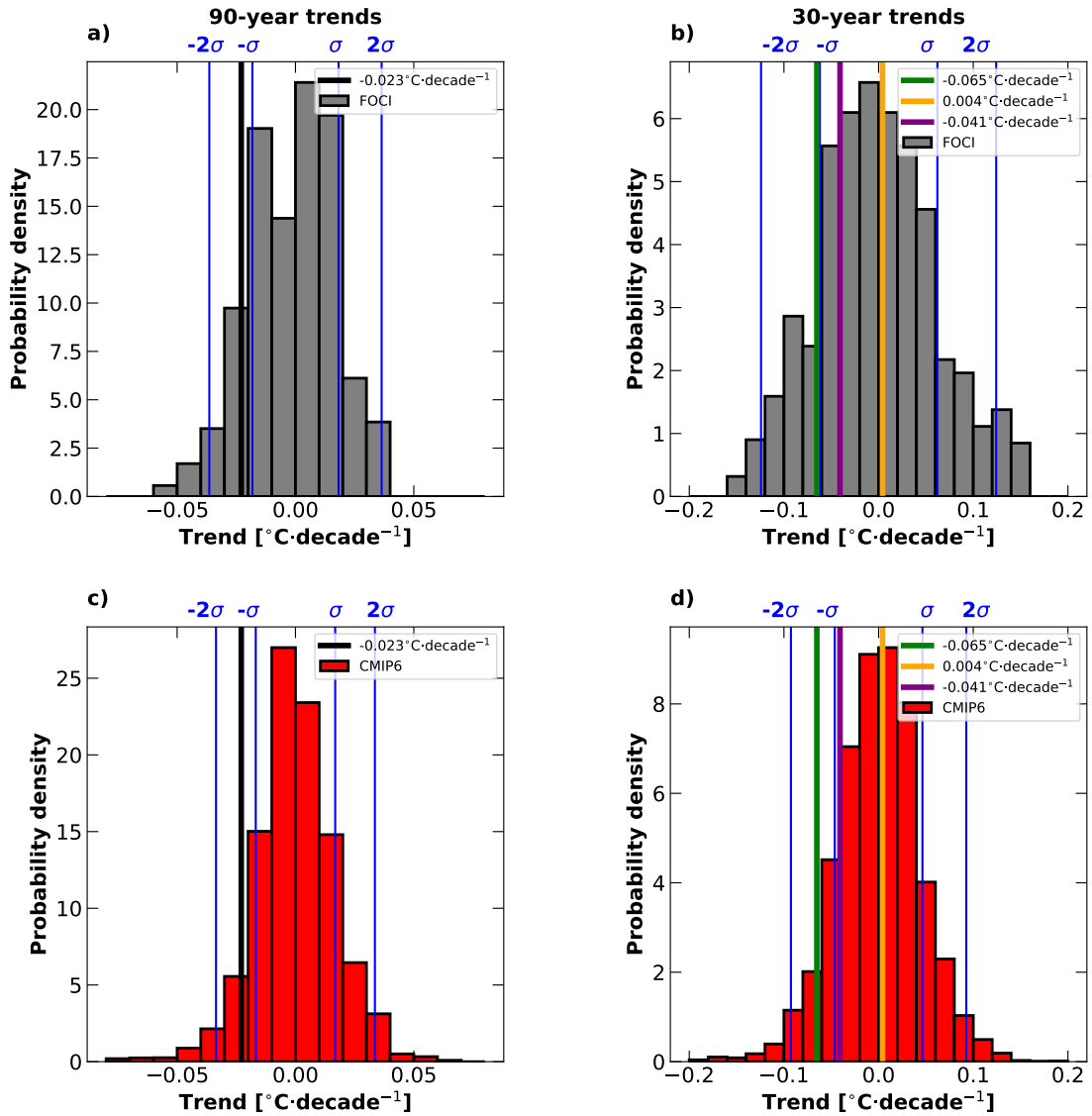
Figure 5.11: ABA-averaged model SST trend distributions in MJJ (a, b) Distribution of multidecadal (90-year and 30-year, respectively) SST-variability trends calculated from the preindustrial control run from FOCI. (c, d) same as (a, b) but for the CMIP6 models. The vertical lines are the multidecadal trends from the FOCI ensembles shown in Fig. 10. $\pm 2\sigma$ and $\pm \sigma$ denote the two and one standard deviations of the multidecadal trend distributions, respectively.

As the internal variability in FOCI and in the CMIP6 models is high, a reduced SST variability observed within a multidecadal period has to be "extreme". For example, the reduction of the interannual SST variability in the ABA reported by Prigent et al. (2020b), comparing the periods 1982-1999 and 2000-2017, would be still within the range of internal variability.

Finally, we note some caveats about the FOCI model. Despite some improvements in the simulation quality by the usage of a high-resolution nest in the ocean, a relatively large SST bias remains along the Southwest African coast, which may be the result of a too coarse atmospheric resolution leading to a poor representation of the near-coastal winds. Nevertheless, the SST bias is smaller than the averaged bias of the CMIP6 models analyzed here. This provides some confidence to our analyses, yet it does not necessarily imply that the real world will respond in the same way. A better understanding of the processes at play in the southeastern tropical Atlantic, which determine the mean state and variability of the SST and upper-ocean temperature in the region, is required to reduce uncertainty regarding the externally forced climate response over the region.

Acknowledgments

Data availability Statement

The model data used in this study can be found at (10.5281/zenodo.5094524). The CMIP6 data can be found at https://esgf-data.dkrz.de/search/cmip6-dkrz/. The ERA5 data used in this study can be found at https://cds.climate.copernicus.eu/cdsapp#!/dataset/reanalysis-era5-single-levels-monthly-means?tab=form. The HadISST is publicly available at https://www.metoffice.gov.uk/hadobs/hadiSST/.

5.7 Supplementary material

Table S1. CMIP6 model simulations used in this study.

Model	Atmosphere model Atmosphere resolution	Ocean model Ocean resolution
ACCESS-CM2	MetUM-HadGEM3-GA7.1 N96; 192 x 144 longitude/latitude; 85 levels	ACCESS-OM2 GFDL-MOM5, tripolar primarily 1deg; 360 x 300 longitude/latitude; 50 levels
ACCESS-ESM1-5	HadGAM2 r1.1, N96; 192 x 145 longitude/latitude; 38 levels	ACCESS-OM2 MOM5, tripolar primarily 1deg; 360 x 300 longitude/latitude; 50 levels
BCC-CSM2-MR	BCC_AGCM3_MR T106 (~ 1.125˚ x 1.125˚); 46 levels	MOM4 1/3 deg 10S-10N, 1/3-1 deg 10-30 N/S, and 1 deg in high latitudes; 360 x 232 longitude/latitude; 40 levels
CAMS-CSM1-0	ECHAM5_CAMS T106; 320 x 160 longitude/latitude; 31 levels	MOM4 tripolar; 360 x 200 longitude/latitude, primarily 1deg latitude/longitude, down to 1/3deg within 30deg of the equatorial tropics; 50 levels
EC-Earth3-Veg	IFS cy36r4 TL255, linearly reduced Gaussian grid equivalent to 512 x 256 longitude/latitude; 91 levels	NEMO3.6 ORCA1 tripolar primarily 1 degree with meridional refinement down to 1/3 degree in the tropics; 362 x 292 longitude/latitude; 75 levels
EC-Earth3	IFS cy36r4 TL255, linearly reduced Gaussian grid equivalent to 512 x 256 longitude/latitude; 91 levels	NEMO3.6 ORCA1 tripolar primarily 1 deg with meridional refinement down to 1/3 degree in the tropics; 362 x 292 longitude/latitude; 75 levels
GFDL-ESM4	GFDL-AM4.1 Cubed-sphere (c96) - 1-degree nominal horizontal resolution; 360 x 180 longitude/latitude; 49 levels	GFDL-OM4p5 GFDL-MOM6, tripolar - nominal 0.5 deg; 720 x 576 longitude/latitude; 75 levels
INM-CM4-8	INM-AM4-8 2x1.5; 180 x 120 longitude/latitude; 21 levels	INM-OM5 North Pole shifted to 60N, 90E; 360 x 318 longitude/latitude; 40 levels
INM-CM5-0	INM-AM5-0 2x1.5; 180 x 120 longitude/latitude; 73 levels	INM-OM5 North Pole shifted to 60N, 90E. 0.5x0.25; 720 x 720 longitude/latitude; 40 levels
IPSL-CM6A-LR	LMDZ NPv6, N96; 144 x 143 longitude/latitude; 79 levels	NEMO-OPA eORCA1.3, tripolar primarily 1deg; 362 x 332 longitude/latitude; 75 levels
MIROC6	CCSR AGCM T85; 256 x 128 longitude/latitude; 81 levels	COCO4.9 tripolar primarily 1deg; 360 x 256 longitude/latitude; 63 levels
MPI-ESM1-2-HR	ECHAM6.3 spectral T127; 384 x 192 longitude/latitude; 95 levels	MPIOM1.63 tripolar TP04, approximately 0.4deg; 802 x 404 longitude/latitude; 40 levels
MPI-ESM1-2-LR	ECHAM6.3 spectral T63; 192 x 96 longitude/latitude; 47 levels	MPIOM1.63 bipolar GR1.5, approximately 1.5deg; 256 x 220 longitude/latitude; 40 levels

MRI-ESM2-0	MRI-AGCM3.5 TL159; 320 x 160 longitude/latitude; 80 levels	MRI.COM4.4 tripolar primarily 0.5 deg latitude/1 deg longitude with meridional refinement down to 0.3 deg within 10 degrees north and south of the equator; 360 x 364 longitude/latitude; 61 levels
NESM3	ECHAM v6.3 T63; 192 x 96 longitude/latitude; 47 levels	NEMO v3.4 NEMO v3.4, tripolar primarily 1deg; 384 x 362 longitude/latitude; 46 levels

Chapter 6

Summary, discussion and outlook

6.1 Summary

The aim of this thesis was to better understand the relationship between tropical At-
lantic mean-state changes and changes in tropical Atlantic interannual SST variability
during past, present and future conditions. Towards this end, observational and reanaly-
sis datasets together with global coupled climate models were assessed. Over the satel-
lite era the interannual SST variability changes were evaluated for the eastern equatorial
Atlantic (Chapter 2), and for the southeastern tropical Atlantic (Chapter 3). Finally, the
influence of global warming on future projections of interannual SST variability was
investigated in the eastern equatorial (Chapter 4) and southeastern tropical (Chapter 5)
Atlantic. Below, the answers to the questions raised in Chapter 1 are summarized.

- **How did the interannual SST variability in the eastern equatorial Atlantic
  change over the satellite era? What are the mechanisms driving this change?
  Is this change related to mean-state changes?**

  In Chapter 2, changes in interannual SST variability in the eastern equatorial
  Atlantic (ATL3, $20°$W-$0°$; $3°$S-$3°$N) over the period 1982-2017 were explored
  (Prigent et al., 2020a). Using observational and reanalysis datasets, results show
  that relative to the 1982-1999 period, during 2000-2017 the interannual May-
  June-July (MJJ) SST variability in the ATL3 region has weakened by 31% (Fig-
  ure 2.2 and table 2.1). The reduced interannual SST variability after 2000 was
  partly attributed to an overall reduction of the Bjerknes feedback in boreal sum-
  mer (Figure 2.4). In addition, the net heat flux damping, which is the dominant

negative feedback over the equatorial Atlantic (Lübbecke and McPhaden, 2013), has strongly increased since 2000 (Table 2.3). It is also shown that zonal wind interannual variability in the western equatorial Atlantic has weakened. However, these changes in net heat flux damping and zonal wind variability have large uncertainties as observational and reanalysis datasets tend to differ. The results found in Chapter 2 (Prigent et al., 2020a) were later confirmed by Silva et al. (2021) who investigated the Bjerknes feedback index changes before and after the year 2000. Regarding the mean-state changes, the mean MJJ SST change from 2000-2017 to 1982-1999 is significant, and amounts to about $0.3°C$ only north of the equator (Figure 2.5). There is also a weak SST change in the cold tongue region which is consistent with Nnamchi et al. (2020) who indicated that over the period 1979-2018 the equatorial Atlantic cold tongue depicted a warming hole. In addition, a slight northward shift of the ITCZ position is observed after 2000, which might have resulted in a reduction of the western equatorial zonal wind variability. More research is needed to conclude on this point. Relative to 1982-1999, after 2000 a minor intensification of the easterlies over the eastern equatorial Atlantic is observed. Consequently, a slight shoaling (deepening) of the thermocline is detected in the eastern (western) equatorial Atlantic. Furthermore, compared to 1982-1999, since 2000 a strengthening and minor westward shift of the rising branch of the Walker circulation is depicted (Figure 2.6). A westward shift of the Walker circulation might have also contributed to reduced western equatorial Atlantic zonal wind variability observed after 2000. However, the aforementioned mean-state changes are hardly significant, and therefore can likely not explain completely the weakened Bjerknes feedback and interannual SST variability.

- **How did the interannual SST variability in the southeastern tropical Atlantic change over the satellite era? What are the origins of this interannual SST variability change? Is this change in interannual SST variability related to mean-state changes?**

  In Chapter 3, changes in interannual SST variability in the southeastern tropical Atlantic were examined (Prigent et al., 2020b). The Angola-Benguela-area

(ABA, 8°E-20°E; 20°S-10°S) averaged March-April-May (MAM) interannual SST variability has weakened by 30.5% (Figure 3.1 and table 3.1) during 2000-2017, relative to 1982-1999. The reduced interannual SST variability goes along with the smaller influence of remote forcing associated with equatorial zonal wind variability (Figure 3.3). Indeed, lower zonal wind variability in the western equatorial Atlantic tends to reduce equatorial Kelvin wave (EKW) activity (Figure 3.3), which is an important driver of interannual SST variability in the ABA (see Chapter 1). Furthermore, since 2000, the importance of the local forcing through near-coastal meridional wind stress and wind stress curl is enhanced (Figure 3.2). Regarding mean-state changes relative to the pre-2000 period, during the post-2000 period a significant warming of 0.3°C is observed during MAM (Figures S1a and S4a). This surface warming might have reduced the surface-subsurface coupling, which might partly explain the reduced ABA-averaged interannual SST variability in MAM. This Chapter has implications for the predictability of Benguela Niño/Niña events. Thus, the strong link between equatorial thermocline variations leading the ABA SST anomalies by one to two months has strongly reduced during 2000-2017 relative to 1982-1999 (Figure 3.3). Finally, a strong link between the SAA strength and the ABA SST anomalies was observed during the pre-2000 period, consistent with (Lübbecke et al., 2010). However, this link has also reduced during the post-2000 period (Figure 3.4). Hence, these results raise the question whether predictors based on equatorial variables or SAA strength are still useful to forecast Benguela Niño/Niña events.

- **How is global warming influencing the Atlantic Niño? What are the future changes in interannual SST variability in the eastern equatorial Atlantic?**
  Based on the comparison of historical (1950-1999) and future (2050-2099) highest emission scenario simulations of 40 CMIP5 and CMIP6 models, Chapter 4 shows that the eastern equatorial Atlantic interannual SST variability in June-July-August is projected to weaken under global warming (Figure 4.1). This change in boreal summer SST variability is related to changes in the Bjerknes feedback components, and in particular to the third component of the Bjerknes feedback, i.e the thermocline feedback. Indeed, the change in the 3$^{\text{rd}}$ Bjerknes feedback component explains up to 61% of the change in the eastern equatorial

interannual SST variability (Figure 4.2). Relative to 1950-1999, during 2050-2099 the equatorial Atlantic in the top 50 m depicts a considerable warming (> 2.5°C) along with a deepening of the mean thermocline and surface weakening of the equatorial Atlantic trade winds (Figure 4.3). This chapter also highlights that more than 80% of the 40 CMIP5 and CMIP6 models agree on a reduction of the eastern equatorial boreal summer interannual SST variability (Table 4.1). In addition, the use of several emission scenarios assists in showing that the reduction of interannual SST variability seems independent of the emissions scenario (Figures S3 and S4). Finally, Chapter 4 highlights that models with less SST biases in the eastern equatorial Atlantic exhibit stronger reduction of the future boreal summer interannual SST variability (Figure 4.4).

- **How does the interannual SST variability change in the southeastern tropical Atlantic under a global warming scenario? What are the mean-state changes?**

  Future changes in interannual SST variability in the southeastern tropical Atlantic were investigated in Chapter 5. To do so, a historical ensemble (1970-1999) was compared to a set of future simulations (2070-2099) and ran under the SSP5-8.5 scenario (Table 5.1) using the coupled climate model FOCI. The ABA-averaged SST variability in MJJ (interannual variability peak in the FOCI model) weakens by 24.4% during 2070-2099 relative to 1970-1999 (Figures 5.3 and 5.4). Interannual temperature variability in the upper 35 m also weakens in 2070-2099 relative to 1970-1999 (Figure 5.4). The reduction in interannual SST and temperature variability appears to be driven by weaker thermocline feedback (Figures 5.6 and 5.7). The weaker thermocline feedback is co-located with the regions where the mean thermocline deepens the most, linking mean-state changes to interannual SST variability changes (Figure 5.6). In addition, the ABA depicts the strongest SST increase of the whole tropical Atlantic Ocean, amounting to 2.82 ± 0.6°C in MJJ when comparing 2070-2099 to 1970-1999. Furthermore, subsurface temperatures in the top 50 m from 0°S to 15°S exhibit a substantial increase (> 2.5°C) supporting weaker surface/subsurface coupling. While the 30-year running mean ABA-averaged MJJ SST displays a strong increasing trend throughout the 21st century, the 30-year running standard deviation of the

ABA-averaged MJJ SST anomalies depicts a downward trend (Figure 5.10). The preindustrial control runs of the FOCI and CMIP6 models were used to estimate the internal variability in order to evaluate the significance of the forced trends found in the ABA. This analysis suggests that the trends in the externally forced simulation could be due to internal variability. The internal variability in the FOCI and CMIP6 models is large and thus a reduction of the interannual SST variability would need to be extreme to emerge as a clearly externally forced signal.

6.2 Discussion

Although the observational record of Atlantic SST extends from the mid-1850s to present, its spatial coverage was limited principally to commercial shipping routes until 1979 (Richter and Tokinaga, 2021). The first satellites able to measure SST through multiple infrared channels as well as microwave radiometers were deployed in 1979 (Minnett et al., 2019), making the reliable observational record of the whole tropical Atlantic SST rather short (~ 40 years). Hence, one caveat for the observational studies, such as Chapters 2 and 3, is the relatively short observational period over which they are based. Indeed, in these chapters two 18-year periods are compared: 1982-1999 and 2000-2017. This makes the statistical robustness of the results feeble, particularly for the mean-state changes. In addition, these results might also be influenced by multi-decadal variability coming from the AMV. As mentioned in Chapter 1, Martín-Rey et al. (2018) revealed that during a negative phase of the AMV the interannual SST variability in the eastern equatorial Atlantic is enhanced by 150% in boreal summer. The AMV changed from a negative to a positive phase around the year 1997 (Figure 1.4) and thus it could have contributed to the weakening of eastern equatorial Atlantic interannual SST variability during 2000-2017 relative to 1982-1999.

Other potential sources for multidecadal changes in the tropical Atlantic interannual SST variability

A possible source for multidecadal changes in the tropical Atlantic interannual SST variability can be of remote origin. Indeed, around the year 2000, the interannual SST

variability in the tropical Pacific also experienced a reduction (Hu et al., 2013; Lübbecke and McPhaden, 2014). This shift has been explained by changes in the equatorial Pacific mean-state. Hu et al. (2013) compared the period 1979-1999 to the period 2000-2011, and found that during the post-2000 period the equatorial Pacific thermocline tilt was steeper due to stronger surface trade winds. They proposed that it might have hampered the eastward migration of the warm water along the equatorial Pacific. As a result, the variability of the warm water volume (WWV) was reduced, and thus ENSO amplitude also decreased. McPhaden (2012) showed that during 2000-2010 relative to 1980-1999 WWV variations decreased, and its lead time was reduced to only one season. These changes were linked to a shift towards more central Pacific El Niños versus eastern Pacific El Niños (McPhaden, 2012). Therefore, the question whether the reduced interannual SST variations in the tropical Pacific lead to reduced interannual SST variability in the tropical Atlantic or vice-versa deserves more investigation. Martín-Rey et al. (2014) showed that the Atlantic-Pacific Niños connection is modulated by the AMV with strong negative relationships, i.e. a warm (cold) event in the equatorial Atlantic drives a cold (warm) event in the equatorial Pacific, coinciding with negative AMV. Hence, since the AMV became positive in 1997 (Figure 1.4), the Atlantic-Pacific Niños connection is likely reduced during the post-2000 period. Changes in the tropical Pacific interannual SST variability also has implications for the southeastern tropical Atlantic interannual SST variability. Indeed, Rouault et al. (2010) and Dufois and Rouault (2012) showed over the 1979-2008 period that during El Niño (La Niña) events weaker (stronger) southeasterly winds prevail, leading to reduced (enhanced) upwelling in the Southern Benguela (3° off the coast; 20°S-35°S) which could then lead to SST anomalies. Tim et al. (2015) indicated that ENSO significantly influences the winds in the Southern Benguela but not in the Northern Benguela. Hence, the impact of ENSO on the ABA interannual SST variability seems relatively weak but deserves more investigation.

A recent study from Zhang and Han (2021) using observational datasets and by performing model experiments, shows that the Atlantic Niño can be induced by the Indian Ocean Dipole (IOD). In fact, a positive IOD generates westerly wind anomalies over the tropical Atlantic leading to warm SST anomalies in the central and eastern tropical Atlantic thereby triggering an Atlantic Niño event 3 to 5 months after the IOD peak.

Hence, multidecadal modulations of the eastern equatorial Atlantic SST response to the IOD could also contribute to multidecadal changes in the tropical Atlantic interannual SST variability.

Another potential source for multidecadal changes of interannual SST variability in the eastern equatorial Atlantic and at the eastern boundary off Angola is the multidecadal changes of the subtropical cells (STCs). STCs are shallow meridional overturning circulation that connect the subduction zones of subtropical gyres with the equator and eastern tropical upwelling regions (McCreary and Lu, 1994; Schott et al., 2004; Tuchen et al., 2019). For the tropical Atlantic basin, Tuchen et al. (2020) quantified the SST response to STC changes. They found a strong negative SST response to positive interior transport convergence, with the interior transport convergence leading the SST by 2 months on the equator between 30°W and 10°W, as well as off Angola between 5°S and 15°S. Therefore, a reduction in the interior transport convergence variability could lead to reduced interannual SST variability in the eastern equatorial Atlantic and off Angola. The contribution of multidecadal changes of Atlantic STCs to the multidecadal changes of interannual SST variability in the eastern equatorial Atlantic and at the eastern boundary requires more investigation.

Discussion on models' limitations

While investigating the lag between Atlantic Niños and Benguela Niños using model experiments, Illig et al. (2020) demonstrated that neither the differences in ocean stratification between the eastern equatorial and southeastern tropical Atlantic nor the seasonal phasing of events explains the lag between the two climate modes. Instead, they show that only the coastal wind stress anomalies are responsible for initiating the coastal SST anomalies before the eastern equatorial SST anomalies. Hence, the authors have highlighted the importance of a good representation of the coastal winds in order to obtain the correct lag between the Benguela Niños/Niñas and Atlantic Niños/Niñas. The majority of the CMIP6 models used in this thesis have a relatively coarse atmospheric resolution ($> 1.5°$ horizontal, < 70 vertical levels) which is insufficient to simulate the narrow coastal surface winds found in the southeastern tropical Atlantic (Harlaß et al., 2018). Hence, it is not surprising that state-of-the-art coupled models still underestimate and misrepresent the seasonality of the tropical Atlantic interannual SST vari-

ability (Richter and Tokinaga, 2020). In the CMIP6 ensemble, the eastern equatorial (southeastern tropical) Atlantic interannual SST variability peaks in July (Figure 5.1), which is one (three) month(s) later than the observations. Results of Chapter 5 rely on the outputs of a global coupled model (FOCI) at 0.5° horizontal resolution with an enhanced oceanic resolution at 1/10° over the tropical Atlantic. While the high-resolution ocean allows a reduction in southeastern tropical Atlantic warm SST bias, and simulates a more realistic amplitude of the interannual SST variability in the ABA, a considerable bias remains (Figure 5.1). As for the CMIP6 models, the FOCI model seasonality of the interannual SST variability in the ABA is incorrect, as it peaks in June instead of April. As mentioned above, the good representation of coastal wind variability seems crucial to simulate the correct seasonality of the interannual variability in the ABA. Hence, the coarse atmospheric resolution of approximately 1.8° horizontal with 95 vertical levels (T65L95) used for the model setup of Chapter 5 could potentially explain the two months lag between the FOCI model and observations.

Implications for tropical Atlantic interannual SST variability predictability

In contrast to the equatorial Pacific, the prediction of tropical Atlantic SST anomalies is still a challenge for global coupled models (Stockdale et al., 2006). Indeed, dynamical prediction models struggle to match persistence forecasts in the tropical Atlantic (Richter et al., 2018; Lübbecke et al., 2018). Richter and Tokinaga (2021) pointed to two possible explanations for the low predictability skills for the Atlantic: (1) current prediction models are inadequate because of systematic errors in the model formulation or/and insufficient observations for the initialization of the models, (2) the theoretical predictability of the equatorial Atlantic is inherently low due to weak coupled feedbacks or high internal variability. Indeed, the Bjerknes feedback, the main dynamical driver of eastern equatorial Atlantic interannual SST variability, is weaker than in the Pacific (Keenlyside and Latif, 2007). In addition, Chapter 2 shows that relative to 1982-1999, during 2000-2017 the Bjerknes feedback explained less variance indicating that dynamical processes became less important drivers of equatorial Atlantic SST variability. Hence, the relative multidecadal importance of dynamical processes in driving equatorial Atlantic SST variability might have implications for its predictability.

Stockdale et al. (2006) found no prediction skill above that of persistence south of the equator in the Atlantic and indicated that models were performing particularly badly in the southern tropical Atlantic (60°W-20°E; 20°S-5°N). Yet, Imbol Koungue et al. (2017) found a promising approach towards the prediction of SST anomalies in the ABA based on equatorial Kelvin wave activity between 1998 and 2012. They showed a high correlation between the second mode EKW leading the SST anomalies in the ABA by one month. However, Chapter 3 revealed that, relative to 1982-1999, during 2000-2017 the relationship between the EKW activity and the ABA SST anomalies has reduced (Figure 3.3). Thus, the predictability of ABA SST anomalies based on EKW might be subject to multidecadal variations. Another promising approach towards prediction of ABA SST anomalies is based on the fluctuations of the strength of the SAA (Lübbecke et al., 2010; Richter et al., 2010). However, Chapter 3 also shows that the strong relationship between the SAA and the ABA SSTs that existed during 1982-1999, with the SAA leading the ABA SSTs by one month, dropped during 2000-2017 (Figure 3.4). Chapters 2 and 3 suggested multidecadal changes in the forcing mechanisms of the Atlantic Niños/Niñas and Benguela Niños/Niñas which can make their already difficult predictability, subject to multidecadal modulation.

6.3   Outlook

Will the Tropical Atlantic annual cycle change?

As discussed throughout this thesis, Atlantic and Benguela Niños/Niñas have significant impacts on the climate of the surrounding countries, and therefore understanding their multidecadal changes is crucial. However, as introduced in Chapter 1, both climate modes are phase-locked to their seasonal cycle. Both seasonal cycles are dominated by their annual harmonic, and thus changes in their annual cycle could lead to socio-economic consequences. Preliminary results suggest that under the global warming scenario SSP5-8.5, the amplitude of the annual cycle of the SST from a CMIP6 ensemble is projected to reduce during 2070-2099 relative to 1970-1999 in both the equatorial Atlantic and in the ABA (Figure 4.1). The mechanisms driving the reduced amplitude of the annual cycle in 2070-2099 relative to 1970-1999 as well as the consequences of such a reduction require more research.
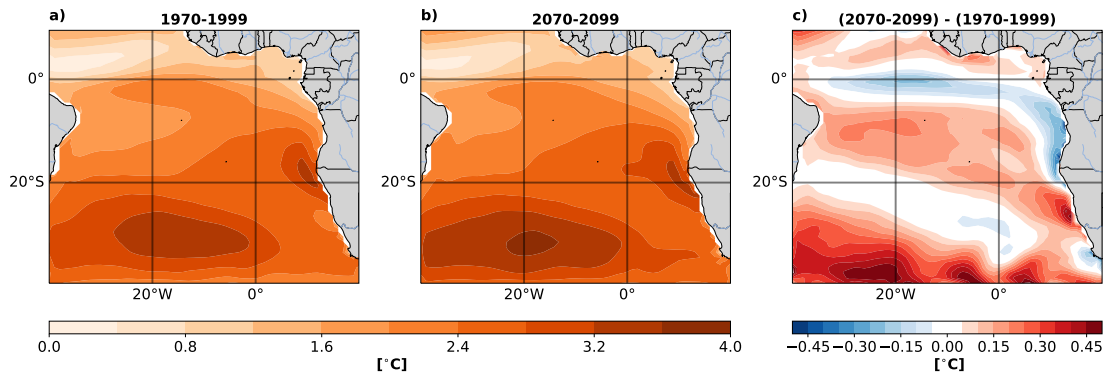
Figure 6.1: Ensemble mean amplitude of the annual harmonic of the detrended SSTs pointwise during (a) 1970-1999 and (b) 2070-2099. (c) is the difference (b) minus (a). The amplitude of the annual cycle (A_{ac}) is estimated as follows: $A_{ac} = \sqrt{A^2 + B^2}$ with the coefficients A and B obtained from the non-linear least mean squares fit of the function $f(t) = A\cos(\omega t) + B\sin(\omega t) + C$ on the SST with $\omega = 2\pi/T$ and T the corresponding period of the harmonic fit. The CMIP6 ensemble is composed of the following models: ACCESS-CM2, CAMS-CSM1-0, CMCC-CM2-SR5, CMCC-ESM2, CNRM-CM6-1, CNRM-CM6-1-HR, CNRM-ESM2-1, CanESM5-CanOE, FGOALS-f3-L, HadGEM3-GC31-LL, HadGEM3-GC31-MM, IITM-ESM, INM-CM4-8, INM-CM5-0, MCM-UA-1-0, MIROC-ES2L, MIROC6, MPI-ESM1-2-LR, NESM3, UKESM1-0-LL.

Are tropical instability waves important for the eastern equatorial Atlantic SST variability?

Wengel et al. (2021) investigated the response of ENSO amplitude to CO_2-doubling and CO_2-quadrupling in ultra-high-resolution simulations, i.e. with $0.25°$ horizontal resolution in the atmosphere and $0.1°$ in the ocean. They indicate that ultra-high-resolution simulations allow for a better representation of the tropical Pacific mean-state and mesoscale oceanic processes, in particular the tropical instability waves (TIWs). These waves are generated by the shear of the tropical zonal current system. They argue that TIWs provide a strong negative feedback for ENSO, and are thus a crucial element in ENSO dynamics. They found a robust weakening of the future simulated ENSO amplitude due to quadrupling atmospheric CO_2. This reduction in ENSO amplitude is found to be the consequence of a stronger thermal latent heat flux damping and weaker advective feedbacks. Therefore, TIWs could be another potential negative feedback to consider for the eastern equatorial Atlantic interannual SST.

How certain are the changes in Atlantic Niño and Benguela Niño amplitude?

Lastly, this thesis showed that the interannual SST variability in the tropical Atlantic (Chapters 2 and 3) has decreased in 2000-2017 relative to 1982-1999. In addition, using CMIP5 and CMIP6 models as well as an ensemble of the coupled climate model FOCI, ran under a global warming scenario, it is shown that the interannual SST variability in the ATL3 (Chapter 4) and in the ABA (Chapter 5) is projected to decrease. However, in the last couple of years the interannual SST variability in the tropical Atlantic Ocean could be increasing again with the occurrence of two Atlantic Niños (2019, 2021) and two Benguela Niños (2019/2020 and 2021). Therefore, a question arises: how certain are the Atlantic Niños/Niñas and Benguela Niños/Niñas amplitudes projections? The study from Beobide-Arsuaga et al. (2021) addressed this question for ENSO amplitude projections using CMIP5 and CMIP6 models. They indicate that future ENSO amplitudes in CMIP5 and CMIP6 models highly diverge, with the projected amplitude changes ranging from a decrease of -0.4°C to an increase of 0.6°C. Beobide-Arsuaga et al. (2021) found that internal variability is the main source of uncertainty in the first three decades of projection and that model uncertainty dominates thereafter. They also note that relative to the internal variability and model uncertainty, the scenario uncertainty remains small throughout the twenty-first century. In contrast to future ENSO amplitude projection, Chapter 4 shows that 80% of the 40 CMIP5 and CMIP6 models used in this chapter agree on a future reduction of the interannual SST variability. Worou et al. (2021) showed that 84% of their CMIP6 ensemble composed of 31 models agree on a decrease of the future Atlantic Niño amplitude projection. They found an ensemble mean decrease of -21% of the JAS interannual SST variability in the ATL3 region during 2070-2099 relative to 1985-2014. This result agrees with Figures 4.1 and 5.3 which show a decrease of the interannual SST variability in 2070-2099 relative to 1970-1999 in the CMIP5 and CMIP6 and in the FOCI ensemble. The future Atlantic Niño amplitude projection seems less uncertain than the one of ENSO. However, the identification and quantification of the sources of uncertainty for the future Atlantic Niños/Niñas and Benguela Niños/Niñas amplitudes requires more research.

References

Adler R, Sapiano M, Huffman G, Wang JJ, Gu G, Bolvin D, Chiu L, Schneider U, Becker A, Nelkin E, Xie P, Ferraro R, Shin DB (2018) The Global Precipitation Climatology Project (GPCP) Monthly Analysis (New Version 2.3) and a Review of 2017 Global Precipitation. Atmosphere 9(4):138, DOI 10.3390/atmos9040138, URL http://www.mdpi.com/2073-4433/9/4/138

Amaya DJ, DeFlorio MJ, Miller AJ, Xie SP (2017) Wes feedback and the atlantic meridional mode: observations and cmip5 comparisons. Climate Dynamics 49(5):1665–1679, DOI 10.1007/s00382-016-3411-1, URL https://doi.org/10.1007/s00382-016-3411-1

Bachèlery ML, Illig S, Dadou I (2016a) Forcings of nutrient, oxygen, and primary production interannual variability in the southeast atlantic ocean. Geophysical Research Letters 43(16):8617–8625, DOI https://doi.org/10.1002/2016GL070288, URL https://agupubs.onlinelibrary.wiley.com/doi/abs/10.1002/2016GL070288, https://agupubs.onlinelibrary.wiley.com/doi/pdf/10.1002/2016GL070288

Bachèlery ML, Illig S, Dadou I (2016b) Interannual variability in the south-east atlantic ocean, focusing on the benguela upwelling system: Remote versus local forcing. Journal of Geophysical Research: Oceans 121(1):284–310, DOI https://doi.org/10.1002/2015JC011168, URL https://agupubs.onlinelibrary.wiley.com/doi/abs/10.1002/2015JC011168, https://agupubs.onlinelibrary.wiley.com/doi/pdf/10.1002/2015JC011168

Bachèlery ML, Illig S, Rouault M (2020) Interannual coastal trapped waves in the angola-benguela upwelling system and benguela niño and niña events. Journal

of Marine Systems 203:103,262, DOI https://doi.org/10.1016/j.jmarsys.2019.10326 2, URL https://www.sciencedirect.com/science/article/pii/S0924796 319303999

Bakun A, Black BA, Bograd SJ, García-Reyes M, Miller AJ, Rykaczewski RR, Sydeman WJ (2015) Anticipated effects of climate change on coastal upwelling ecosystems. Current Climate Change Reports 1(2):85–93, DOI 10.1007/s40641-015-0008-4, URL https://doi.org/10.1007/s40641-015-0008-4

Balmaseda MA, Mogensen K, Weaver AT (2013) Evaluation of the ECMWF ocean reanalysis system ORAS4. Quarterly Journal of the Royal Meteorological Society 139(674):1132–1161, DOI 10.1002/qj.2063, URL http://doi.wiley.com/10.1 002/qj.2063

Bayr T, Dommenget D, Martin T, Power SB (2014) The eastward shift of the Walker Circulation in response to global warming and its relationship to ENSO variability. Climate Dynamics 43(9-10):2747–2763, DOI 10.1007/s00382-014-2091-y, URL ht tp://link.springer.com/10.1007/s00382-014-2091-y

Bayr T, Latif M, Dommenget D, Wengel C, Harlaß J, Park W (2018) Mean-state dependence of ENSO atmospheric feedbacks in climate models. Climate Dynamics 50(9-10):3171–3194, DOI 10.1007/s00382-017-3799-2, URL http://link.sprin ger.com/10.1007/s00382-017-3799-2

Bayr T, Wengel C, Latif M, Dommenget D, Lübbecke J, Park W (2019) Error compensation of ENSO atmospheric feedbacks in climate models and its influence on simulated ENSO dynamics. Climate Dynamics 53(1-2):155–172, DOI 10.1007/s00382-0 18-4575-7, URL http://link.springer.com/10.1007/s00382-018-4575-7

Behera SK (2021) 1 - introduction to atmosphere and ocean variability and air–sea interactions. In: Behera SK (ed) Tropical and Extratropical Air-Sea Interactions, Elsevier, pp 1–16, DOI https://doi.org/10.1016/B978-0-12-818156-0.00013-7, URL https://www.sciencedirect.com/science/article/pii/B9780128181560000137

Bentamy A, Katsaros KB, Mestas-Nuñez AM, Drennan WM, Forde EB, Roquet H (2003) Satellite Estimates of Wind Speed and Latent Heat

Flux over the Global Oceans. Journal of Climate 16(4):637–656, DOI 10.1175/1520-0442(2003)016⟨0637:SEOWSA⟩2.0.CO;2, URL http://journals.ametsoc.org/doi/abs/10.1175/1520-0442{%}282003{%}29016{%}3C0637{%}3ASEOWSA{%}3E2.0.CO{%}3B2

Bentamy A, Piollé J, Grouazel A, Danielson R, Gulev S, Paul F, Azelmat H, Mathieu P, von Schuckmann K, Sathyendranath S, Evers-King H, Esau I, Johannessen J, Clayson C, Pinker R, Grodsky S, Bourassa M, Smith S, Haines K, Valdivieso M, Merchant C, Chapron B, Anderson A, Hollmann R, Josey S (2017) Review and assessment of latent and sensible heat flux accuracy over the global oceans. Remote Sensing of Environment 201(November):196–218, DOI 10.1016/j.rse.2017.08.016, URL https://linkinghub.elsevier.com/retrieve/pii/S0034425717303826

Beobide-Arsuaga G, Bayr T, Reintges A, Latif M (2021) Uncertainty of enso-amplitude projections in cmip5 and cmip6 models. Climate Dynamics 56(11):3875–3888, DOI 10.1007/s00382-021-05673-4, URL https://doi.org/10.1007/s00382-021-05673-4

Biastoch A, Böning CW, Getzlaff J, Molines JM, Madec G (2008) Causes of interannual–decadal variability in the meridional overturning circulation of the midlatitude north atlantic ocean. Journal of Climate 21(24):6599 – 6615, DOI 10.1175/2008JCLI2404.1, URL https://journals.ametsoc.org/view/journals/clim/21/24/2008jcli2404.1.xml

Binet D, Gobert B, Maloueki L (2001) El Niño-like warm events in the Eastern Atlantic (6°N, 20°S) and fish availability from Congo to Angola (1964-1999). Aquatic Living Resources 14(2):99–113, DOI 10.1016/S0990-7440(01)01105-6

Bjerknes J (1969) Atmospheric teleconnections from the equatorial pacific. Monthly Weather Review 97(3):163 – 172, DOI 10.1175/1520-0493(1969)097⟨0163:ATFTEP⟩2.3.CO;2, URL https://journals.ametsoc.org/view/journals/mwre/97/3/1520-0493_1969_097_0163_atftep_2_3_co_2.xml

Boyd AJ, Taunton-Clark J, Oberholster GPJ (1992) Spatial features of the near-surface and midwater circulation patterns off western and southern south africa and their role in the life histories of various commercially fished species. South

African Journal of Marine Science 12(1):189–206, DOI 10.2989/02577619209504
702, URL https://doi.org/10.2989/02577619209504702, https://doi.or
g/10.2989/02577619209504702

Brandt P, Hormann V, Bourlès B, Fischer J, Schott FA, Stramma L, Dengler M
(2008) Oxygen tongues and zonal currents in the equatorial atlantic. Journal of
Geophysical Research: Oceans 113(C4), DOI https://doi.org/10.1029/2007JC0044
35, URL https://agupubs.onlinelibrary.wiley.com/doi/abs/10.1029/20
07JC004435, https://agupubs.onlinelibrary.wiley.com/doi/pdf/10.102
9/2007JC004435

Brandt P, Caniaux G, Bourlès B, Lazar A, Dengler M, Funk A, Hor-
mann V, Giordani H, Marin F (2011a) Equatorial upper-ocean dynam-
ics and their interaction with the west african monsoon. Atmospheric
Science Letters 12(1):24–30, DOI https://doi.org/10.1002/asl.287, URL
https://rmets.onlinelibrary.wiley.com/doi/abs/10.1002/asl.287,
https://rmets.onlinelibrary.wiley.com/doi/pdf/10.1002/asl.287

Brandt P, Funk A, Hormann V, Dengler M, Greatbatch RJ, Toole JM (2011b) Inter-
annual atmospheric variability forced by the deep equatorial atlantic ocean. Nature
473(7348):497–500, DOI 10.1038/nature10013, URL https://doi.org/10.103
8/nature10013

Burgers G, Jin FF, van Oldenborgh GJ (2005) The simplest enso recharge oscilla-
tor. Geophysical Research Letters 32(13), DOI https://doi.org/10.1029/2005GL0229
51, URL https://agupubs.onlinelibrary.wiley.com/doi/abs/10.1029/20
05GL022951, https://agupubs.onlinelibrary.wiley.com/doi/pdf/10.102
9/2005GL022951

Burmeister K, Brandt P, Lübbecke JF (2016) Revisiting the cause of the eastern
equatorial atlantic cold event in 2009. Journal of Geophysical Research: Oceans
121(7):4777–4789, DOI https://doi.org/10.1002/2016JC011719, URL https://ag
upubs.onlinelibrary.wiley.com/doi/abs/10.1002/2016JC011719, https:
//agupubs.onlinelibrary.wiley.com/doi/pdf/10.1002/2016JC011719

Cabos W, de la Vara A, Koseki S (2019) Tropical atlantic variability: Observations and modeling. Atmosphere 10(9), DOI 10.3390/atmos10090502, URL https://www.mdpi.com/2073-4433/10/9/502

Cai W, Borlace S, Lengaigne M, van Rensch P, Collins M, Vecchi G, Timmermann A, Santoso A, McPhaden MJ, Wu L, England MH, Wang G, Guilyardi E, Jin FF (2014) Increasing frequency of extreme el niño events due to greenhouse warming. Nature Climate Change 4(2):111–116, DOI 10.1038/nclimate2100, URL https://doi.org/10.1038/nclimate2100

Cai W, Wang G, Santoso A, McPhaden MJ, Wu L, Jin FF, Timmermann A, Collins M, Vecchi G, Lengaigne M, England MH, Dommenget D, Takahashi K, Guilyardi E (2015) Increased frequency of extreme la niña events under greenhouse warming. Nature Climate Change 5(2):132–137, DOI 10.1038/nclimate2492, URL https://doi.org/10.1038/nclimate2492

Cai W, Wu L, Lengaigne M, Li T, McGregor S, Kug JS, Yu JY, Stuecker MF, Santoso A, Li X, Ham YG, Chikamoto Y, Ng B, McPhaden MJ, Du Y, Dommenget D, Jia F, Kajtar JB, Keenlyside N, Lin X, Luo JJ, Martín-Rey M, Ruprich-Robert Y, Wang G, Xie SP, Yang Y, Kang SM, Choi JY, Gan B, Kim GI, Kim CE, Kim S, Kim JH, Chang P (2019) Pantropical climate interactions. Science 363(6430):eaav4236, DOI 10.1126/science.aav4236, URL http://www.sciencemag.org/lookup/doi/10.1126/science.aav4236

Caniaux G, Giordani H, Redelsperger JL, Guichard F, Key E, Wade M (2011) Coupling between the atlantic cold tongue and the west african monsoon in boreal spring and summer. Journal of Geophysical Research: Oceans 116(C4), DOI https://doi.org/10.1029/2010JC006570, URL https://agupubs.onlinelibrary.wiley.com/doi/abs/10.1029/2010JC006570, https://agupubs.onlinelibrary.wiley.com/doi/pdf/10.1029/2010JC006570

Castaño-Tierno A, Mohino E, Rodríguez-Fonseca B, Losada T (2018) Revisiting the cmip5 thermocline in the equatorial pacific and atlantic oceans. Geophysical Research Letters 45(23):12,963–12,971, DOI https://doi.org/10.1029/2018GL079847, URL https://agupubs.onlinelibrary.wiley.com/doi/abs/10.1029/20

18GL079847, `https://agupubs.onlinelibrary.wiley.com/doi/pdf/10.1029/2018GL079847`

Chang P, Fang Y, Saravanan R, Ji L, Seidel H (2006) The cause of the fragile relationship between the Pacific El Niño and the Atlantic Niño. Nature 443(7109):324–328, DOI 10.1038/nature05053, URL `http://www.nature.com/articles/nature05053`

Chang P, Zhang R, Hazeleger W, Wen C, Wan X, Ji L, Haarsma RJ, Breugem WP, Seidel H (2008) Oceanic link between abrupt changes in the north atlantic ocean and the african monsoon. Nature Geoscience 1(7):444–448, DOI 10.1038/ngeo218, URL `https://doi.org/10.1038/ngeo218`

Chavez FP, Messié M (2009) A comparison of eastern boundary upwelling ecosystems. Progress in Oceanography 83(1):80–96, DOI https://doi.org/10.1016/j.pocean.2009.07.032, URL `https://www.sciencedirect.com/science/article/pii/S0079661109000998`, eastern Boundary Upwelling Ecosystems: Integrative and Comparative Approaches

Chenillat F, Illig S, Jouanno J, Awo FM, Alory G, Brehmer P (2021) How do climate modes shape the chlorophyll-a interannual variability in the tropical atlantic? Geophysical Research Letters 48(14):e2021GL093,769, DOI https://doi.org/10.1029/2021GL093769, URL `https://agupubs.onlinelibrary.wiley.com/doi/abs/10.1029/2021GL093769`, e2021GL093769 2021GL093769, `https://agupubs.onlinelibrary.wiley.com/doi/pdf/10.1029/2021GL093769`

Clarke AJ (1983) The Reflection of Equatorial Waves from Oceanic Boundaries. Journal of Physical Oceanography 13(7):1193–1207, DOI 10.1175/1520-0485(1983)013⟨1193:TROEWF⟩2.0.CO;2, URL `https://doi.org/10.1175/1520-0485(1983)013{%}3C1193:TROEWF{%}3E2.0.COhttp://0.0.0.2`

Collins M, An SI, Cai W, Ganachaud A, Guilyardi E, Jin FF, Jochum M, Lengaigne M, Power S, Timmermann A, Vecchi G, Wittenberg A (2010) The impact of global warming on the tropical pacific ocean and el niño. Nature Geoscience 3(6):391–397, DOI 10.1038/ngeo868, URL `https://doi.org/10.1038/ngeo868`

Davey M, Huddleston M, Sperber K, Braconnot P, Bryan F, Chen D, Colman R, Cooper C, Cubasch U, Delecluse P, DeWitt D, Fairhead L, Flato G, Gordon C, Hogan T, Ji M, Kimoto M, Kitoh A, Knutson T, Latif M, Le Treut H, Li T, Manabe S, Mechoso C, Meehl G, Power S, Roeckner E, Terray L, Vintzileos A, Voss R, Wang B, Washington W, Yoshikawa I, Yu J, Yukimoto S, Zebiak S (2002) Stoic: a study of coupled model climatology and variability in tropical ocean regions. Climate Dynamics 18(5):403–420, DOI 10.1007/s00382-001-0188-6, URL https://doi.org/10.1007/s00382-001-0188-6

Dee DP, Uppala SM, Simmons AJ, Berrisford P, Poli P, Kobayashi S, Andrae U, Balmaseda MA, Balsamo G, Bauer P, Bechtold P, Beljaars ACM, van de Berg L, Bidlot J, Bormann N, Delsol C, Dragani R, Fuentes M, Geer AJ, Haimberger L, Healy SB, Hersbach H, Hólm EV, Isaksen L, Kållberg P, Köhler M, Matricardi M, McNally AP, Monge-Sanz BM, Morcrette JJ, Park BK, Peubey C, de Rosnay P, Tavolato C, Thépaut JN, Vitart F (2011) The ERA-Interim reanalysis: configuration and performance of the data assimilation system. Quarterly Journal of the Royal Meteorological Society 137(656):553–597, DOI 10.1002/qj.828, URL http://doi.wiley.com/10.1002/qj.828

Delecluse P, Servain J, Levy C, Arpe K, Bengtsson L (1994) On the connection between the 1984 atlantic warm event and the 1982—1983 enso. Tellus A: Dynamic Meteorology and Oceanography 46(4):448–464, DOI 10.3402/tellusa.v46i4.15491, URL https://doi.org/10.3402/tellusa.v46i4.15491, https://doi.org/10.3402/tellusa.v46i4.15491

Deppenmeier AL, Haarsma RJ, Hazeleger W (2016) The bjerknes feedback in the tropical atlantic in cmip5 models. Climate Dynamics 47(7):2691–2707, DOI 10.1007/s00382-016-2992-z, URL https://doi.org/10.1007/s00382-016-2992-z

Dewitte B, Yeh SW, Thual S (2013) Reinterpreting the thermocline feedback in the western-central equatorial pacific and its relationship with the enso modulation. Climate Dynamics 41(3):819–830, DOI 10.1007/s00382-012-1504-z, URL https://doi.org/10.1007/s00382-012-1504-z

DiNezio PN, Kirtman BP, Clement AC, Lee SK, Vecchi GA, Wittenberg A (2012)

Mean climate controls on the simulated response of enso to increasing green-house gases. Journal of Climate 25(21):7399 – 7420, DOI 10.1175/JCLI-D-11-00 494.1, URL https://journals.ametsoc.org/view/journals/clim/25/21/jcli-d-11-00494.1.xml

Ding H, Keenlyside NS, Latif M (2009) Seasonal cycle in the upper equatorial atlantic ocean. Journal of Geophysical Research: Oceans 114(C9), DOI https://doi.org/10.1029/2009JC005418, URL https://agupubs.onlinelibrary.wiley.com/doi/abs/10.1029/2009JC005418, https://agupubs.onlinelibrary.wiley.com/doi/pdf/10.1029/2009JC005418

Ding H, Keenlyside NS, Latif M (2012) Impact of the Equatorial Atlantic on the El Niño Southern Oscillation. Climate Dynamics 38(9-10):1965–1972, DOI 10.1007/s00382-011-1097-y, URL http://link.springer.com/10.1007/s00382-011-1097-y

Ding H, Keenlyside N, Latif M, Park W, Wahl S (2015) The impact of mean state errors on equatorial atlantic interannual variability in a climate model. Journal of Geophysical Research: Oceans 120(2):1133–1151, DOI https://doi.org/10.1002/2014JC010384, URL https://agupubs.onlinelibrary.wiley.com/doi/abs/10.1002/2014JC010384, https://agupubs.onlinelibrary.wiley.com/doi/pdf/10.1002/2014JC010384

Dippe T, Greatbatch RJ, Ding H (2018) On the relationship between atlantic niño variability and ocean dynamics. Climate Dynamics 51(1):597–612, DOI 10.1007/s00382-017-3943-z, URL https://doi.org/10.1007/s00382-017-3943-z

Dippe T, Lübbecke JF, Greatbatch RJ (2019) A Comparison of the Atlantic and Pacific Bjerknes Feedbacks: Seasonality, Symmetry, and Stationarity. Journal of Geophysical Research: Oceans 124(4):2374–2403, DOI 10.1029/2018JC014700, URL https://onlinelibrary.wiley.com/doi/abs/10.1029/2018JC014700

Dommenget D, Vijayeta A (2019) Simulated future changes in enso dynamics in the framework of the linear recharge oscillator model. Climate Dynamics 53(7):4233–4248, DOI 10.1007/s00382-019-04780-7, URL https://doi.org/10.1007/s00382-019-04780-7

Dufois F, Rouault M (2012) Sea surface temperature in false bay (south africa): Towards a better understanding of its seasonal and inter-annual variability. Continental Shelf Research 43:24–35, DOI https://doi.org/10.1016/j.csr.2012.04.009, URL https://www.sciencedirect.com/science/article/pii/S0278434312000970

Enfield DB, Mayer DA (1997) Tropical atlantic sea surface temperature variability and its relation to el niño-southern oscillation. Journal of Geophysical Research: Oceans 102(C1):929–945, DOI https://doi.org/10.1029/96JC03296, URL https://agupubs.onlinelibrary.wiley.com/doi/abs/10.1029/96JC03296, https://agupubs.onlinelibrary.wiley.com/doi/pdf/10.1029/96JC03296

Enfield DB, Mestas-Nuñez AM, Trimble PJ (2001) The atlantic multidecadal oscillation and its relation to rainfall and river flows in the continental u.s. Geophysical Research Letters 28(10):2077–2080, DOI https://doi.org/10.1029/2000GL012745, URL https://agupubs.onlinelibrary.wiley.com/doi/abs/10.1029/2000GL012745, https://agupubs.onlinelibrary.wiley.com/doi/pdf/10.1029/2000GL012745

Exarchou E, Prodhomme C, Brodeau L, Guemas V, Doblas-Reyes F (2018) Origin of the warm eastern tropical atlantic sst bias in a climate model. Climate Dynamics 51(5):1819–1840, DOI 10.1007/s00382-017-3984-3, URL https://doi.org/10.1007/s00382-017-3984-3

Exarchou E, Ortega P, Rodríguez-Fonseca B, Losada T, Polo I, Prodhomme C (2021) Impact of equatorial atlantic variability on enso predictive skill. Nature Communications 12(1):1612, DOI 10.1038/s41467-021-21857-2, URL https://doi.org/10.1038/s41467-021-21857-2

Eyring V, Bony S, Meehl GA, Senior CA, Stevens B, Stouffer RJ, Taylor KE (2016) Overview of the coupled model intercomparison project phase 6 (cmip6) experimental design and organization. Geoscientific Model Development 9(5):1937–1958, DOI 10.5194/gmd-9-1937-2016, URL https://gmd.copernicus.org/articles/9/1937/2016/

Florenchie P, Lutjeharms JRE, Reason CJC, Masson S, Rouault M (2003) The source of benguela niños in the south atlantic ocean. Geophysical Research Letters 30(10),

DOI https://doi.org/10.1029/2003GL017172, URL https://agupubs.onlineli
brary.wiley.com/doi/abs/10.1029/2003GL017172, https://agupubs.onli
nelibrary.wiley.com/doi/pdf/10.1029/2003GL017172

Florenchie P, Reason CJC, Lutjeharms JRE, Rouault M, Roy C, Masson S (2004)
Evolution of interannual warm and cold events in the southeast atlantic ocean.
Journal of Climate 17(12):2318 – 2334, DOI 10.1175/1520-0442(2004)017⟨2318:
EOIWAC⟩2.0.CO;2, URL https://journals.ametsoc.org/view/journals/c
lim/17/12/1520-0442_2004_017_2318_eoiwac_2.0.co_2.xml

Folland CK, Palmer TN, Parker DE (1986) Sahel rainfall and worldwide sea tempera-
tures, 1901–85. Nature 320(6063):602–607, DOI 10.1038/320602a0, URL https:
//doi.org/10.1038/320602a0

Foltz GR, McPhaden MJ (2010) Abrupt equatorial wave-induced cooling of the atlantic
cold tongue in 2009. Geophysical Research Letters 37(24), DOI https://doi.org/10.1
029/2010GL045522, URL https://agupubs.onlinelibrary.wiley.com/doi/
abs/10.1029/2010GL045522, https://agupubs.onlinelibrary.wiley.com/
doi/pdf/10.1029/2010GL045522

Foltz GR, McPhaden MJ, Lumpkin R (2012) A strong atlantic meridional mode event
in 2009: The role of mixed layer dynamics. Journal of Climate 25(1):363 – 380,
DOI 10.1175/JCLI-D-11-00150.1, URL https://journals.ametsoc.org/view/
journals/clim/25/1/jcli-d-11-00150.1.xml

Frankignoul C, Kestenare E, Mignot J (2002) The surface heat flux feedback. Part II:
direct and indirect estimates in the ECHAM4/OPA8 coupled GCM. Climate Dynam-
ics 19(8):649–655, DOI 10.1007/s00382-002-0253-9, URL http://link.springe
r.com/10.1007/s00382-002-0253-9

Frauen C, Dommenget D (2010) El Niño and La Niña amplitude asymmetry caused by
atmospheric feedbacks. Geophysical Research Letters 37(18):n/a–n/a, DOI 10.1029/
2010GL044444, URL http://doi.wiley.com/10.1029/2010GL044444

Gammelsrød T, Bartholomae CH, Boyer DC, Filipe VLL, O'Toole MJ (1998) Intrusion
of warm surface water along the Angolan-Namibian coast in February–March 1995:

the 1995 Benguela Nino. South African Journal of Marine Science 19(1):41–56, DOI 10.2989/025776198784126719, URL https://doi.org/10.2989/025776198784 126719

García-Serrano J, Losada T, Rodríguez-Fonseca B, Polo I (2008) Tropical atlantic variability modes (1979–2002). part ii: Time-evolving atmospheric circulation related to sst-forced tropical convection. Journal of Climate 21(24):6476 – 6497, DOI 10.1175/2008JCLI2191.1, URL https://journals.ametsoc.org/view/journa ls/clim/21/24/2008jcli2191.1.xml

Gu G, Adler RF (2004) Seasonal evolution and variability associated with the west african monsoon system. Journal of Climate 17(17):3364 – 3377, DOI 10.1175/1520-0442(2004)017⟨3364:SEAVAW⟩2.0.CO;2, URL https://journals.ametsoc.org/view/journals/clim/17/17/1520-044 2_2004_017_3364_seavaw_2.0.co_2.xml

Guan C, McPhaden MJ (2016) Ocean Processes Affecting the Twenty-First-Century Shift in ENSO SST Variability. Journal of Climate 29(19):6861–6879, DOI 10.1175/ JCLI-D-15-0870.1, URL http://journals.ametsoc.org/doi/10.1175/JCLI-D-15-0870.1

Haarsma RJ, Hazeleger W (2007) Extratropical atmospheric response to equatorial atlantic cold tongue anomalies. Journal of Climate 20(10):2076 – 2091, DOI 10.1175/JCLI4130.1, URL https://journals.ametsoc.org/view/journals/c lim/20/10/jcli4130.1.xml

Hansingo K, Reason CJC (2009) Modelling the atmospheric response over southern Africa to SST forcing in the southeast tropical Atlantic and southwest subtropical Indian Oceans. International Journal of Climatology 29(7):1001–1012, DOI https://doi.org/10.1002/joc.1919, URL https://doi.org/10.1002/joc.1919

Harlaß J, Latif M, Park W (2018) Alleviating tropical atlantic sector biases in the kiel climate model by enhancing horizontal and vertical atmosphere model resolution: climatology and interannual variability. Climate Dynamics 50(7):2605–2635, DOI 10.1007/s00382-017-3760-4, URL https://doi.org/10.1007/s00382-017-3760-4

Harlaß J, Latif M, Park W (2015) Improving climate model simulation of tropical atlantic sea surface temperature: The importance of enhanced vertical atmosphere model resolution. Geophysical Research Letters 42(7):2401–2408, DOI https://doi.org/10.1002/2015GL063310, URL https://agupubs.onlinelibrary.wiley.com/doi/abs/10.1002/2015GL063310, https://agupubs.onlinelibrary.wiley.com/doi/pdf/10.1002/2015GL063310

Heede UK, Fedorov AV, Burls NJ (2020) Time scales and mechanisms for the tropical pacific response to global warming: A tug of war between the ocean thermostat and weaker walker. Journal of Climate 33(14):6101 – 6118, DOI 10.1175/JCLI-D-19-0690.1, URL https://journals.ametsoc.org/view/journals/clim/33/14/JCLI-D-19-0690.1.xml

Heede UK, Fedorov AV, Burls NJ (2021) A stronger versus weaker walker: understanding model differences in fast and slow tropical pacific responses to global warming. Climate Dynamics 57(9):2505–2522, DOI 10.1007/s00382-021-05818-5, URL https://doi.org/10.1007/s00382-021-05818-5

Hersbach H, Bell B, Berrisford P, Hirahara S, Horányi A, Muñoz-Sabater J, Nicolas J, Peubey C, Radu R, Schepers D, Simmons A, Soci C, Abdalla S, Abellan X, Balsamo G, Bechtold P, Biavati G, Bidlot J, Bonavita M, De Chiara G, Dahlgren P, Dee D, Diamantakis M, Dragani R, Flemming J, Forbes R, Fuentes M, Geer A, Haimberger L, Healy S, Hogan RJ, Hólm E, Janisková M, Keeley S, Laloyaux P, Lopez P, Lupu C, Radnoti G, de Rosnay P, Rozum I, Vamborg F, Villaume S, Thépaut JN (2020) The era5 global reanalysis. Quarterly Journal of the Royal Meteorological Society 146(730):1999–2049, DOI https://doi.org/10.1002/qj.3803, URL https://rmets.onlinelibrary.wiley.com/doi/abs/10.1002/qj.3803, https://rmets.onlinelibrary.wiley.com/doi/pdf/10.1002/qj.3803

Hersbach, Hans and Dee D (2016) ERA5 reanalysis is in production. ECMWF newsletter 147(7):5–6

Hirst AC, Hastenrath S (1983) Atmosphere-Ocean Mechanisms of Climate Anomalies in the Angola-Tropical Atlantic Sector. Journal of Physical Oceanography 13(7):1146–1157, DOI 10.1175/1520-0485(1983)013⟨1146:AOMOCA⟩2.0.CO;2,

URL `http://journals.ametsoc.org/doi/abs/10.1175/1520-0485{%}28198`
`3{%}29013{%}3C1146{%}3AAOMOCA{%}3E2.0.CO{%}3B2`

Hu ZZ, Huang B (2007) Physical processes associated with the tropical atlantic sst gradient during the anomalous evolution in the southeastern ocean. Journal of Climate 20(14):3366 – 3378, DOI 10.1175/JCLI4189.1, URL `https://journals.ametsoc`
`.org/view/journals/clim/20/14/jcli4189.1.xml`

Hu ZZ, Kumar A, Ren HL, Wang H, L'Heureux M, Jin FF (2013) Weakened Interannual Variability in the Tropical Pacific Ocean since 2000. Journal of Climate 26(8):2601–2613, DOI 10.1175/JCLI-D-12-00265.1, URL `http://journals.ametsoc.org/d`
`oi/abs/10.1175/JCLI-D-12-00265.1`

Hu ZZ, Kumar A, Huang B, Zhu J, Ren HL (2017) Interdecadal variations of enso around 1999/2000. Journal of Meteorological Research 31(1):73–81, DOI 10.1007/s13351-017-6074-x, URL `https://doi.org/10.1007/s13351-017-6074-x`

Hu ZZ, Kumar A, Huang B, Zhu J, L'Heureux M, McPhaden MJ, Yu JY (2020) The interdecadal shift of enso properties in 1999/2000: A review. Journal of Climate 33(11):4441 – 4462, DOI 10.1175/JCLI-D-19-0316.1, URL `https://journals.a`
`metsoc.org/view/journals/clim/33/11/jcli-d-19-0316.1.xml`

Huang B, Hu ZZ, Jha B (2007) Evolution of model systematic errors in the tropical atlantic basin from coupled climate hindcasts. Climate Dynamics 28(7):661–682, DOI 10.1007/s00382-006-0223-8, URL `https://doi.org/10.1007/s00382-006`
`-0223-8`

Illig S, Bachèlery ML (2019) Propagation of Subseasonal Equatorially-Forced Coastal Trapped Waves down to the Benguela Upwelling System. Scientific Reports 9(1):5306, DOI 10.1038/s41598-019-41847-1, URL `http://www.nature.com/a`
`rticles/s41598-019-41847-1`

Illig S, Dewitte B, Ayoub N, du Penhoat Y, Reverdin G, De Mey P, Bonjean F, Lagerloef GSE (2004) Interannual long equatorial waves in the tropical atlantic from a high-resolution ocean general circulation model experiment in 1981–2000. Journal of Geophysical Research: Oceans 109(C2), DOI https://doi.org/10.1029/2003JC00

1771, URL https://agupubs.onlinelibrary.wiley.com/doi/abs/10.1029/2003JC001771, https://agupubs.onlinelibrary.wiley.com/doi/pdf/10.1029/2003JC001771

Illig S, Bachèlery ML, Cadier E (2018a) Subseasonal coastal-trapped wave propagations in the southeastern pacific and atlantic oceans: 2. wave characteristics and connection with the equatorial variability. Journal of Geophysical Research: Oceans 123(6):3942–3961, DOI https://doi.org/10.1029/2017JC013540, URL https://agupubs.onlinelibrary.wiley.com/doi/abs/10.1029/2017JC013540, https://agupubs.onlinelibrary.wiley.com/doi/pdf/10.1029/2017JC013540

Illig S, Cadier E, Bachèlery ML, Kersalé M (2018b) Subseasonal coastal-trapped wave propagations in the southeastern pacific and atlantic oceans: 1. a new approach to estimate wave amplitude. Journal of Geophysical Research: Oceans 123(6):3915–3941, DOI https://doi.org/10.1029/2017JC013539, URL https://agupubs.onlinelibrary.wiley.com/doi/abs/10.1029/2017JC013539, https://agupubs.onlinelibrary.wiley.com/doi/pdf/10.1029/2017JC013539

Illig S, Bachèlery ML, Lübbecke JF (2020) Why do benguela niños lead atlantic niños? Journal of Geophysical Research: Oceans 125(9):e2019JC016,003, DOI https://doi.org/10.1029/2019JC016003, URL https://agupubs.onlinelibrary.wiley.com/doi/abs/10.1029/2019JC016003, e2019JC016003 2019JC016003, https://agupubs.onlinelibrary.wiley.com/doi/pdf/10.1029/2019JC016003

Imbol Koungue RA, Brandt P (2021) Impact of intraseasonal waves on angolan warm and cold events. Journal of Geophysical Research: Oceans 126(4):e2020JC017,088, DOI https://doi.org/10.1029/2020JC017088, URL https://agupubs.onlinelibrary.wiley.com/doi/abs/10.1029/2020JC017088, e2020JC017088 2020JC017088, https://agupubs.onlinelibrary.wiley.com/doi/pdf/10.1029/2020JC017088

Imbol Koungue RA, Illig S, Rouault M (2017) Role of interannual kelvin wave propagations in the equatorial atlantic on the angola benguela current system. Journal of Geophysical Research: Oceans 122(6):4685–4703, DOI https://doi.org/10.1002/2016JC012463, URL https://agupubs.onlinelibrary.wiley.com/doi/abs/10

.1002/2016JC012463, https://agupubs.onlinelibrary.wiley.com/doi/pd
f/10.1002/2016JC012463

Imbol Koungue RA, Rouault M, Illig S, Brandt P, Jouanno J (2019) Benguela niños
and benguela niñas in forced ocean simulation from 1958 to 2015. Journal of Geo-
physical Research: Oceans 124(8):5923–5951, DOI https://doi.org/10.1029/2019JC
015013, URL https://agupubs.onlinelibrary.wiley.com/doi/abs/10.102
9/2019JC015013, https://agupubs.onlinelibrary.wiley.com/doi/pdf/10
.1029/2019JC015013

Imbol Nkwinkwa ASN, Latif M, Park W (2021) Mean-state dependence of co2-
forced tropical atlantic sector climate change. Geophysical Research Letters
48(19):e2021GL093,803, DOI https://doi.org/10.1029/2021GL093803, URL http
s://agupubs.onlinelibrary.wiley.com/doi/abs/10.1029/2021GL093803,
e2021GL093803 2021GL093803, https://agupubs.onlinelibrary.wiley.co
m/doi/pdf/10.1029/2021GL093803

Ishii M, Shouji A, Sugimoto S, Matsumoto T (2005) Objective analyses of sea-surface
temperature and marine meteorological variables for the 20th century using ICOADS
and the Kobe Collection. International Journal of Climatology 25(7):865–879, DOI
https://doi.org/10.1002/joc.1169, URL https://doi.org/10.1002/joc.1169

Jansen MF, Dommenget D, Keenlyside N (2009) Tropical Atmosphere–Ocean Interac-
tions in a Conceptual Framework. Journal of Climate 22(3):550–567, DOI 10.1175/
2008JCLI2243.1, URL http://journals.ametsoc.org/doi/abs/10.1175/200
8JCLI2243.1

Jin FF, Kim ST, Bejarano L (2006) A coupled-stability index for ENSO. Geophysical
Research Letters 33(23):2–5, DOI 10.1029/2006GL027221

Jouanno J, Hernandez O, Sanchez-Gomez E (2017) Equatorial Atlantic interannual
variability and its relation to dynamic and thermodynamic processes. Earth System
Dynamics 8(4):1061–1069, DOI 10.5194/esd-8-1061-2017, URL https://www.ea
rth-syst-dynam.net/8/1061/2017/

Junker T, Mohrholz V, Siegfried L, van der Plas A (2017) Seasonal to interannual

variability of water mass characteristics and currents on the namibian shelf. Journal of Marine Systems 165:36–46, DOI https://doi.org/10.1016/j.jmarsys.2016.09.003, URL https://www.sciencedirect.com/science/article/pii/S0924796316302810

Kalnay E, Kanamitsu M, Kistler R, Collins W, Deaven D, Gandin L, Iredell M, Saha S, White G, Woollen J, Zhu Y, Chelliah M, Ebisuzaki W, Higgins W, Janowiak J, Mo KC, Ropelewski C, Wang J, Leetmaa A, Reynolds R, Jenne R, Joseph D (1996) The ncep/ncar 40-year reanalysis project. Bulletin of the American Meteorological Society 77(3):437 – 472, DOI 10.1175/1520-0477(1996)077⟨0437:TNYRP⟩2.0.CO;2, URL https://journals.ametsoc.org/view/journals/bams/77/3/1520-0477_1996_077_0437_tnyrp_2_0_co_2.xml

Kanamitsu M, Ebisuzaki W, Woollen J, Yang SK, Hnilo JJ, Fiorino M, Potter GL (2002) Ncep–doe amip-ii reanalysis (r-2). Bulletin of the American Meteorological Society 83(11):1631 – 1644, DOI 10.1175/BAMS-83-11-1631, URL https://journals.ametsoc.org/view/journals/bams/83/11/bams-83-11-1631.xml

Kaplan A, Cane MA, Kushnir Y, Clement AC, Blumenthal MB, Rajagopalan B (1998) Analyses of global sea surface temperature 1856–1991. Journal of Geophysical Research: Oceans 103(C9):18,567–18,589, DOI https://doi.org/10.1029/97JC01736, URL https://agupubs.onlinelibrary.wiley.com/doi/abs/10.1029/97JC01736, https://agupubs.onlinelibrary.wiley.com/doi/pdf/10.1029/97JC01736

Keenlyside NS, Latif M (2007) Understanding Equatorial Atlantic Interannual Variability. Journal of Climate 20(1):131–142, DOI 10.1175/JCLI3992.1, URL http://journals.ametsoc.org/doi/abs/10.1175/JCLI3992.1

Kerr RA (2000) A north atlantic climate pacemaker for the centuries. Science 288(5473):1984–1985, DOI 10.1126/science.288.5473.1984, URL https://www.science.org/doi/abs/10.1126/science.288.5473.1984, https://www.science.org/doi/pdf/10.1126/science.288.5473.1984

Kim ST, Cai W, Jin FF, Santoso A, Wu L, Guilyardi E, An SI (2014) Response of el niño sea surface temperature variability to greenhouse warming. Nature Climate

Change 4(9):786–790, DOI 10.1038/nclimate2326, URL https://doi.org/10.1038/nclimate2326

Kinnison DE, Brasseur GP, Walters S, Garcia RR, Marsh DR, Sassi F, Harvey VL, Randall CE, Emmons L, Lamarque JF, Hess P, Orlando JJ, Tie XX, Randel W, Pan LL, Gettelman A, Granier C, Diehl T, Niemeier U, Simmons AJ (2007) Sensitivity of chemical tracers to meteorological parameters in the mozart-3 chemical transport model. Journal of Geophysical Research: Atmospheres 112(D20), DOI https://doi.org/10.1029/2006JD007879, URL https://agupubs.onlinelibrary.wiley.com/doi/abs/10.1029/2006JD007879, https://agupubs.onlinelibrary.wiley.com/doi/pdf/10.1029/2006JD007879

Knight JR, Folland CK, Scaife AA (2006) Climate impacts of the atlantic multidecadal oscillation. Geophysical Research Letters 33(17), DOI https://doi.org/10.1029/2006GL026242, URL https://agupubs.onlinelibrary.wiley.com/doi/abs/10.1029/2006GL026242, https://agupubs.onlinelibrary.wiley.com/doi/pdf/10.1029/2006GL026242

Kopte R, Brandt P, Dengler M, Tchipalanga PCM, Macuéria M, Ostrowski M (2017) The angola current: Flow and hydrographic characteristics as observed at 11°s. Journal of Geophysical Research: Oceans 122(2):1177–1189, DOI https://doi.org/10.1002/2016JC012374, URL https://agupubs.onlinelibrary.wiley.com/doi/abs/10.1002/2016JC012374, https://agupubs.onlinelibrary.wiley.com/doi/pdf/10.1002/2016JC012374

Koseki S, Imbol Koungue RA (2021) Regional atmospheric response to the benguela niñas. International Journal of Climatology 41(S1):E1483–E1497, DOI https://doi.org/10.1002/joc.6782, URL https://rmets.onlinelibrary.wiley.com/doi/abs/10.1002/joc.6782, https://rmets.onlinelibrary.wiley.com/doi/pdf/10.1002/joc.6782

Kumar A, Hu ZZ (2012) Uncertainty in the ocean–atmosphere feedbacks associated with enso in the reanalysis products. Climate Dynamics 39(3):575–588, DOI 10.1007/s00382-011-1104-3, URL https://doi.org/10.1007/s00382-011-1104-3

Kurian J, Li P, Chang P, Patricola CM, Small J (2021) Impact of the benguela coastal low-level jet on the southeast tropical atlantic sst bias in a regional ocean model. Climate Dynamics 56(9):2773–2800, DOI 10.1007/s00382-020-05616-5, URL https://doi.org/10.1007/s00382-020-05616-5

Latif M, Grötzner A (2000) The equatorial Atlantic oscillation and its response to ENSO. Climate Dynamics 16(2-3):213–218, DOI 10.1007/s003820050014, URL http://link.springer.com/10.1007/s003820050014

Levine A, Jin FF, McPhaden MJ (2016) Extreme noise–extreme el niño: How state-dependent noise forcing creates el niño–la niña asymmetry. Journal of Climate 29(15):5483 – 5499, DOI 10.1175/JCLI-D-16-0091.1, URL https://journals.ametsoc.org/view/journals/clim/29/15/jcli-d-16-0091.1.xml

Li G, Xie SP (2012) Origins of tropical-wide sst biases in cmip multi-model ensembles. Geophysical Research Letters 39(22), DOI https://doi.org/10.1029/2012GL053777, URL https://agupubs.onlinelibrary.wiley.com/doi/abs/10.1029/2012GL053777, https://agupubs.onlinelibrary.wiley.com/doi/pdf/10.1029/2012GL053777

Li X, Hu ZZ, Becker E (2019) On the westward shift of tropical pacific climate variability since 2000. Climate Dynamics 53(5):2905–2918, DOI 10.1007/s00382-019-04666-8, URL https://doi.org/10.1007/s00382-019-04666-8

Lloyd J, Guilyardi E, Weller H (2011) The role of atmosphere feedbacks during enso in the cmip3 models. part ii: using amip runs to understand the heat flux feedback mechanisms. Climate Dynamics 37(7):1271–1292, DOI 10.1007/s00382-010-0895-y, URL https://doi.org/10.1007/s00382-010-0895-y

Losada T, Rodríguez-Fonseca B, Kucharski F (2012) Tropical influence on the summer mediterranean climate. Atmospheric Science Letters 13(1):36–42, DOI https://doi.org/10.1002/asl.359, URL https://rmets.onlinelibrary.wiley.com/doi/abs/10.1002/asl.359, https://rmets.onlinelibrary.wiley.com/doi/pdf/10.1002/asl.359

Lübbecke JF, McPhaden MJ (2012) On the inconsistent relationship between pacific and atlantic niños. Journal of Climate 25(12):4294 – 4303, DOI 10.1175/JCLI-D-1

1-00553.1, URL https://journals.ametsoc.org/view/journals/clim/25/12/jcli-d-11-00553.1.xml

Lübbecke JF, McPhaden MJ (2013) A Comparative Stability Analysis of Atlantic and Pacific Niño Modes. Journal of Climate 26(16):5965–5980, DOI 10.1175/JCLI-D-12-00758.1, URL http://journals.ametsoc.org/doi/10.1175/JCLI-D-12-00758.1

Lübbecke JF, McPhaden MJ (2014) Assessing the twenty-first-century shift in enso variability in terms of the bjerknes stability index. Journal of Climate 27(7):2577 – 2587, DOI 10.1175/JCLI-D-13-00438.1, URL https://journals.ametsoc.org/view/journals/clim/27/7/jcli-d-13-00438.1.xml

Lübbecke JF, McPhaden MJ (2017) Symmetry of the Atlantic Niño mode. Geophysical Research Letters 44(2):965–973, DOI 10.1002/2016GL071829, URL http://doi.wiley.com/10.1002/2016GL071829

Lübbecke JF, Böning CW, Keenlyside NS, Xie SP (2010) On the connection between benguela and equatorial atlantic niños and the role of the south atlantic anticyclone. Journal of Geophysical Research: Oceans 115(C9), DOI https://doi.org/10.1029/2009JC005964, URL https://agupubs.onlinelibrary.wiley.com/doi/abs/10.1029/2009JC005964, https://agupubs.onlinelibrary.wiley.com/doi/pdf/10.1029/2009JC005964

Lübbecke JF, Burls NJ, Reason CJC, McPhaden MJ (2014) Variability in the south atlantic anticyclone and the atlantic niño mode. Journal of Climate 27(21):8135 – 8150, DOI 10.1175/JCLI-D-14-00202.1, URL https://journals.ametsoc.org/view/journals/clim/27/21/jcli-d-14-00202.1.xml

Lübbecke JF, Rodríguez-Fonseca B, Richter I, Martín-Rey M, Losada T, Polo I, Keenlyside NS (2018) Equatorial Atlantic variability-Modes, mechanisms, and global teleconnections. Wiley Interdisciplinary Reviews: Climate Change 9(4):e527, DOI 10.1002/wcc.527, URL http://doi.wiley.com/10.1002/wcc.527

Lübbecke JF, Brandt P, Dengler M, Kopte R, Lüdke J, Richter I, Sena Martins M, Tchipalanga PCM (2019) Causes and evolution of the southeastern tropical atlantic

warm event in early 2016. Climate Dynamics 53(1):261–274, DOI 10.1007/s00382 -018-4582-8, URL https://doi.org/10.1007/s00382-018-4582-8

Lutz K, Rathmann J, Jacobeit J (2013) Classification of warm and cold water events in the eastern tropical atlantic ocean. Atmospheric Science Letters 14(2):102–106, DOI https://doi.org/10.1002/asl2.424, URL https://rmets.onlinelibrary.wiley.com/doi/abs/10.1002/asl2.424, https://rmets.onlinelibrary.wiley.com/doi/pdf/10.1002/asl2.424

Madec G, Bourdallé-Badie R, Bouttier PA, Bricaud C, Bruciaferri D, Calvert D, Chanut J, Clementi E, Coward A, Delrosso D, et al. (2017) Nemo ocean engine

Majumder S, Schmid C (2018) A study of the variability in the benguela current volume transport. Ocean Science 14(2):273–283, DOI 10.5194/os-14-273-2018, URL https://os.copernicus.org/articles/14/273/2018/

Maloney ED, Xie SP (2013) Sensitivity of tropical intraseasonal variability to the pattern of climate warming. Journal of Advances in Modeling Earth Systems 5(1):32–47, DOI https://doi.org/10.1029/2012MS000171, URL https://agupubs.onlinelibrary.wiley.com/doi/abs/10.1029/2012MS000171, https://agupubs.onlinelibrary.wiley.com/doi/pdf/10.1029/2012MS000171

Martín-Rey M, Rodríguez-Fonseca B, Polo I, Kucharski F (2014) On the atlantic–pacific niños connection: a multidecadal modulated mode. Climate Dynamics 43(11):3163–3178, DOI 10.1007/s00382-014-2305-3, URL https://doi.org/10.1007/s00382-014-2305-3

Martín-Rey M, Rodríguez-Fonseca B, Polo I (2015) Atlantic opportunities for enso prediction. Geophysical Research Letters 42(16):6802–6810, DOI https://doi.org/10.1002/2015GL065062, URL https://agupubs.onlinelibrary.wiley.com/doi/abs/10.1002/2015GL065062, https://agupubs.onlinelibrary.wiley.com/doi/pdf/10.1002/2015GL065062

Martín-Rey M, Polo I, Rodríguez-Fonseca B, Losada T, Lazar A (2018) Is there evidence of changes in tropical atlantic variability modes under amo phases in the observational record? Journal of Climate 31(2):515 – 536, DOI 10.1175/JCLI-D-16-0459

.1, URL `https://journals.ametsoc.org/view/journals/clim/31/2/jcli-d-16-0459.1.xml`

Matthes K, Funke B, Andersson ME, Barnard L, Beer J, Charbonneau P, Clilverd MA, Dudok de Wit T, Haberreiter M, Hendry A, Jackman CH, Kretzschmar M, Kruschke T, Kunze M, Langematz U, Marsh DR, Maycock AC, Misios S, Rodger CJ, Scaife AA, Seppälä A, Shangguan M, Sinnhuber M, Tourpali K, Usoskin I, van de Kamp M, Verronen PT, Versick S (2017) Solar forcing for cmip6 (v3.2). Geoscientific Model Development 10(6):2247–2302, DOI 10.5194/gmd-10-2247-2017, URL `https://gmd.copernicus.org/articles/10/2247/2017/`

Matthes K, Biastoch A, Wahl S, Harlaß J, Martin T, Brücher T, Drews A, Ehlert D, Getzlaff K, Krüger F, Rath W, Scheinert M, Schwarzkopf FU, Bayr T, Schmidt H, Park W (2020) The flexible ocean and climate infrastructure version 1 (foci1): mean state and variability. Geoscientific Model Development 13(6):2533–2568, DOI 10.5194/gmd-13-2533-2020, URL `https://gmd.copernicus.org/articles/13/2533/2020/`

McCreary JP, Lu P (1994) Interaction between the subtropical and equatorial ocean circulations: The subtropical cell. Journal of Physical Oceanography 24(2):466 – 497, DOI 10.1175/1520-0485(1994)024⟨0466:IBTSAE⟩2.0.CO;2, URL `https://journals.ametsoc.org/view/journals/phoc/24/2/1520-0485_1994_024_0466_ibtsae_2_0_co_2.xml`

McPhaden MJ (2012) A 21st century shift in the relationship between enso sst and warm water volume anomalies. Geophysical Research Letters 39(9), DOI https://doi.org/10.1029/2012GL051826, URL `https://agupubs.onlinelibrary.wiley.com/doi/abs/10.1029/2012GL051826`, `https://agupubs.onlinelibrary.wiley.com/doi/pdf/10.1029/2012GL051826`

McPhaden MJ, Zebiak SE, Glantz MH (2006) Enso as an integrating concept in earth science. Science 314(5806):1740–1745, DOI 10.1126/science.1132588

Merle J (1980) Variabilité thermique annuelle et interannuelle de l'océan atlantique équatorial est. l'hypothèse d'un el niño atlantique. Oceanologica Acta 3(2):209–220

Minnett P, Alvera-Azcárate A, Chin T, Corlett G, Gentemann C, Karagali I, Li X, Marsouin A, Marullo S, Maturi E, Santoleri R, Saux Picart S, Steele M, Vazquez-Cuervo J (2019) Half a century of satellite remote sensing of sea-surface temperature. Remote Sensing of Environment 233:111,366, DOI https://doi.org/10.1016/j.rse.2019.111366, URL https://www.sciencedirect.com/science/article/pii/S0034425719303852

Mohino E, Losada T (2015) Impacts of the atlantic equatorial mode in a warmer climate. Climate Dynamics 45(7):2255–2271, DOI 10.1007/s00382-015-2471-y, URL https://doi.org/10.1007/s00382-015-2471-y

Nicholson SE, Entekhabi D (1987) Rainfall variability in equatorial and southern africa: Relationships with sea surface temperatures along the southwestern coast of africa. Journal of Applied Meteorology and Climatology 26(5):561 – 578, DOI 10.1175/1520-0450(1987)026⟨0561:RVIEAS⟩2.0.CO;2, URL https://journals.ametsoc.org/view/journals/apme/26/5/1520-0450_1987_026_0561_rvieas_2_0_co_2.xml

Nnamchi HC, Li J, Kucharski F, Kang IS, Keenlyside NS, Chang P, Farneti R (2015) Thermodynamic controls of the Atlantic Niño. Nature Communications 6(1):8895, DOI 10.1038/ncomms9895, URL http://www.nature.com/articles/ncomms9895

Nnamchi HC, Latif M, Keenlyside NS, Park W (2020) A satellite era warming hole in the equatorial atlantic ocean. Journal of Geophysical Research: Oceans 125(4):e2019JC015,834, DOI https://doi.org/10.1029/2019JC015834, URL https://agupubs.onlinelibrary.wiley.com/doi/abs/10.1029/2019JC015834, e2019JC015834 2019JC015834, https://agupubs.onlinelibrary.wiley.com/doi/pdf/10.1029/2019JC015834

Nobre P, Shukla J (1996) Variations of sea surface temperature, wind stress, and rainfall over the tropical atlantic and south america. Journal of Climate 9(10):2464 – 2479, DOI 10.1175/1520-0442(1996)009⟨2464:VOSSTW⟩2.0.CO;2, URL https://journals.ametsoc.org/view/journals/clim/9/10/1520-0442_1996_009_2464_vosstw_2_0_co_2.xml

Okumura Y, Xie SP (2006) Some Overlooked Features of Tropical Atlantic Climate Leading to a New Niño-Like Phenomenon*. Journal of Climate 19(22):5859–5874, DOI 10.1175/JCLI3928.1, URL http://journals.ametsoc.org/doi/abs/10.1175/JCLI3928.1

O'Neill BC, Tebaldi C, van Vuuren DP, Eyring V, Friedlingstein P, Hurtt G, Knutti R, Kriegler E, Lamarque JF, Lowe J, Meehl GA, Moss R, Riahi K, Sanderson BM (2016) The scenario model intercomparison project (scenariomip) for cmip6. Geoscientific Model Development 9(9):3461–3482, DOI 10.5194/gmd-9-3461-2016, URL https://gmd.copernicus.org/articles/9/3461/2016/

Ostrowski M, da Silva JCB, Bazik-Sangolay B (2009) The response of sound scatterers to el niño- and la niña-like oceanographic regimes in the southeastern atlantic. ICES Journal of Marine Science 66(6):1063–1072, DOI 10.1093/icesjms/fsp102, URL https://doi.org/10.1093/icesjms/fsp102

Park W, Latif M (2020) Resolution dependence of co2-induced tropical atlantic sector climate changes. npj Climate and Atmospheric Science 3(1):36, DOI 10.1038/s41612-020-00139-6, URL https://doi.org/10.1038/s41612-020-00139-6

Peterson RG, Stramma L (1991) Upper-level circulation in the south atlantic ocean. Progress in Oceanography 26(1):1–73, DOI https://doi.org/10.1016/0079-6611(91)90006-8, URL https://www.sciencedirect.com/science/article/pii/0079661191900068

Philander SG (ed) (1990) El Niño, La Niña, and the Southern Oscillatio. International Geophysics, Academic Press, DOI https://doi.org/10.1016/S0074-6142(08)60171-0, URL https://www.sciencedirect.com/science/article/pii/S0074614208601710

Polo I, Lazar A, Rodriguez-Fonseca B, Arnault S (2008) Oceanic kelvin waves and tropical atlantic intraseasonal variability: 1. kelvin wave characterization. Journal of Geophysical Research: Oceans 113(C7), DOI https://doi.org/10.1029/2007JC004495, URL https://agupubs.onlinelibrary.wiley.com/doi/abs/10.1029/2007JC004495, https://agupubs.onlinelibrary.wiley.com/doi/pdf/10.1029/2007JC004495

Polo I, Martin-Rey M, Rodriguez-Fonseca B, Kucharski F, Mechoso CR (2015) Processes in the pacific la niña onset triggered by the atlantic niño. Climate Dynamics 44(1):115–131, DOI 10.1007/s00382-014-2354-7, URL https://doi.org/10.1007/s00382-014-2354-7

Prigent A, Lübbecke JF, Bayr T, Latif M, Wengel C (2020a) Weakened SST variability in the tropical Atlantic Ocean since 2000. Climate Dynamics 54(5):2731–2744, DOI 10.1007/s00382-020-05138-0, URL https://doi.org/10.1007/s00382-020-05138-0

Prigent A, Imbol Koungue RA, Lübbecke JF, Brandt P, Latif M (2020b) Origin of weakened interannual sea surface temperature variability in the southeastern tropical atlantic ocean. Geophysical Research Letters 47(20):e2020GL089,348, DOI https://doi.org/10.1029/2020GL089348, URL https://agupubs.onlinelibrary.wiley.com/doi/abs/10.1029/2020GL089348, e2020GL089348 2020GL089348, https://agupubs.onlinelibrary.wiley.com/doi/pdf/10.1029/2020GL089348

Rayner NA (2003) Global analyses of sea surface temperature, sea ice, and night marine air temperature since the late nineteenth century. Journal of Geophysical Research 108(D14):4407, DOI 10.1029/2002JD002670, URL http://doi.wiley.com/10.1029/2002JD002670

Reason CJC, Florenchie P, Rouault M, Veitch J (2006) 10 Influences of large scale climate modes and agulhas system variability on the BCLME region. In: Shannon V, Hempel G, Malanotte-Rizzoli P, Moloney C, Woods JBTLME (eds) Benguela, vol 14, Elsevier, pp 223–238, DOI https://doi.org/10.1016/S1570-0461(06)80015-7, URL http://www.sciencedirect.com/science/article/pii/S157004610680015 7

Reboita MS, Ambrizzi T, Silva BA, Pinheiro RF, da Rocha RP (2019) The south atlantic subtropical anticyclone: Present and future climate. Frontiers in Earth Science 7:8, DOI 10.3389/feart.2019.00008, URL https://www.frontiersin.org/article/10.3389/feart.2019.00008

Reynolds RW, Smith TM, Liu C, Chelton DB, Casey KS, Schlax MG (2007) Daily High-Resolution-Blended Analyses for Sea Surface Temperature. Journal of Climate

20(22):5473–5496, DOI 10.1175/2007JCLI1824.1, URL http://journals.amets
oc.org/doi/abs/10.1175/2007JCLI1824.1

Richter I (2015) Climate model biases in the eastern tropical oceans: causes, impacts and ways forward. WIREs Climate Change 6(3):345–358, DOI https://doi.org/10.1002/wcc.338, URL https://wires.onlinelibrary.wile y.com/doi/abs/10.1002/wcc.338, https://wires.onlinelibrary.wiley. com/doi/pdf/10.1002/wcc.338

Richter I, Tokinaga H (2020) An overview of the performance of cmip6 models in the tropical atlantic: mean state, variability, and remote impacts. Climate Dynamics 55(9):2579–2601, DOI 10.1007/s00382-020-05409-w, URL https://doi.org/10 .1007/s00382-020-05409-w

Richter I, Tokinaga H (2021) 7 - the atlantic zonal mode: Dynamics, thermodynamics, and teleconnections. In: Behera SK (ed) Tropical and Extratropical Air-Sea Interactions, Elsevier, pp 171–206, DOI https://doi.org/10.1016/B978-0-12-818156-0.000 08-3, URL https://www.sciencedirect.com/science/article/pii/B97801 28181560000083

Richter I, Xie SP (2008) On the origin of equatorial atlantic biases in coupled general circulation models. Climate Dynamics 31(5):587–598, DOI 10.1007/s00382-008-0 364-z, URL https://doi.org/10.1007/s00382-008-0364-z

Richter I, Behera SK, Masumoto Y, Taguchi B, Komori N, Yamagata T (2010) On the triggering of benguela niños: Remote equatorial versus local influences. Geophysical Research Letters 37(20), DOI https://doi.org/10.1029/2010GL0444 61, URL https://agupubs.onlinelibrary.wiley.com/doi/abs/10.1029/20 10GL044461, https://agupubs.onlinelibrary.wiley.com/doi/pdf/10.102 9/2010GL044461

Richter I, Xie SP, Wittenberg AT, Masumoto Y (2012) Tropical atlantic biases and their relation to surface wind stress and terrestrial precipitation. Climate Dynamics 38(5):985–1001, DOI 10.1007/s00382-011-1038-9, URL https://doi.org/10.1 007/s00382-011-1038-9

Richter I, Behera SK, Masumoto Y, Taguchi B, Sasaki H, Yamagata T (2013) Multiple causes of interannual sea surface temperature variability in the equatorial atlantic ocean. Nature Geoscience 6(1):43–47, DOI 10.1038/ngeo1660, URL https://doi.org/10.1038/ngeo1660

Richter I, Xie SP, Behera SK, Doi T, Masumoto Y (2014) Equatorial atlantic variability and its relation to mean state biases in cmip5. Climate Dynamics 42(1):171–188, DOI 10.1007/s00382-012-1624-5, URL https://doi.org/10.1007/s00382-012-1624-5

Richter I, Xie SP, Morioka Y, Doi T, Taguchi B, Behera S (2017) Phase locking of equatorial atlantic variability through the seasonal migration of the itcz. Climate Dynamics 48(11):3615–3629, DOI 10.1007/s00382-016-3289-y, URL https://doi.org/10.1007/s00382-016-3289-y

Richter I, Doi T, Behera SK, Keenlyside N (2018) On the link between mean state biases and prediction skill in the tropics: an atmospheric perspective. Climate Dynamics 50(9):3355–3374, DOI 10.1007/s00382-017-3809-4, URL https://doi.org/10.1007/s00382-017-3809-4

Rodríguez-Fonseca B, Polo I, García-Serrano J, Losada T, Mohino E, Mechoso CR, Kucharski F (2009) Are atlantic niños enhancing pacific enso events in recent decades? Geophysical Research Letters 36(20), DOI https://doi.org/10.1029/2009GL040048, URL https://agupubs.onlinelibrary.wiley.com/doi/abs/10.1029/2009GL040048, https://agupubs.onlinelibrary.wiley.com/doi/pdf/10.1029/2009GL040048

Rouault M (2012) Bi-annual intrusion of tropical water in the northern benguela upwelling. Geophysical Research Letters 39(12), DOI https://doi.org/10.1029/2012GL052099, URL https://agupubs.onlinelibrary.wiley.com/doi/abs/10.1029/2012GL052099, https://agupubs.onlinelibrary.wiley.com/doi/pdf/10.1029/2012GL052099

Rouault M, Florenchie P, Fauchereau N, Reason CJC (2003) South east tropical atlantic warm events and southern african rainfall. Geophysical Research Letters 30(5), DOI https://doi.org/10.1029/2002GL014840, URL https://agupubs.onli

nelibrary.wiley.com/doi/abs/10.1029/2002GL014840, https://agupubs.
onlinelibrary.wiley.com/doi/pdf/10.1029/2002GL014840

Rouault M, Illig S, Bartholomae C, Reason CJC, Bentamy A (2007) Propagation and
origin of warm anomalies in the Angola Benguela upwelling system in 2001. Journal
of Marine Systems 68(3):473–488, DOI https://doi.org/10.1016/j.jmarsys.2006.11.
010, URL http://www.sciencedirect.com/science/article/pii/S0924796
306003538

Rouault M, Pohl B, Penven P (2010) Coastal oceanic climate change and variability
from 1982 to 2009 around south africa. African Journal of Marine Science 32(2):237–
246, DOI 10.2989/1814232X.2010.501563, URL https://doi.org/10.2989/18
14232X.2010.501563, https://doi.org/10.2989/1814232X.2010.501563

Rouault M, Illig S, Lübbecke J, Koungue RAI (2018) Origin, development and demise
of the 2010–2011 Benguela Niño. Journal of Marine Systems 188(July 2017):39–48,
DOI 10.1016/j.jmarsys.2017.07.007, URL https://doi.org/10.1016/j.jmarsy
s.2017.07.007

Saha S, Moorthi S, Wu X, Wang J, Nadiga S, Tripp P, Behringer D, Hou YT, Chuang
Hy, Iredell M, Ek M, Meng J, Yang R, Mendez MP, van den Dool H, Zhang Q, Wang
W, Chen M, Becker E (2013) The NCEP Climate Forecast System Version 2. Journal
of Climate 27(6):2185–2208, DOI 10.1175/JCLI-D-12-00823.1, URL https://do
i.org/10.1175/JCLI-D-12-00823.1

Saha S, Moorthi S, Wu X, Wang J, Nadiga S, Tripp P, Behringer D, Hou YT, ya Chuang
H, Iredell M, Ek M, Meng J, Yang R, Mendez MP, van den Dool H, Zhang Q, Wang
W, Chen M, Becker E (2014) The ncep climate forecast system version 2. Journal of
Climate 27(6):2185 – 2208, DOI 10.1175/JCLI-D-12-00823.1, URL https://jour
nals.ametsoc.org/view/journals/clim/27/6/jcli-d-12-00823.1.xml

Schott FA, McCreary Jr JP, Johnson GC (2004) Shallow overturning circulations of the
tropical-subtropical oceans. Earth's Climate 147:261–304

Schultz MG, Stadtler S, Schröder S, Taraborrelli D, Franco B, Krefting J, Henrot A,
Ferrachat S, Lohmann U, Neubauer D, Siegenthaler-Le Drian C, Wahl S, Kokkola

H, Kühn T, Rast S, Schmidt H, Stier P, Kinnison D, Tyndall GS, Orlando JJ, Wespes C (2018) The chemistry–climate model echam6.3-ham2.3-moz1.0. Geoscientific Model Development 11(5):1695–1723, DOI 10.5194/gmd-11-1695-2018, URL https://gmd.copernicus.org/articles/11/1695/2018/

Schwarzkopf FU, Biastoch A, Böning CW, Chanut J, Durgadoo JV, Getzlaff K, Harlaß J, Rieck JK, Roth C, Scheinert MM, Schubert R (2019) The inalt family – a set of high-resolution nests for the agulhas current system within global nemo ocean/sea-ice configurations. Geoscientific Model Development 12(7):3329–3355, DOI 10.5194/gmd-12-3329-2019, URL https://gmd.copernicus.org/articles/12/3329/2019/

Servain J, Picaut J, Merle J (1982) Evidence of Remote Forcing in the Equatorial Atlantic Ocean. Journal of Physical Oceanography 12(5):457–463, DOI 10.1175/1520-0485(1982)012⟨0457:EORFIT⟩2.0.CO;2, URL http://journals.ametsoc.org/doi/abs/10.1175/1520-0485{%}281982{%}29012{%}3C0457{%}3AEORFIT{%}3E2.0.CO{%}3B2

Servain J, Caniaux G, Kouadio YK, McPhaden MJ, Araujo M (2014) Recent climatic trends in the tropical Atlantic. Climate Dynamics 43(11):3071–3089, DOI 10.1007/s00382-014-2168-7, URL http://link.springer.com/10.1007/s00382-014-2168-7

Shannon LV, Boyd AJ, Brundrit GB, Taunton-Clark J (1986) On the existence of an el niño-type phenomenon in the benguela system. Journal of Marine Research 44(3):495–520, DOI doi:10.1357/002224086788403105, URL https://www.ingentaconnect.com/content/jmr/jmr/1986/00000044/00000003/art00005

Siegfried L, Schmidt M, Mohrholz V, Pogrzeba H, Nardini P, Böttinger M, Scheuermann G (2019) The tropical-subtropical coupling in the southeast atlantic from the perspective of the northern benguela upwelling system. PLOS ONE 14(1):1–31, DOI 10.1371/journal.pone.0210083, URL https://doi.org/10.1371/journal.pone.0210083

Silva P, Wainer I, Khodri M (2021) Changes in the equatorial mode of the tropical atlantic in terms of the bjerknes feedback index. Climate Dynamics 56(9):3005–3024,

DOI 10.1007/s00382-021-05627-w, URL https://doi.org/10.1007/s00382-0
21-05627-w

Small RJ, Curchitser E, Hedstrom K, Kauffman B, Large WG (2015) The benguela upwelling system: Quantifying the sensitivity to resolution and coastal wind representation in a global climate model. Journal of Climate 28(23):9409 – 9432, DOI 10.1175/JCLI-D-15-0192.1, URL https://journals.ametsoc.org/view/jour nals/clim/28/23/jcli-d-15-0192.1.xml

Steele M, Morley R, Ermold W (2001) Phc: A global ocean hydrography with a high-quality arctic ocean. Journal of Climate 14(9):2079 – 2087, DOI 10.1175/1520-0442(2001)014⟨2079:PAGOHW⟩2.0.CO;2, URL https://journals.ametsoc.org/view/journals/clim/14/9/1520-0442 _2001_014_2079_pagohw_2.0.co_2.xml

Stevens B, Giorgetta M, Esch M, Mauritsen T, Crueger T, Rast S, Salzmann M, Schmidt H, Bader J, Block K, Brokopf R, Fast I, Kinne S, Kornblueh L, Lohmann U, Pincus R, Reichler T, Roeckner E (2013) Atmospheric component of the mpi-m earth system model: Echam6. Journal of Advances in Modeling Earth Systems 5(2):146–172, DOI https://doi.org/10.1002/jame.20015, URL https://agupubs.onlinelibrar y.wiley.com/doi/abs/10.1002/jame.20015, https://agupubs.onlinelibr ary.wiley.com/doi/pdf/10.1002/jame.20015

Stockdale TN, Balmaseda MA, Vidard A (2006) Tropical atlantic sst prediction with coupled ocean–atmosphere gcms. Journal of Climate 19(23):6047 – 6061, DOI 10 .1175/JCLI3947.1, URL https://journals.ametsoc.org/view/journals/cli m/19/23/jcli3947.1.xml

Sutton RT, Hodson DLR (2003) Influence of the ocean on north atlantic climate variability 1871–1999. Journal of Climate 16(20):3296 – 3313, DOI 10.1175/1520-0442(20 03)016⟨3296:IOTOON⟩2.0.CO;2, URL https://journals.ametsoc.org/view/ journals/clim/16/20/1520-0442_2003_016_3296_iotoon_2.0.co_2.xml

Sutton RT, Jewson SP, Rowell DP (2000) The elements of climate variability in the tropical atlantic region. Journal of Climate 13(18):3261 – 3284, DOI 10.1175/1520-044

2(2000)013⟨3261:TEOCVI⟩2.0.CO;2, URL https://journals.ametsoc.org/view/journals/clim/13/18/1520-0442_2000_013_3261_teocvi_2.0.co_2.xml

Svendsen L, Kvamstø NG, Keenlyside N (2014) Weakening amoc connects equatorial atlantic and pacific interannual variability. Climate Dynamics 43(11):2931–2941, DOI 10.1007/s00382-013-1904-8, URL https://doi.org/10.1007/s00382-013-1904-8

Taylor KE, Stouffer RJ, Meehl GA (2012) An overview of cmip5 and the experiment design. Bulletin of the American Meteorological Society 93(4):485 – 498, DOI 10.1175/BAMS-D-11-00094.1, URL https://journals.ametsoc.org/view/journals/bams/93/4/bams-d-11-00094.1.xml

Tchipalanga P, Dengler M, Brandt P, Kopte R, Macuéria M, Coelho P, Ostrowski M, Keenlyside NS (2018) Eastern Boundary Circulation and Hydrography Off Angola: Building Angolan Oceanographic Capacities. Bulletin of the American Meteorological Society 99(8):1589–1605, DOI 10.1175/BAMS-D-17-0197.1, URL http://journals.ametsoc.org/doi/10.1175/BAMS-D-17-0197.1

Tim N, Zorita E, Hünicke B (2015) Decadal variability and trends of the benguela upwelling system as simulated in a high-resolution ocean simulation. Ocean Science 11(3):483–502, DOI 10.5194/os-11-483-2015, URL https://os.copernicus.org/articles/11/483/2015/

Timmermann A, An SI, Kug JS, Jin FF, Cai W, Capotondi A, Cobb KM, Lengaigne M, McPhaden MJ, Stuecker MF, Stein K, Wittenberg AT, Yun KS, Bayr T, Chen HC, Chikamoto Y, Dewitte B, Dommenget D, Grothe P, Guilyardi E, Ham YG, Hayashi M, Ineson S, Kang D, Kim S, Kim W, Lee JY, Li T, Luo JJ, McGregor S, Planton Y, Power S, Rashid H, Ren HL, Santoso A, Takahashi K, Todd A, Wang G, Wang G, Xie R, Yang WH, Yeh SW, Yoon J, Zeller E, Zhang X (2018) El niño–southern oscillation complexity. Nature 559(7715):535–545, DOI 10.1038/s41586-018-0252-6, URL https://doi.org/10.1038/s41586-018-0252-6

Tokinaga H, Xie SP (2011) Weakening of the equatorial Atlantic cold tongue over the past six decades. Nature Geoscience 4(4):222–226, DOI 10.1038/ngeo1078, URL http://www.nature.com/articles/ngeo1078

Tuchen FP, Lübbecke JF, Schmidtko S, Hummels R, Böning CW (2019) The atlantic subtropical cells inferred from observations. Journal of Geophysical Research: Oceans 124(11):7591–7605, DOI https://doi.org/10.1029/2019JC015396, URL https://agupubs.onlinelibrary.wiley.com/doi/abs/10.1029/2019JC015396, https://agupubs.onlinelibrary.wiley.com/doi/pdf/10.1029/2019JC015396

Tuchen FP, Lübbecke JF, Brandt P, Fu Y (2020) Observed transport variability of the atlantic subtropical cells and their connection to tropical sea surface temperature variability. Journal of Geophysical Research: Oceans 125(12):e2020JC016,592, DOI https://doi.org/10.1029/2020JC016592, URL https://agupubs.onlinelibrary.wiley.com/doi/abs/10.1029/2020JC016592, e2020JC016592 2020JC016592, https://agupubs.onlinelibrary.wiley.com/doi/pdf/10.1029/2020JC016592

Valcke S (2013) The oasis3 coupler: a european climate modelling community software. Geoscientific Model Development 6(2):373–388, DOI 10.5194/gmd-6-373-2013, URL https://gmd.copernicus.org/articles/6/373/2013/

Veitch JA, Florenchie P, Shillington FA (2006) Seasonal and interannual fluctuations of the angola–benguela frontal zone (abfz) using 4.5 km resolution satellite imagery from 1982 to 1999. International Journal of Remote Sensing 27(5):987–998, DOI 10.1080/01431160500127914, URL https://doi.org/10.1080/01431160500127914, https://doi.org/10.1080/01431160500127914

Vijayeta A, Dommenget D (2018) An evaluation of ENSO dynamics in CMIP simulations in the framework of the recharge oscillator model. Climate Dynamics 51(5-6):1753–1771, DOI 10.1007/s00382-017-3981-6, URL http://dx.doi.org/10.1007/s00382-017-3981-6http://link.springer.com/10.1007/s00382-017-3981-6

Vizy EK, Cook KH (2016) Understanding long-term (1982–2013) multi-decadal change in the equatorial and subtropical South Atlantic climate. Climate Dynamics 46(7-8):2087–2113, DOI 10.1007/s00382-015-2691-1

Vizy EK, Cook KH, Sun X (2018) Decadal change of the south Atlantic ocean Angola–Benguela frontal zone since 1980. Climate Dynamics 51(9-10):3251–3273, DOI 10.1007/s00382-018-4077-7, URL http://dx.doi.org/10.1007/s00382-018-4077-7

Voldoire A, Exarchou E, Sanchez-Gomez E, Demissie T, Deppenmeier AL, Frauen C, Goubanova K, Hazeleger W, Keenlyside N, Koseki S, Prodhomme C, Shonk J, Toniazzo T, Traoré AK (2019) Role of wind stress in driving sst biases in the tropical atlantic. Climate Dynamics 53(5):3481–3504, DOI 10.1007/s00382-019-04717-0, URL https://doi.org/10.1007/s00382-019-04717-0

Wang C, Zhang L (2013) Multidecadal ocean temperature and salinity variability in the tropical north atlantic: Linking with the amo, amoc, and subtropical cell. Journal of Climate 26(16):6137 – 6162, DOI 10.1175/JCLI-D-12-00721.1, URL https://journals.ametsoc.org/view/journals/clim/26/16/jcli-d-12-00721.1.xml

Wang D, Gouhier TC, Menge BA, Ganguly AR (2015) Intensification and spatial homogenization of coastal upwelling under climate change. Nature 518(7539):390–394, DOI 10.1038/nature14235, URL https://doi.org/10.1038/nature14235

Wang L (2017) Weakened interannual variability of the contrast in rainfall between the eastern equatorial Pacific and equatorial Atlantic since 2000. Atmospheric and Oceanic Science Letters 10(3):198–205, DOI 10.1080/16742834.2017.1286632, URL http://dx.doi.org/10.1080/16742834.2017.1286632

Wengel C, Dommenget D, Latif M, Bayr T, Vijayeta A (2018) What Controls ENSO-Amplitude Diversity in Climate Models? Geophysical Research Letters 45(4):1989–1996, DOI 10.1002/2017GL076849, URL http://doi.wiley.com/10.1002/2017GL076849

Wengel C, Lee SS, Stuecker MF, Timmermann A, Chu JE, Schloesser F (2021) Future high-resolution el niño/southern oscillation dynamics. Nature Climate Change 11(9):758–765, DOI 10.1038/s41558-021-01132-4, URL https://doi.org/10.1038/s41558-021-01132-4

Worou K, Goosse H, Fichefet T, Kucharski F (2021) Weakened impact of the atlantic niño on the future equatorial atlantic and guinean coast rainfall. Earth Sys-

tem Dynamics Discussions 2021:1–45, DOI 10.5194/esd-2021-46, URL https://esd.copernicus.org/preprints/esd-2021-46/

Xie SP (2009) Ocean–atmosphere interaction and tropical climate. The Encyclopedia of Life Support Systems (EOLSS)

Xie SP, Philander SGH (1994) A coupled ocean-atmosphere model of relevance to the itcz in the eastern pacific. Tellus A 46(4):340–350, DOI https://doi.org/10.1034/j.1600-0870.1994.t01-1-00001.x, URL https://onlinelibrary.wiley.com/doi/abs/10.1034/j.1600-0870.1994.t01-1-00001.x, https://onlinelibrary.wiley.com/doi/pdf/10.1034/j.1600-0870.1994.t01-1-00001.x

Xu K, Wang W, Liu B, Zhu C (2019) Weakening of the El Niño amplitude since the late 1990s and its link to decadal change in the North Pacific climate. International Journal of Climatology p joc.6063, DOI 10.1002/joc.6063, URL https://onlinelibrary.wiley.com/doi/abs/10.1002/joc.6063

Yu, Lisan and Jin, Xiangze and Weller R (2008) Multidecade Global Flux Datasets from the Objectively Analyzed Air-sea Fluxes (OAFlux) Project: Latent and Sensible Heat Fluxes, Ocean Evaporation, and Related Surface Meteorological Variables. OAFlux Project Tech Rep OA-2008-01

Zebiak SE (1986) Atmospheric convergence feedback in a simple model for El Niño. Mon Wea Rev 114:1263–1271, URL https://doi.org/10.1175/1520-0493(1986)114{%}3C1263:ACFIAS{%}3E2.0.CO;2.

Zebiak SE (1993) Air–Sea Interaction in the Equatorial Atlantic Region. Journal of Climate 6(8):1567–1586, DOI 10.1175/1520-0442(1993)006⟨1567:AIITEA⟩2.0.CO;2, URL http://journals.ametsoc.org/doi/abs/10.1175/1520-0442{%}281993{%}29006{%}3C1567{%}3AAIITEA{%}3E2.0.CO{%}3B2

Zhang L, Han W (2021) Indian ocean dipole leads to atlantic niño. Nature Communications 12(1):5952, DOI 10.1038/s41467-021-26223-w, URL https://doi.org/10.1038/s41467-021-26223-w

Own publications

- **Prigent, A.**, Lübbecke, J. F., Bayr, T., Latif, M., & Wengel, C. (2020a). Weakened SST variability in the tropical Atlantic Ocean since 2000. Climate Dynamics, 54, 2731–2744. https://doi.org/10.1007/s00382-020-05138-0

- **Prigent, A.**, Imbol Koungue, R. A., Lübbecke, J. F., Brandt, P., & Latif, M. (2020b). Origin of weakened interannual sea surface temperature variability in the southeastern tropical Atlantic Ocean. Geophysical Research Letters, 47, e2020GL089348. https://doi.org/10.1029/2020GL089348

- Crespo, L. R., **Prigent, A.**, Keenlyside, K., Koseki, S., Svendsen, L., Richter, I., & Sánchez-Gómez, E. (In preparation). Weakening of the Atlantic Niño variability under global warming

- **Prigent, A.**, Imbol Koungue, R. A., Lübbecke, J. F., Brandt, P., Bayr, T., Harlaß, J., & Latif, M. (Under revision at Journal of Climate). Future weakening of southeastern Tropical Atlantic Ocean interannual SST variability in a nested coupled model.

- Imbol Koungue, R. A., Brandt, P., Lübbecke, J. F., **Prigent, A.**, Sena Martins, M., Rodrigues, R. R. (Accepted in Frontiers in Marine Science). The 2019 Benguela Niño event.

Acknowledgements

Declaration

I hereby declare that - apart from my supervisor's guidance and acknowledged assistance - the content and design of this thesis is my own work. This thesis has not been submitted either partially or wholly as part of a doctoral degree to another examining body and has not been published or submitted for publication except for the chapters where this is explicitly stated. This thesis has been prepared in accordance with the Rules of Good Scientific Practice of the German Research Foundation. An academic degree has never been withdrawn from me.

Kiel, December 2021, _15/12/2021 Arthur Prigent_

(Arthur Prigent)